TÉCNICO LISBOA

Interchangeability Analysis of a Domestic Cooktop Burner

Eduardo Maria Soares Rodrigues

Thesis to obtain the Master of Science Degree in

Mechanical Engineering

Supervisors: Prof. Ana Filipa da Silva Ferreira
Prof. Edgar Caetano Fernandes

Examination Committee

Chairperson: Prof. António Luís Nobre Moreira
Supervisor: Prof. Edgar Caetano Fernandes
Member of the Committee: Prof. Teodoro José Pereira Trindade

July 2022

Declaration

I declare that this document is an original work of my own authorship and that it fulfills all the requirements of the Code of Conduct and Good Practices of the Universidade de Lisboa.

Acknowledgments

All my journey in the faculty of the Instituto Superior Técnico was made through much effort and dedication, in constant need of exceeding again and again my own capabilities. Consequently, this master's dissertation could not have been achieved in any other way. Fortunately, I am one of the lucky ones who could share such challenge with plenty of true and tireless friends.

The current work results from a great synergy created with Professor Edgar, who incredibly shared with me the same enthusiasm, curiosity and pro-activity, to overcome countless barriers until the end. Professor Edgar truly has a priceless contribution to the work developed. I would like to express my special gratitude to Professor Ana, who challenged me to engage in this subject and placed her entire trust in me. In addition, Professor Sandra Dias was always concerned and available to solve any inconvenience, concerning the laboratory facilities.

Also to all the people that contributed during the development of this thesis: Diogo Almeida - for its thermocouples and PIV expertise; Diogo Vozone and Francisco Silva - for all the intelligent solutions suggested; Vasco Centeno - for the spectrometry measurements conducted; Gonçalo Madeira and Bruno Gouveia - for all the camaraderie and support.

Still, I couldn't be more grateful to: my grandparents, brother, and specially to my parents, who have always been there fighting, guiding and praying for my utmost success and happiness. At last, I would like to leave a kindly note to Margarida, who remarkably managed to cope with all the stress and difficulties, supporting me all the way.

This work was developed at the Thermofluids, Combustion and Energy Systems laboratory of the IN+ - Center for Innovation, Technology and Policy Research.

Resumo

O hidrogénio é cada vez mais considerado a chave para enfrentar as alterações climáticas e alcançar uma economia descarbonizada. Em períodos de excesso de produção de energia renovável, este pode ser utilizado para produzir hidrogénio verde, reduzindo assim a necessidade de baterias. Além disso, o hidrogénio apresenta também potencial como portador energético, podendo ser injetado na rede de gás natural. Neste contexto, fatores de segurança e desempenho dos aparelhos domésticos, são fundamentais para a sua viabilidade.

O trabalho estudou o impacto de misturas $NG - H_2$ num fogão doméstico, no sentido de avaliar a estabilidade da chama, o risco de flashback e o ruído do queimador. Para isso, foram realizados testes laboratoriais onde se aqueceu água dentro de uma panela, e através de balanços energéticos foi possível obter a eficiência do processo de aquecimento. Entretanto, com a ajuda da tecnologia de PIV foi possível estudar o comportamento do escoamento em redor da panela. Assim, desenvolveu-se um segundo método para determinar a eficiência, este baseado nas equações de transferência de calor. Além disso, as experiências foram realizadas para queimadores de diferentes tamanhos, para explorar o impacto da sua potência e dimensão nos parâmetros mencionados até agora.

Processos de cozedura lenta provaram ter eficiências mais altas ($\approx +15\%$) e custos mais reduzidos ($\approx -25\%$), quando comparados com processos de cozedura rápida. Finalmente, os resultados de ambos os métodos coincidiram e foi desenvolvido um modelo matemático, que utiliza condições de funcionamento para prever a eficiência.

Palavras-chave: Hidrogénio, Permutabilidade, Aparelhos Domésticos, Cozedura Lenta, Custos para o Consumidor

Abstract

Hydrogen is increasingly being placed on the road to face climate change and achieve a decarbonised economy. In fact, green hydrogen can be produced by renewable energy during periods of over production, thus reducing the need for batteries. In addition, hydrogen is a great energy carrier, that could be injected into the natural gas network. Therefore, the interchangeability of household appliances, either for safety reasons or fitness for purpose, is key to progress towards sustainability.

The current work studied the impact of several $NG - H_2$ mixtures on a domestic cooktop burner, in order to assess the flame stability, flashback risk and burner noise. The fitness for purpose was examined by conducting cooking efficiency experiments, which relied on heating water inside a pan and conduct its energy balance. A second cooking efficiency method based on the heat transfer equations was developed, which relied on PIV experiments to study the flow behaviour. In addition, the experiments were conducted through 3 different sized burners, to explore the impact of the burner power and dimensions, on the parameters mentioned so far.

Slow cooking proved to be the path for sustainability and cost reduction, by providing a higher cooking efficiency ($\approx +15\%$) and lower costs ($\approx -25\%$) when compared to fast cooking. Finally, the results from both methods met and a mathematical model was developed. This model uses the operating conditions to predict the cooking efficiency, thus extrapolating the results.

Keywords: Hydrogen, Interchangeability, Household Appliances, Slow Cooking, End User Costs

Contents

List of Tables

List of Figures

Nomenclature

Acronyms

ATR	Auto thermal reforming.
B05	Burner with $5cm$ diameter.
B07	Burner with $7cm$ diameter.
B10	Burner with $10cm$ diameter.
CRS	Constant returns of scale.
DRS	Decreasing returns of scale.
FG	Fluorinated gases.
HHV	High heating value.
IRS	Increasing returns of scale.
LHV	Low heating value.
MF1	Modelling function 1.
MF2	Modelling function 2.
NG	Natural gas.
PIV	Particle image velocimetry.
POX	Partial oxidation.
RMF1	Refined modelling function 1.
RMF2	Refined modelling function 2.
SLPM	Standard liters per minute.
SMR	Steam methane reforming.

Chemical Species

CH_4	Methane.

CO Carbon monoxide.

CO_2 Carbon dioxide.

H_2 Hydrogen (molecule).

KOH Potassium hydroxide.

N_2 Nitrogen (molecule).

N_2O Nitrous oxide.

$NaOH$ Sodium hydroxide.

NO_x Nitrogen oxides.

O_2 Oxygen (molecule).

Greek symbols

α Correction value.

β Coefficient of volume expansion.

η Cooking efficiency.

κ Thermal conductivity coefficient.

μ Dynamic viscosity coefficient.

ρ Density.

ρ_r Relative density of fuel compared to air.

τ Time constant.

θ Curvature angle.

Roman symbols

A Area.

C^+ Best cost prediction.

C^- Worst cost prediction.

Cp Specific heat capacity.

f Hydrogen molar fraction.

g Gravitational acceleration.

Gr Grashof number.

h Convection coefficient.

h_{fg} Water evaporation enthalpy.

L_{dv} Volumetric stoichiometric air requirement.

L_d Molar stoichiometric air requirement.

$\dot{m}_{evap}$ Rate of the water mass evaporated.

M Molar mass.

m Mass.

nh Number of burner holes.

Nm^3 Normal cubic meter.

Nu Nusselt number.

P Burner power.

p Perimeter.

Pr Prandtl number.

$\dot{Q}_{comb}$ Combustion heat rate.

$\dot{Q}_{cond}$ Heat from conduction.

$\dot{Q}_{conv}$ Heat from convection.

$\dot{Q}_{in}$ Heat rate entering the system.

$\dot{Q}_{out}$ Heat rate exiting the system.

$\dot{Q}_{rad}$ Heat from radiation.

$Q^i_{\max}$ Controller maximum flow rate capacity.

Q_m Measured flow rate.

R Ideal gas constant.

R_b Radius of the burner.

R_p Radius of the pan.

Re Reynolds number.

S_L Laminar burning velocity.

t Time.

T_b Tip temperature.

T_f Fluid temperature.

T_w Water temperature.

U Internal energy.

$U_{f_{H_2}}$ Hydrogen fraction uncertainty.

U_P Power uncertainty.

U_Q Flow rate uncertainty.

$\dot{V}$ Volumetric flow rate.

V Volume.

v kinematic viscosity coefficient.

W_i Wobbe number.

x Axial distance.

y Molar fraction.

Subscripts

∞ Free-stream condition.

i, j, k Computational indexes.

max Maximum.

n Normal component.

st Stoichiometric conditions.

X, Y, Z Cartesian components.

ref Reference condition.

Chapter 1

Introduction

1.1 Motivation

Climate change is a fundamental topic that concerns today's World and one that will deeply shape the future of not only the human specie but also of life as it is known in Earth. Indeed, the only way to face climate change is to change one's behaviour as an individual so that a whole new sustainable society can be reborn. Actually, it is known that climate change is deeply linked to the greenhouse gas emissions, representing a major problem to be tackled. Nowadays, the emissions of greenhouse gas results greatly from the energy production process in order to supply electricity and heat (31%) as well as transportation (16%) [1, 2], leading to $0.8° \, C$ increase of the worlds' temperature in the last 50 years [2]. In Europe, the household sector ends up accountable for 72% of greenhouse gases emissions [3]. Indeed, one can look at its own behaviour and easily realize that performing simple home tasks such as cooking, taking a bath, washing, or simply turning on the electricity may contribute to the greenhouse gas effect [3].

As a matter of fact, the energy consumption in Europe has been almost entirely relying on fossil fuels until the last decade [4, 5]. However, in the last decade the production of energy through renewable energies have been increasingly growing due to a few reasons. First of all, the costs associated to this energies have been decreasing considerably, being most of that due to the so called learning curve [6, 7]. While in the past the fossil fuels were considered way cheaper and cost effective than renewable energies, today's reality has changed and renewable energy industry appear as a growing market full of interesting opportunities. Plus, the Paris Agreement was a landmark which brought all nations together to combat the climate change [8]. From then on, huge steps towards achieving a net zero carbon emissions had been taking place, and in that scenario hydrogen as a cleaner energy source is more and more being regarded as a solution [9–12].

In that context, the hydrogen role can be essential to achieve the established goals for 2050, as it's a very possible substitute of Natural Gas. Indeed, NG is a fossil fuel widely used for power generation [13]. It can be burned to generate pressurized gas into a turbine producing electricity. Plus, it has also plenty of household utilities. Usually, water heating systems rely on burning natural gas to heat the hot water that circulates inside pipes along the house. Moreover, basic necessities are dependent

on domestic appliances such as cookers and boilers, that rely on the combustion of NG as the heat source. While the combustion of natural gas results in considerable emissions of greenhouse gases, the hydrogen combustion is free of CO_2 emissions. Instead, its combustion is eco-friendly by mainly producing water vapor. Although hydrogen combustion is extremely interesting from an environmental point of view, the turning point for hydrogen as a sustainable economic energy carrier, was due to two major factors: the decrease of its production costs (by implementing economies of scale) and the increase of the electrolysis process efficiency, used to obtain hydrogen [14, 15]. However, from an interchangeability perspective, implementing hydrogen still rises a few challenges to overcome, leaving a few open questions. Hydrogen has a low energy density in a mass basis, being able to store up to 3 times the energy stored by natural gas. As hydrogen is a powerful energy carrier, the aim is to inject it into the gas grid network while maintaining the same infrastructure. Yet, it isn't proved to be fully compatible with the gas grid composition requirements [16]. Therefore, a few countries such as Portugal, have chosen a gradual change in the gas network supply. Nevertheless, ensure that all end users have access to an uniform hydrogen supply may turn out to be a challenge, due to the fact that the behaviour of a blended mixture is not the same as it was pure H_2 or pure NG. Moreover, the domestic appliances fueled by natural gas may not have the same operating behaviour when fueled by hydrogen, which may result in different efficiencies and safety margins [17]. Indeed, flashback risk is a phenomenon that has already been accounted for and can be dangerous to both the lifetime of the appliance and to the security of the end user. Therefore, it is crucial to ensure that the end user needs and safety issues are going to be met no matter the fuel type.

From the economic point of view, it has already been mentioned that the production costs of hydrogen are now competitive and the tendency is to decrease, yet it does not necessarily mean that for the end user it's going to be economically interesting. It depends on the performance of the appliances, on the market behaviour and on the the charging method to the end user. Ultimately, one's contribution to the implementation of hydrogen in the world's energetic context, can make the difference.

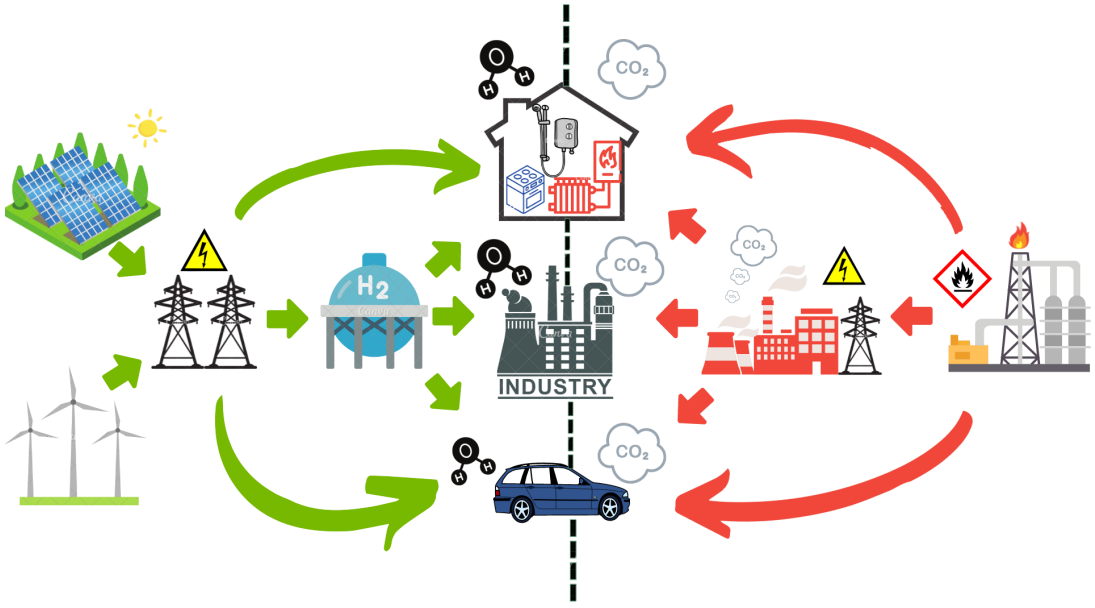

Figure 1.1: Green Energy Value Chain VS Fossil Energy Value Chain

1.2 Energetic Reality in Portugal and Europe

Since the Industrial Revolution that fossil fuels, natural gas, oil and mainly coal lead the society towards a new era. In fact, these energy sources supplied a mass production economy and have made it possible to boost the life quality standards known today. Unfortunately, apart from possessing a few coal mines, Portugal has been an energy dependent country struggling to meet its energy demand. Indeed, according to "Direcao Geral de Energia-Geologia", in 2020 Portugal imported 72% of its energy consumption. Figure 1.2 (a) and (b) shows Portugal primary energy consumption sources, in particular for 2020 but also over time since 1990, respectively. In fact, figure 1.2 (a) shows that Portugal is still dangerously relying on fossil fuels, as its slice corresponds to 70% of all primary energy sources.

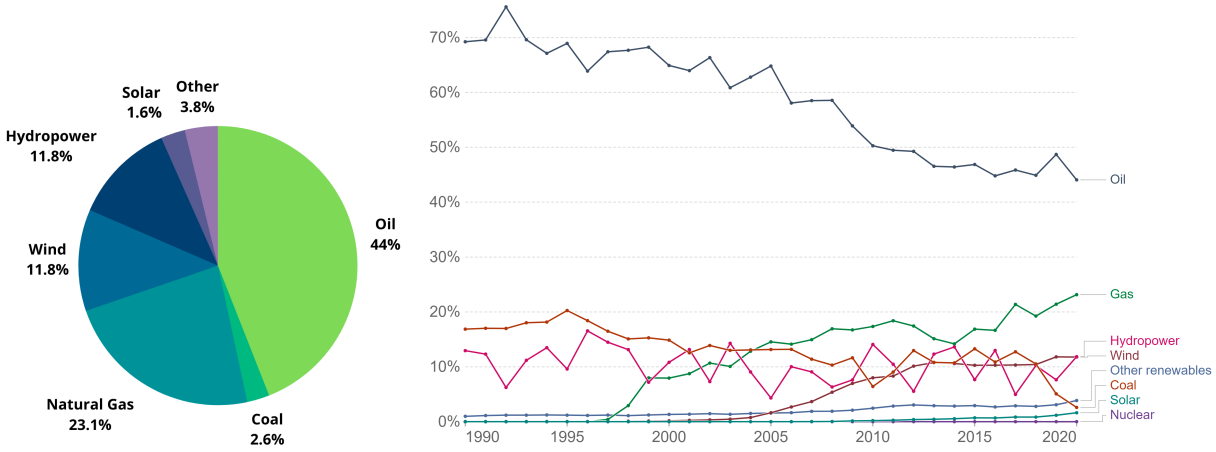

(a) Energy Sources in 2020

(b) Energy Sources over time

Figure 1.2: Portugal Primary Consumption Sources of Energy [18, 19]

In turn, figure 1.2 (b) shows that the energy policy in Portugal has sought to reduce oil consumption, which has been counterbalanced by an increase in both natural gas and wind energy consumption. Moreover, solar energy is becoming increasingly popular has its costs have been decreasing while its efficiency has been growing, [20, 21]. Indeed, it's considered an extremely interesting market with high expectancy to grow, plus Portuguese government with the support of European funds are promoting the purchase of solar panels by introducing economic benefits to the household sector, [22–25]. Indeed, renewable energy generation has already been increasing since the lats decade. For instance, it was inaugurated in 2008 the "Alto do Minho" onshore wind farm providing $263MW$, or more recently in 2021 it was inaugurated Portugal's largest solar farm in "Alcoutim" providing up to $200MW$. In fact, several projects have been inaugurated since the beginning of the century, which can be seen through to the ascending lines in the figure 1.3. In particular, figure 1.3 shows that since 2005 wind production was given an huge boost, steeping from $1TWh$ to today's $12TWh$. Nevertheless, since 2014 it has stabilised, sometimes suffering slight reductions.

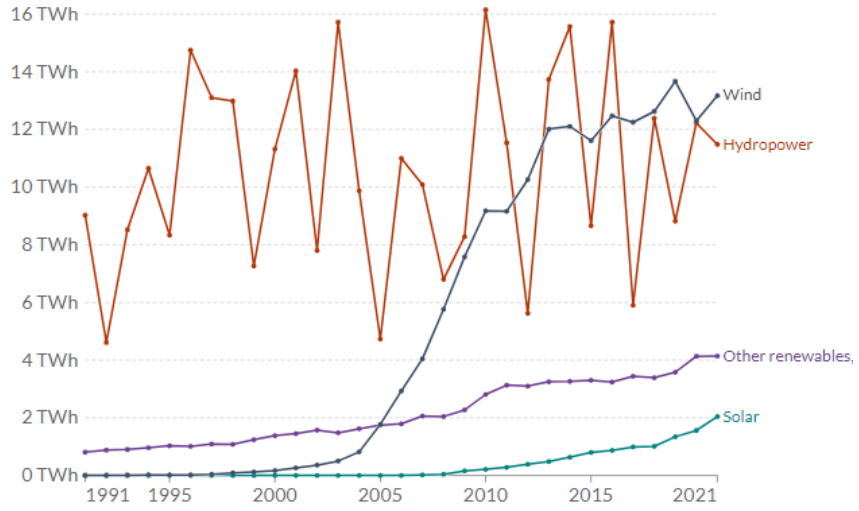

Figure 1.3: Portugal Renewables Energy Generation by year [18, 19]

In fact, these investments in renewable energies were reflected in the greenhouse gas emissions. Figure 1.4 shows the greenhouse gas emissions over time, according to the emission of CH_4, N_2O, FG and $CO2$. Undeniably, $CO2$ emission (blue) is overwhelmingly more significant than all the other gases. Moreover, since 2005 the increase in the wind generation was followed by a steady decrease of the greenhouse gas emissions. However, since 2014 the tendency has become unstable, sometimes resulting in an increase in emissions. Interestingly, such happened at the same time as wind energy generation stopped increasing.

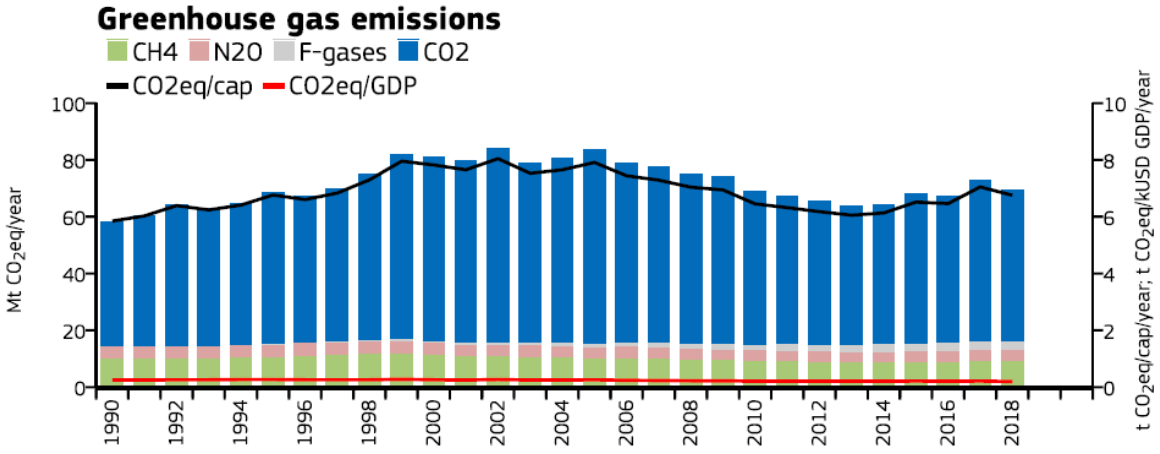

Figure 1.4: Portugal Greenhouse Gas Emissions [26]

As the CO_2 emissions are significantly higher than any of the other greenhouse gases, if one considers only CO_2, it's expected to obtain the same variations as before. Indeed, figure 1.5 is very much alike the figure above, yet this one shows the CO_2 emissions by sector. It shows that over the years since 1990, transports and power industry have been the main sectors contributing to the CO_2 emissions. Whereas, emissions in particular due to buildings, which are directly linked to the household sector, have a minor share of only close to 5%.

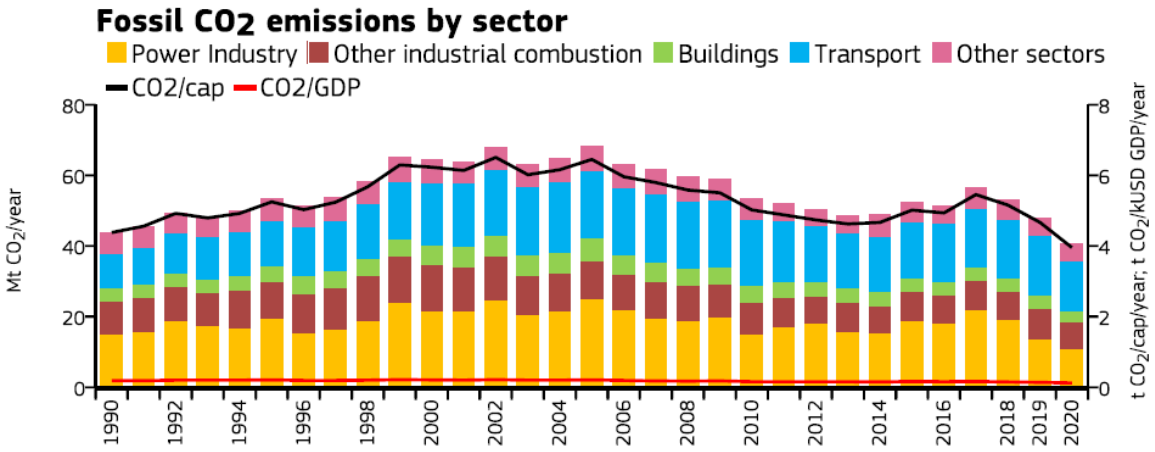

Figure 1.5: Portugal CO_2 Emissions [26]

Although the household sector isn't an active agent causing the emissions from the power industry, it should be regarded as a passive agent because it greatly uses that energy. Therefore, the household real CO_2 emissions are higher than what the figures suggest at first sight. The direct and indirect greenhouse gas emissions have been a topic of study in past years. Several studies have found different approaches to estimate the household share in the greenhouse emissions. Its particularly value changes from study to study: [3] suggests 72%; [27] suggested 60% for Portugal in 2001; [28] suggests more than 60%. Plus, [28] stands that the emissions are unevenly distributed across countries, according to the household consumption.

Actually, figure 1.6 (a) and (b) show the energy consumption by sector both in Portugal and in Europe. In Portugal, the transports and the industry sectors stand as the sectors that largely require most energy, overshadowing the household sector (which has the third larger slice in figure 1.6 (a)). In the mean while, for the average Europe, there is a balanced distribution of the energy consumption. Figure 1.6 (b) shows that transports, industry and the household are the main energy consumption sectors, sharing similar slices.

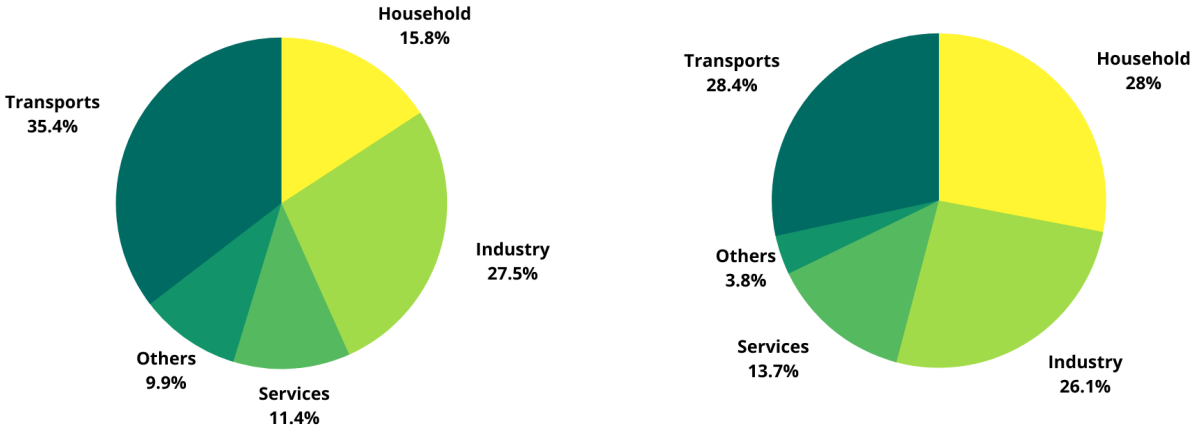

(a) Portugal

(b) Average Europe

Figure 1.6: Energy Consumption by Sector 2020 [4, 29]

Indeed, the clear difference of the household share in the energy consumption between Portugal and the average Europe, can be easily explained due to weather related factors. Portugal has a warm climate during all seasons over the year. While, Northern and Easter Europe countries are exposed to freezing winters, thus being forced to expend more energy to heat its buildings. In fact, figure 1.7 (a) and (b), which shows the household energy consumption by end user type both for Portugal and Europe, can help realizing precisely that. On one hand, figure 1.7 (a) shows that in Portugal the household sector mainly uses energy by cooking (36%), whereas space heating has a smaller slice (27.4%). On the other hand, figure 1.7 (b) shows that the average Europe household sector uses 63.4% of its energy consumption in space heating. Apart from the energy share used for lightning, water heating and space cooling, figure 1.7 shows a completely different reality between the household sector in Portugal and in Europe.

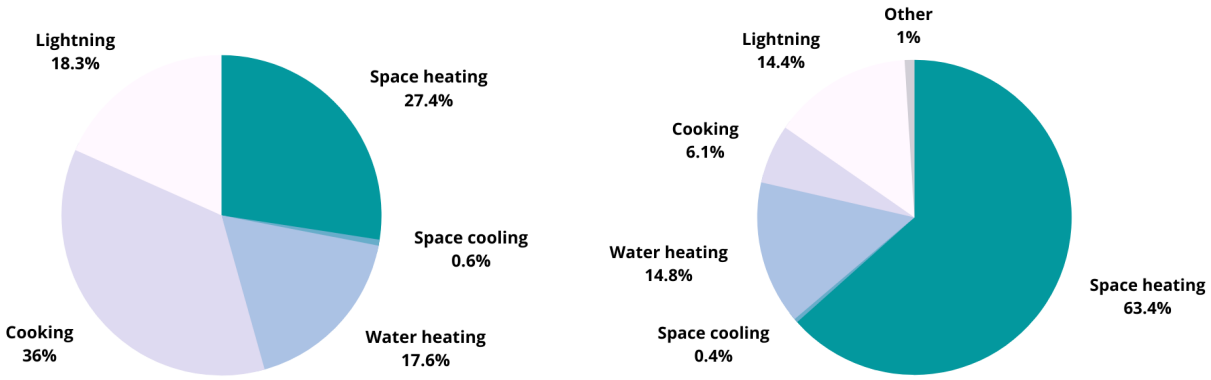

(a) Portugal

(b) Average Europe

Figure 1.7: Household End User Energy Consumption Type 2019 [4]

Nowadays in Portugal the little space heating required can be satisfied by burning wood, which stands as a solid renewable bio fuel. However, Northern and Easter Europe countries rely on furnaces and boilers to space heating, which are fuelled by mainly NG. Thus, most of Europe felt the need to invest in a wide and large gas network (200.000 km of transmission pipelines, over 2 million km of distribution network) in order respond to high household heating demand [30]. Indeed, figure 1.8 (a) and (b) show the household energy sources for Portugal and Europe and, there is a clear difference in the NG slice. While in Portugal, the household consumption relies 9.9% on NG, the European household uses NG to provide for an outstanding 32.1% of its energy consumption. Portugal household fills this large gap by consuming more renewable energy (36.7%) and electricity (39.3%).

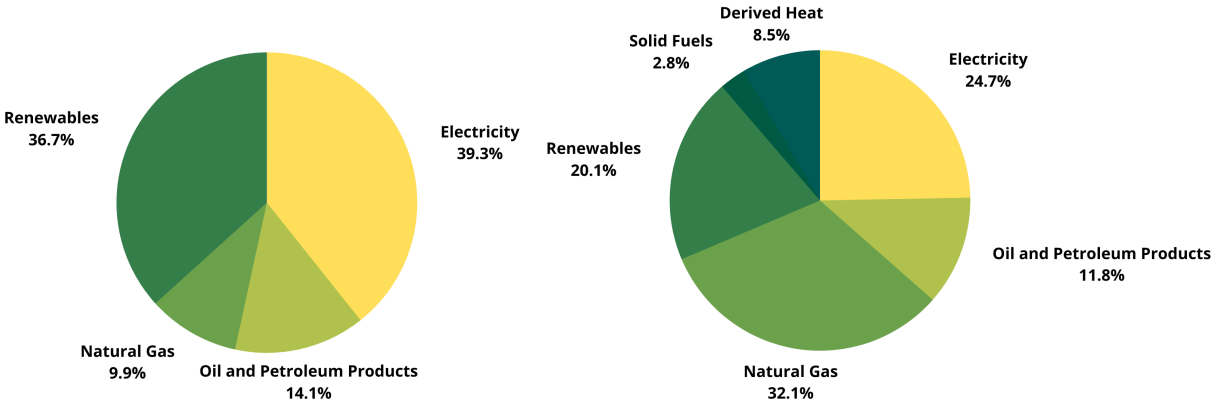

(a) Portugal

(b) Average Europe Union

Figure 1.8: Household Energy Sources in 2020 [4]

Still, it's worth noting that in 2020, Portugal imported a total sum of $5.748.812.000 Nm^3$ of natural gas [31]. Figure 1.9 shows the different countries which in 2020 exported NG for Portugal, either by boat or through pipelines. The port of Sines, which is a small city, plays a fundamental role as up to 90% of the NG importations arrive there by boat.

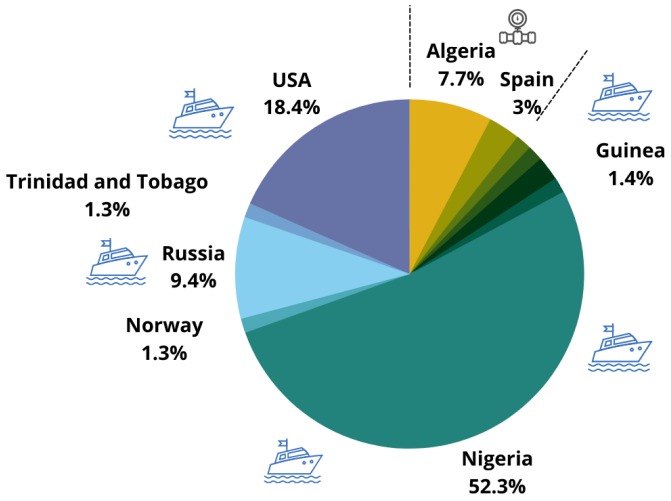

Figure 1.9: Portugal Natural Gas Importation [31]

Actually, the majority of the imported NG, approximately 54%, were used to generate electricity, while only 6% were directly used by residential consumers as fuel to domestic appliances such as ovens, boilers, water heaters and cooktop burners [31]. Still, in Portugal the NG itself as an energy source was responsible for 28% of the CO_2 gas emissions known as the main greenhouse gas [19, 32].

The Paris Agreement [8] signed in 2016, was a landmark to the upcoming environmental and energetic transition. It brought the world together, united to face the climate changes caused by an environmentally careless society. Greenhouse gas emissions, from the use of fossil fuels, have resulted in a higher average world temperature, threatening the health of ecosystems and jeopardising the sustainability of planet Earth. As so, most countries officially pledged to reduce its greenhouse emissions by choosing and investing in energy alternatives that do not require fossil fuels. The aim is to update all the energetic

industry, replacing the fossil fuel power plants by renewable energy sources and achieve zero carbon emissions by 2050. However, while a power plant can produce energy on demand, renewable sources produce energy under certain conditions that are beyond man's control. For instance, the solar panels can only generate energy while there is sunlight, or the wind farms depend on the characteristics of the wind to generate more or less energy. Therefore, the need arises to store energy during periods of overproduction in order to meet the demand during periods of underproduction. To that end, batteries are extremely useful to storage the energy and use it when needed. Yet, batteries have a limited capacity and life span, plus are harmful to the environment. Therefore it requires a proper disposal system to ensure they are eco-friendly recycled. Moreover, the production of batteries implies mining for cobalt and lithium, which requires energy and it's known to not properly consider both the environment and people's health.

In that context, hydrogen can be a very interesting alternative to batteries but also to substitute fossil fuels either in the power generation plants, transports or even in the household domestic appliances. First of all, the hydrogen combustion is free of carbon emissions, thus it doesn't jeopardises the Paris Agreement goals. Secondly, hydrogen ca be stored in pressure tanks to be used when necessary. Even tough, its delivery would require vehicles that, if fueled by fossil fuels would result in greenhouse emissions. Still, like batteries, hydrogen is an option to store energy but there is no disposal system required, as it simply burns harmless to the environment. Finally, hydrogen is able to store up to 3 times the energy stored by natural gas, making it a powerful energy carrier that could be injected into the gas grid. Although, due to its physical and chemical properties, it shortens the durability of existing metal pipelines. Thus, it requires costly modifications to strengthen the gas grid. Hydrogen same as batteries requires energy to be produced. Yet, its production centers could be placed near renewable sources and use its energy excess. As so, hydrogen appears to be a very interesting alternative to batteries for energy storage. Still, it lays on its production costs to realise if hydrogen is a real competitive solution.

Actually, hydrogen can be produced from plenty of resources, such as water, fossil fuels, and biomass through different methods [33–36]. It can be produced by natural gas reforming, either through SMR, POX, or ATR. The steam reforming requires heat input and involves the endothermic conversion of mainly methane. It's the cheapest, though it releases CO_2 emissions. Therefore, the hydrogen produced is usually called grey hydrogen. Nevertheless, if the produced CO_2 is captured and stored underground using a CSS technology then, the hydrogen produced stand as blue hydrogen. In partial oxidation, NG is exposed to not enough O_2 to oxidize completely, thus releasing both H_2 and CO. The auto-thermal reforming goes through the partial oxidation process but then, it is exposed to high temperature steam to product even more H_2. Coal can also be used to produce hydrogen, as by reacting with O_2 and steam under high pressure, it releases CO_2, CO and what is usually called black H_2. The process is called gasification of coal and it's very polluting. In spite of colorless, hydrogen assumes plenty of colors according to its production technique. There is the turquoise hydrogen, which is a thermal process that uses the methane pyrolysis to broken down NG into H_2 and solid carbon. Moreover, there are plenty of water electrolysis processes to produce hydrogen. All operate using an electrolysis cell that contain two electrodes, the cathode negatively charged, and the anode positively charged. It relies on the application

of an electric current that provides the required energy to break the hydrogen and oxygen bond. While the principle remains the same, there are the alkaline electrolyzer and the solid oxide electrolyzer. In figure 1.10, the cathode and the anode are immersed into an electrolyte that contains a high concentration of hydrogen ions, since it was diluted sulfuric acid. When a sufficiently high voltage is applied across the electrodes, the positively charged ions migrate to the ones in the cathode and combine into H_2. In the mean while, water molecules at the anode react to form O_2 while releasing more hydrogen ions into the electrolyte.

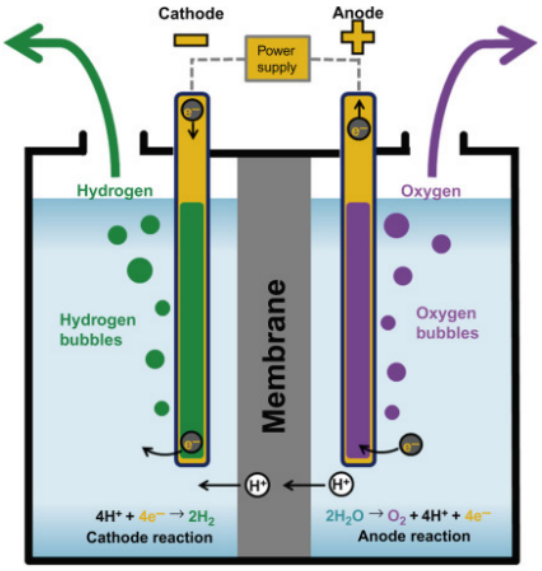

Figure 1.10: Schematic of Electrolysis Process [37]

However, the largest electrolysers produce hydrogen under alkaline solutions [38, 39], like sodium hydroxide ($NaOH$) or potassium hydroxide (KOH) that is added to the water. In this case, water is split at the cathode forming H_2 and driving hydroxide ions across through the diaphragm to the anode, where it is formed O_2. In addition, the water electrolysis results in zero greenhouse emissions and when the hydrogen is produced using electrical energy from renewable sources, it can be called green hydrogen. Worth nothing that high-temperature electrolysis requires less electrical energy to break the bound between the hydrogen and oxygen. Therefore, it is desirable when waste heat from different resources can be used as a heat source for the process. For instance, when the production center can use either solar or geothermal energy. Still, there is the solar thermochemical splitting technique, which uses a high-temperature water splitting technology. The high temperatures, from the concentrated solar power, combined with cerium oxide or copper chloride drive a chemical reaction that splits water. It releases low greenhouse gas emissions and the hydrogen produced is called yellow hydrogen. It must be also mentioned that, it's possible to produce hydrogen from biomass gasification. It's a technique that uses organic or fossil-based carbonaceous materials at high temperatures, that exposed to both O_2 and steam originates mainly H_2, CO_2 and CO. Though CO can go through a water-gas process in which it is exposed to steam and extra heat, forming more H_2 as well as CO_2.

Indeed, there are plenty of techniques to produce H_2 and only a few were mentioned. Nowadays,

electrolysis is about 80% efficient, while steam reforming is 65%. Therefore, green hydrogen obtained through electrolysis has been argued as the solution to achieve a general decarbonisation of all sectors [40–42], as it means producing and storing energy with non greenhouse emissions along all the process [14, 15, 43]. Indeed, Europe is fully committed to invest in the breakthrough hydrogen industry, relying on renewable energy sources. The Europe Green Deal [44] presented in 2019 established production thresholds to be met in the upcoming years. Plus, it's already been identified several regions along all Europe, which are ideal for creating hydrogen hubs [45].

Portugal is on the forefront of such endeavors, and the Portuguese government together with the DGEG ("Direção Geral de Energia e Geologia") designed the "Roteiro e Plano de Ação para o Hidrogénio em Portugal" [46]. This document is a detailed analysis of the Portuguese hydrogen market, but also a step by step program filled with measures to a healthy growing hydrogen production, and to a successful hydrogen distribution to the end user. Moreover, an installation of total electrolysis capacity of $1GW$ is projected in the Portuguese coast city, Sines. It can be energetically feed by all the wind and solar farms in the area, producing up to 465.000 tons of green hydrogen per year. Plus, Sines hydrogen hub can benefit from the already existent seaport of cargo, in order to export the produced green hydrogen. Indeed, a particularly ambitious goal has been set: in 2030, Portugal aims at operating a total $4GW$ electrolysis powered by solar and wind farms installed in the meanwhile. Actually, the $2GW$ solar auctions awarded in the 2019 and 2020 should start any time by now, which will double the installed solar power capacity in Portugal.

While the hydrogen sector is progressing towards economies of scale, the massive transition of natural gas to hydrogen will happen gradually. As hydrogen production increases and adjustments to the pipeline network are being made (so that it's safe to inject higher concentrations of H_2), the hydrogen share injected in the gas grid will increase. It's up to distribution companies such as GALP or REN to cope with the difficulties of providing a proper mix of NG and H_2 to the end users. Moreover, the household sector is relying on the private sector of domestic appliances companies, to update all the cooktop burners such as boilers, water heaters, furnaces. It's fundamental to to ease the transition, without compromising the efficiency of the equipment and ultimately the safety of the end user. At last, unfortunately, the economic factor is key to unlock this new cleaner energy era.

1.3 Economic Impact on the End User

In spite of all the environmental reasons for the upcoming transition, it will only happen if it's economically bearable. As mentioned before, the material costs of implementing hydrogen production have never been lower but still are in a completely misplaced reality. Yet, on the other hand the efficiency of the electrolysis process is increasing as the learning curve progresses [47, 48]. Nevertheless, it has been pointed out that green hydrogen production will only be economically bearable when a significant reduction of material costs happen, combined with a decrease of electricity prices. Fortunately, it is expected that the renewable sources cost decrease will be followed by a decrease in the electric prices, which combined with scale economies of hydrogen production may cut hydrogen costs by 80% [49], figure 1.11.

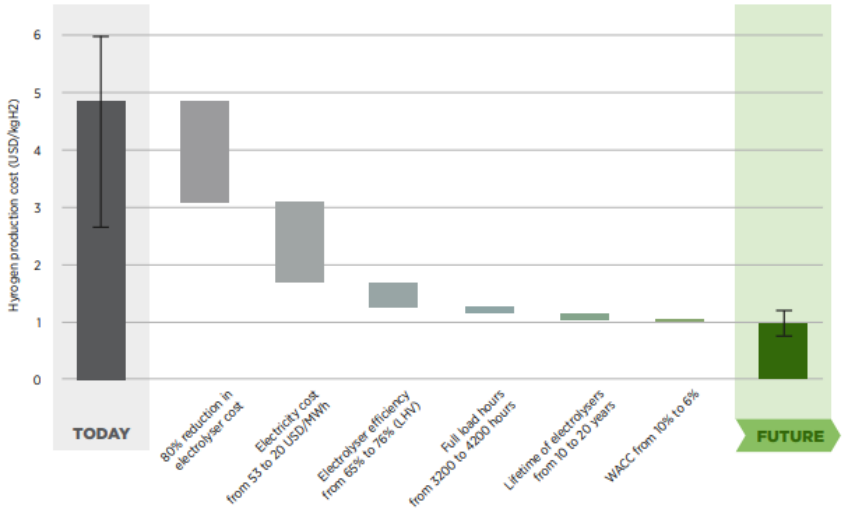

Figure 1.11: Hydrogen Production Costs [49]

Nevertheless, by 2030 the predicted hydrogen production cost will be approximately $2 euros/kg$ which added the predicted costs of storage, transportation, distribution plus taxes will mean approximately $4-8 euros/kg$ to the end user [46], which would be equivalent to approximately $0.12-0.24 euros/kWh$. That range estimation is still wide, and makes it difficult to draw final conclusions about the competitiveness of green hydrogen as a substitute for natural gas in the short term. On the other hand, NG prices for the household sector in Portugal have been constant along the last years, usually suffering $0.005 euros/kWh$ fluctuation around the average price value of $0.09 euros/kWh$, figure 1.12.

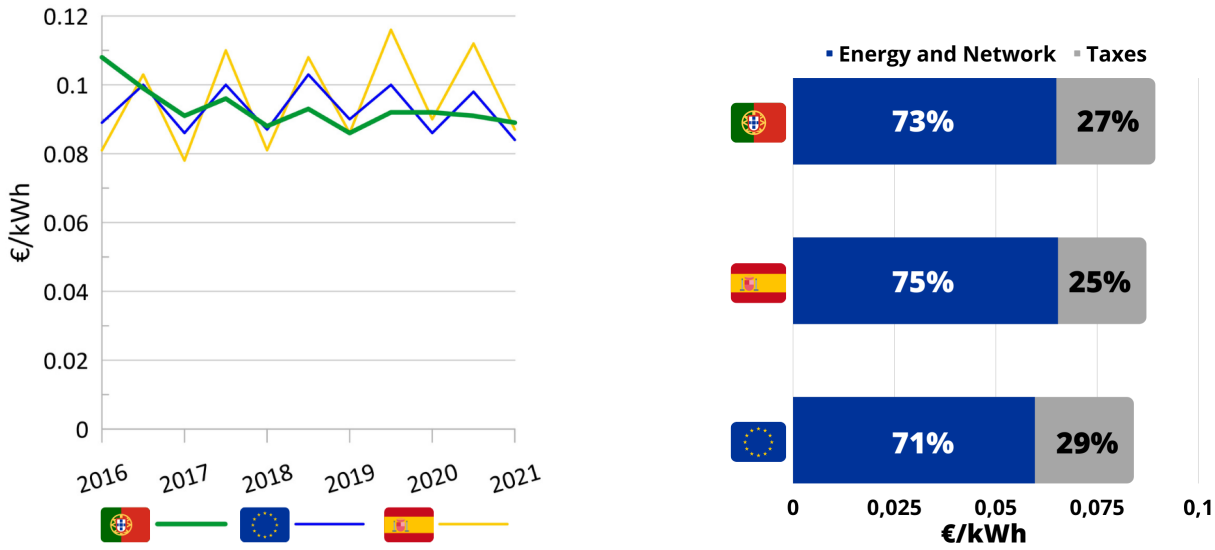

(a) Price Evolution

(b) Price Composition 2021

Figure 1.12: Natural Gas Price [50]

Therefore, in the short term, green hydrogen will most likely be more expensive than natural gas, and only in the most positive scenarios will it be economically competitive. However, as mentioned before, Portugal imports all its NG thus it's dependent on third parties who can influence the market by causing price fluctuations. Fortunately, since 2016 until the end of 2021 no major fluctuations occurred. Yet, by

the end of 2021 and beginning of 2022, the NG prices skyrocketed reaching approximately 5 times the highest value ever reached since the turn of the century, figure 1.13.

Figure 1.13: Europe Natural Gas Market Price (euros/MW) [51]

Although such fluctuation has never been recorded, it will always be a possibility while Portugal relies on NG importation. Moreover, logically, an increase on a commodity price must have repercussions throughout the value chain right up to the end user. Indeed, as long as the NG price doesn't fall close to standard prices, Portugal's government efforts and measures to minimize the NG price fluctuations impact on the final consumer, may eventually not be enough. As so, the competitiveness of green hydrogen, as an economically viable energy source, may well benefit from such unexpected disputes.

Actually, other methods of producing hydrogen were clearly considered cheaper but now are being questioned in favour of green hydrogen production. As a matter of fact, grey hydrogen, produced from fossil fuel by the steam methane reforming (SMR) method which leads to CO_2 emissions, was the most economically attractive process. It was followed by blue hydrogen production, also possible to obtain from SMR or from auto-thermal reforming (ATR), which particularly is a process that uses technologies to capture and storage carbon, thus reducing the CO_2 emissions resulted from its production [52]. As both methods rely on NG or other fossil fuels, since its prices increased then the production costs associated to grey and blue hydrogen also increased:"Green hydrogen cheaper to produce than both blue and grey in Europe" - ICIS report at ending 2021. Yet, there are still plenty of assessments that project real competitive scenarios for green hydrogen, just for the end of the decade [53].

Finally, it does seem that a consensus has been reached that hydrogen, no matter its color, is the center of the energetic transition. Indeed, Portugal aims at providing $NG - H_2$ mixures to the household sector in the upcoming years [46]. Still, the interchangeability of household appliances remains an open question.

1.4 State of the Art

In the last years, hydrogen as a substitute of natural gas have been in the world's agenda. The interchangeability of both gases is achieved when a gas can be substituted by another, without leading to deterioration in the performance of a given appliance. Therefore, gas characteristics plus end user

requirements are the ultimate interchangeability parameters. Table 1.1, clearly states that both gases present different values for a few important parameters.

Table 1.1: Fuel Properties

Property	CH_4	H_2
HHV (MJ/m^3)	39.82	12.75
ρ_r (0°C)	0.716	0.090
W_i (MJ/m^3)	53.45	48.34
L_d (mol/mol)	9.5484	2.3871
L_{dV} (m^3/m^3)	9.5657	2.3845
S_L (cm/s)	36.7	203.9

Moreover, both the H_2 and the NG combustion result in the emission of different combustion products, which are also dependent on the nature of the mixture itself. Combustion mixtures can be classified as lean if the amount of air is higher than the required so that all the fuel burns, or by the opposite, if the fuel doesn't find enough air to burn completely, the reaction is classified as rich. The equivalence ratio, ϕ, is written as the ratio of the actual volumetric flow rates of fuel to air divided by its stoichiometric value: $\phi = (F/A)/(F/A)_{stoich}$. Thus, for a rich mixture $\phi > 1$, while for a lean mixture $\phi < 1$. Still, regardless ϕ, the combustion of pure hydrogen results in zero emissions of CO_2, given by expression 1.1. While the contrary happens with the combustion of NG, given by expression 1.2.

$$\mathrm{H_2} + \frac{0.5}{\phi}\left(\mathrm{O_2} + 3.76\ \mathrm{N_2}\right) \Rightarrow \mathrm{H_2O} + \frac{0.5}{\phi} \times 3.76\ \mathrm{N_2} \tag{1.1}$$

$$\mathrm{CH_4} + \frac{2}{\phi}\left(\mathrm{O_2} + 3.76\ \mathrm{N_2}\right) \Rightarrow \mathrm{CO_2} + 2\mathrm{H_2O} + \frac{2}{\phi} \times 3.76\ \mathrm{N_2} \tag{1.2}$$

Both expressions are given for the stoichiometric reactions, $\phi = 1$, and one can easily realize that the combustion of a $NG - H_2$ mixture will result in less CO_2 emissions as much H_2 is added. Nevertheless, the end user is only concerned about the thermal load delivered by the domestic appliance. Indeed, the thermal input to the appliance is given by multiplying the HHV for the volumetric flow rate of fuel, $TI = HHV \times \dot{V}$. Therefore, according to table 1.1, the heating value of a mixture decreases with hydrogen admixture, requiring a higher volumetric flow of fuel to achieve the same temperature rise. As so, the decrease on the CO_2 emissions is not linear amid H_2 admixture, figure 1.14 (a). For a constant gas supply pressure [54], $\dot{V} \propto 1/\sqrt{\rho_r}$, thus $TI = HHV/ \propto \sqrt{\rho_r}$. In the meanwhile, the Wobbe Index, W_i, stands as an indicator of the interchangeability of a gas. Plus, it is written as the high heating value of a gas divided by the square root of its relative density, $W_i = HHV/\sqrt{\rho_r}$, for a fixed orifice at a fixed pressure [55, 56]. Thus, the Wobbe Index is an interesting parameter to compare the thermal input given by different mixtures, figure 1.14 (b).

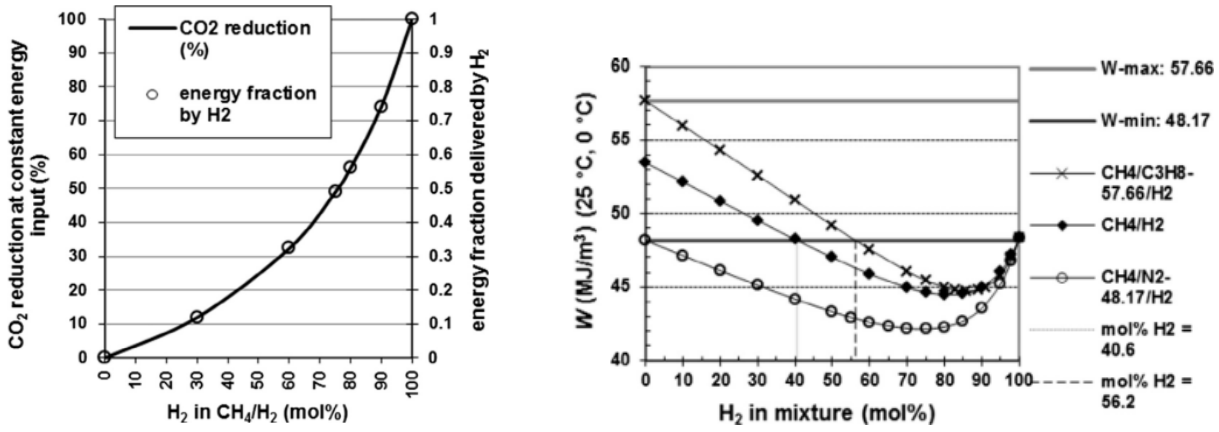

(a) CO_2 Emissions

(b) Wobbe Index

Figure 1.14: Combustion Outputs for Different Fuel Blends [17]

As hydrogen is added to a NG mixture, it decreases the Wobbe Index and increases the so-called burning velocity [57, 58], S_L. Indeed, the burning velocity is deeply connected to the flame's stability issues such as flashback, and it's considered a major safety combustion parameter [54, 59, 60]. Moreover, a significant amount of air is usually mixed to the fuel as it is drawn into the burner head, changing the ϕ value. As mentioned, ϕ stands for the nature of the combustion reaction, thus affecting the S_L as well. Therefore, it's crucial to determine the ϕ variation amid the presence of several amounts of H_2. As a matter of fact, for most of domestic appliances at constant supply pressure, the fuel pressure entering the burner is constant no matter the fuel composition. Under these conditions, in burners that either use a Venturi construction or fans to draw the air into the burner, then the air flow rate will also be constant and independent on the fuel composition [17], so that $\Delta\Phi = \Phi_2 - \Phi_1 = \Phi_1 \times \left[\left\{(L_{dV2}/L_{dV1}) \times \left(\sqrt{\rho_{r_1}}/\sqrt{\rho_{r_2}}\right)\right\} - 1\right]$. Indeed, figure 1.15 (a) shows the ϕ variation for different values of an initial ϕ_1. While figure 1.15 (b) shows its effect on the S_L, for different H_2 blends. As so, the closer ϕ comes to 1, the closer it is to reach the maximum S_L.

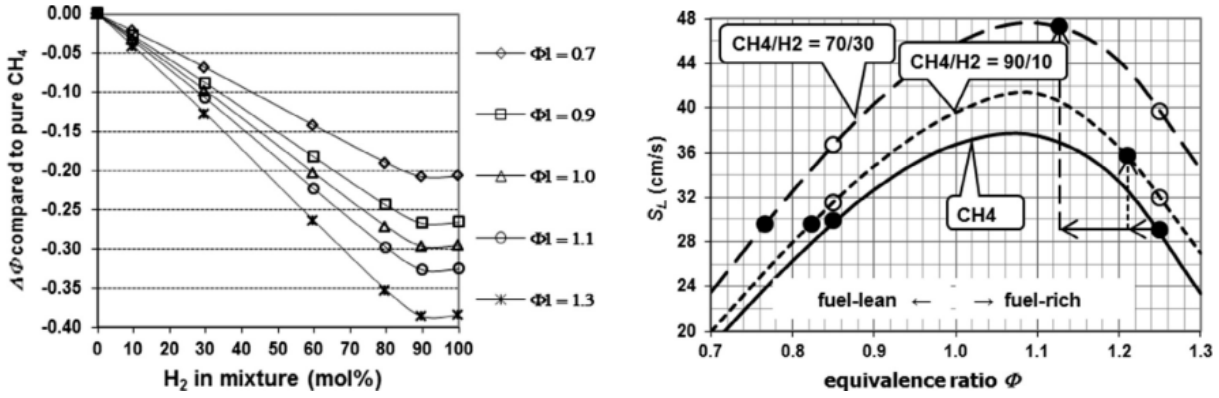

(a) Equivalence Ratio Variation

(b) Burning Velocity Variation

Figure 1.15: Combustion Parameters Variation amid Hydrogen admixture [17]

As mentioned before, there are a few domestic appliances fueled by natural gas that soon will be fueled by a $NG - H_2$ mixture. The literature contemplates the most usual appliances, yet there are not

that many experiments conducted. Moreover, lack of normalised operating conditions lead to divergence into the obtained results.

Oven Burners

First of all, there are two main types of ovens: the conventional ovens and the convection ovens. Both can use gas or electricity as power source, yet the convection ovens have a circulating system that forces the distribution of hot air, usually a fan. In the meanwhile, the conventional ovens use the natural circulation of air. Indeed, it relies on the fact that the density of hot air is lower than the density of the surrounding air. Therefore the hot air rises forcing down the cold air. Clearly, hydrogen will fit in the ovens that rely on the combustion of natural gas, either conventional or convection ovens. In that context, the literature aimed at recent experiments that explore the use of hydrogen, yet this particularly domestic appliance has not been widely explored. Nevertheless, Zhao et al. conducted experiments, which explored the oven's interchangeability [61].

The experiment aimed the oven's overall performance considering its safety and its emissions. Plus, it's to point out that ovens work periodically. The end user sets a target temperature, which sooner or later will be met by the oven. When that happens the flame is extinguished and from that time on the oven will only lose heat to the surrounds, until a minimum temperature is reached. When that happens, the ovens automatically ignites the flames again, until reaching the temperature target by the end user. This cycle occurs until the cooking is finally done and the end user turns off the oven. For this reason, and for the fact that there is non standard method to measure the cooking efficiency, it becomes particularly difficult to determine its cooking efficiency, thus it was not considered in the study.

Now, regarding safety reasons and emissions, one of the studied parameters was the ignition time. Indeed, the ignition time is a pivotal parameter, as it leads to a wider combustion. Plus, the unburnt natural gas emitted isn't beneficial to the environment. Fortunately, the experiment resulted in a decrease of the ignition time by adding hydrogen, since the required ignition energy decreases.

Still, considering safety issues, the stated flashback risk limit was up to 25% addition of hydrogen. Moreover, for 10% of hydrogen, it was noted that the burner temperature increased 63% over the usual operating temperature, which can be an issue regarding the burner's life time. Yet, for higher percentages of hydrogen the burner temperature remained constant.

Regarding the combustion emissions, it was verified that adding hydrogen doesn't change the NO_x emission levels significantly. In addition, it decreased the CO levels, which can be understood as green sign for replacing natural gas for hydrogen. At last, for health reasons, the burner noise was measured and there was no significant increase amid hydrogen addition.

Storage Water Heaters and Boilers

Actually, these appliances are definitely crucial to reduce the greenhouse emissions from the household sector. Indeed, it was already state before that water heater systems are greatly used in plenty of countries along East and North Europe, in order to face the cold winters by providing heat to its homes. Therefore, these appliances have been given more prominence and more works have been developed on the matter.

The following table 1.2 lists a few articles, and resumes the author's, the scope of the work and the main outcomes. The the entries are ordered by the year in which they were published, from most recent to oldest. At last, it remains to point out, the studies suggested that these appliances performance should remain unaffected until up to $10\% - 20\%$ of H_2 admixture, and little or no adjustments are needed.

Table 1.2: Studies of Storage Water Heaters and Boilers Performance

Author	Year	Scope	Results and Conclusions
Hinrichs et al. [62]	2021	Condensing boiler formation of nitric oxide in methane mixed flames	- the flames burning velocity increased by adding hydrogen while the emissions of NO_x sightly decreased; - the flames burning velocity decreased by adding propane, while the emissions of NO_x increased.
Schiro et al. [63]	2020	Eventual adjustments in boilers due to H_2 enriched NG	- the flow of hydrogen is 3.3 times than with pure methane in order to maintain the same thermal load, thus the gas valve must be adjusted; - the condensable water flow increases up to 70% for pure hydrogen, thus the condensate discharge system must be re-dimensioned; - the performance can be ensured with non modifications until up to 20% added hydrogen.
Choudhury et al. [64]	2020	Performance of water heaters H_2 enriched NG	- the performance remains ensured until up to 10% addition of hydrogen; - for low-NO_x heaters, the NO_x emissions further decrease by adding hydrogen; - for conventional water heaters, the NO_x emissions slightly increase by adding hydrogen.
Lo Basso et al. [65]	2017	Boiler's efficiency due to H_2 enriched NG	- the water mass content in air decreases by adding hydrogen; - the condensable water mass decreases as hydrogen increases; - the condensation efficiency increases by adding hydrogen.

Cooktop Burners

This appliance is the one that has delivered the most promising results. Plus, it is the one most explored in the literature, in which multiple parameters have been studied. It's worth nothing that the entries in the following table 1.3 are ordered from most relevant to least relevant, for the current thesis. Again, the table resumes the scope of each work as well as its outcome. Moreover, the assessment conducted by Zhao et al. was given special attention, as it was the most complete. Besides, the conducted experiment was the most similar compared to the one developed in the next chapters.

Table 1.3: Studies of Cooktop Burners Performance

Author	Year	Scope	Results and Conclusions
Zhao et al. [66]	2019	Cooking performance amid $CH_4 - H_2$ mixtures	- shorten ignition time; - flashback limit of 50% of hydrogen; - no significant difference in efficiency and cooking time up to 50% hydrogen; - combustion noise increases; - reduction of pollutant emissions by adding hydrogen.
Karunanithi and Shafer [67]	2016	Efficiency of different cooking methods	- efficiency from 10% up to 40%, according to the pan, under the same operating conditions fueled by natural gas.
Wichangarm et al [68]	2020	Cooking efficiency	- efficiency between 40% and 50% fueled by natural gas; - flow velocity spectrum.
Gimeno-Escobedo et al [69]	2019	Prediction methane hydrogen flames method	- ignition time decreases as hydrogen is added; - flame velocity increases by adding hydrogen and maximum velocity for equivalence ratio of 1.1.
Zhao et al. [70]	2018	Cooking performance $CH_4 - CO_2$ fuel mixtures	- efficiency remains around 32%; - more than 10% addition resulted in shorter flames; - up to 30% addition yields blow off; - it fails to ignite for up to 20% of added CO_2; - cooking time increases by adding CO_2.

Indeed, Zhao et al.[66] work was extremely important for the current study, since it illuminated the initial path adopted to assess the performance of a domestic cooktop burner, fueled by a $H_2 - NG$ mixture.

The present study also focused on parameters such as the flashback risk, burner noise and cooking efficiency. The cooking efficiency was also studied by the process of using a cooktop burner to heat up a pan filled with water, at room temperature until it reaches an uniform boiling state. Actually, in order to ensure that an uniform boiling state had been reached, the use of thermocouples has proved very useful. Plus, a digital weight scale was used to determine the water mass evaporated in the process, so that the internal energy balance of the water could be calculated. Similarly to Zhao et al.[66] study, the flashback risk stands for identifying operational conditions that lead to unstable combustion at the brink of flashback, and consequent extinction of the flame itself. That particularly experiments, relied on the sensitivity and power of observation to detect changes in the stability, colour and size of the flames, as well as in the noise intensity caused by its combustion. Thus, those experiments were combined with burning noise measuring amid hydrogen admixture. The experiments were conducted through out 3 different sized burners, so that its impact on the parameters above could be explored. In addition, the cooktop

burner structure was adjusted, in order to inject different $NG-H_2$ mixtures and impose a certain power, even beyond the possibilities given by the cooktop itself.

Nevertheless, for the current study, two different approaches were explored in order to achieve the cooking efficiency. The first was already mentioned, and its purpose is clear. However, the second aims at fully understanding the heat transfer process between the flames and the pan. To that end, PIV experiments were conducted. PIV technology is a powerful tool to determine the flow velocity, which has a major importance when calculating heat convection coefficients. The second approach allows developing a deeper sensitivity for the relationship between the variables of the energy transfer process, and the operational conditions affecting the cooking efficiency.

Actually, the following section approaches the added value of the present study, compared to what has already been developed in the cooktop burner performance and interchangeability.

1.5 Objectives

The aim of the study is to assess the interchangeability of domestic cookers, fuelled by $NG-H_2$ mixtures, in the face of the upcoming energy transition. Therefore, parameters such as cooking efficiency, flashback risk and burning noise were considered the back bone of the work. Therefore, different experiments aiming at each parameter were conducted. Still, the study explores the impact of several operating conditions on the parameters mentioned, by conducting the experiments through different combinations of burner's diameter and power, water quantity and hydrogen admixture.

The current study also target the advantages and drawbacks of slow cooking versus fast cooking. Therefore, the cooking efficiency results were remarkably valuable to assess the financial impact of this cooking techniques on the end user costs.

Finally, the work aims at extrapolating the results. Therefore, it focused on developing a mathematical function able to use operating conditions to predict the cooking efficiency. So that, the end user can be aware of the best combination between its operating options, to easily choose the most sustainable cooking technique.

1.6 Outline

The master thesis is structured in five chapters. At first, chapter 1 presents some of nowadays environmental concerns, due to the energy use. Then, Portugal and Europe role on the energetic transition is approached. In addition, it is presented a review on previous works over the domestic appliances interchangeability, and finally, it is approached the scope of the current work.

Chapter 2 details the experimental steps and the equipment used for each experiment. Plus, data treatment methods are explained and uncertainties regarding the used equipment are estimated.

In chapter 3 the two different methods to determine the cooking efficiency are duly explained and the fundamentals of the mathematical model developed are approached.

Then, in chapter 4 the results of both flashback and burner noise experiments are addressed. The

cooking efficiency obtained for both methods is compared, focusing on the impact of different operating conditions. In addition, the slow cooking versus fast cooking impact on the end user financial costs is compared. At last, the advantages and limitations of a few changes to the mathematical prediction function are explored.

Finally, the fifth and last chapter summarizes important insights from the work developed, and a few guidelines for future work are suggested.

Chapter 2

Experimental Set Up

2.1 Procedure

In the present work, 4 different experiments conducted: heating water experiments; PIV experiments; flashback and sound experiments. The first 2 experiments, were conducted in order to estimate the cooking efficiency. The flashback experiments addressed the flame stability. Whereas, the sound experiments measured the sound intensity of the flames.

2.1.1 Heating Experiments

The main goal of this experiments, consisted in heating the water inside the pan using the power provided from the cooktop burner. However, different operating options were explored, in order to simulate different cooking behaviours of the end user. Table 2.1 details the experimental conditions applied for the heating water experiments.

Table 2.1: Heating Water Experiments

Experiment	Burner	Power(W)	Water(L)	Hydrogen(%)
1	B10;B07;B05	1500	0.5;1.0	0;0.05;0.10;0.25;0.50
2	B10	3000	0.5;1.0	0;0.05;0.10;0.25;0.50
3	B07	2300	0.5;1.0	0;0.05;0.10;0.25;0.50
4	B05	750;2100	0.5;1.0	0;0.05;0.10;0.25;0.50

The variables that changed along the experiments were the burners used (which were 3), the quantity of water inside the pan, the percentages of hydrogen in the fuel mixture, and the power provided by each burner. All the experiments started by carefully pouring the amount of water into the pan, then it was placed on an electronic balance and its weight was noted. Only then, was the pan properly placed above the burner. After that, the gas valve was opened, allowing the flames to ignite, so that the heating process could start. In that context, figure 2.1 shows that an external connection to the burner had to

be me made, so that flow meters could control the hydrogen admixing, while imposing a certain power.

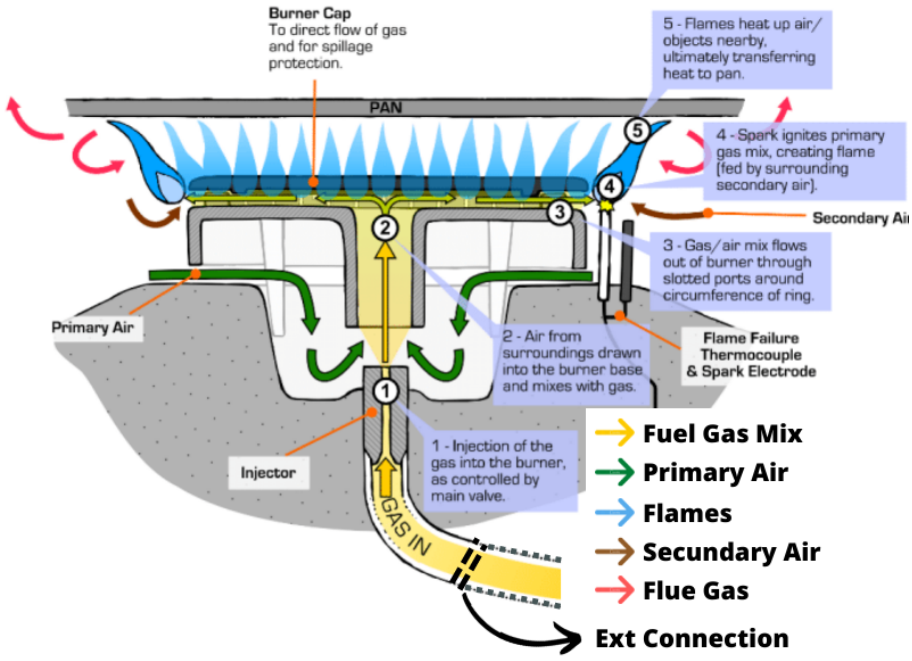

Figure 2.1: Burner Scheme adapted from [71]

Indeed, the hydrogen and the methane volumetric flow, to achieve a certain power and a certain blend, were determined by expression 2.1. The expression uses both the power and hydrogen fraction as input and delivers the total volumetric flow. From then, it's possible to obtain each gas volumetric flow by multiplying its fraction in the mixture by the the total volumetric flow. Therefore, one is allowed to change the percentages of hydrogen in the mixture without changing the power provided, for instance. All in all, one sets the desired power and percentage of hydrogen and obtain the corresponding flow that should be imposed in the flow meters.

$$V_T = \frac{P}{LHV_{H_2}\,\rho_{H_2}\,f \;+\; (1-f)\,LHV_{CH_4}\,\rho_{CH_4}} \tag{2.1}$$

Before the flames ignite and the water inside the pan starts to heat up, a thermocouple was dipped in the water and another was placed near the pan walls. Both thermocouples are connected to an acquisition board, which is a device controlled by the QuickDAQ program, that reads and translates the differential voltage into a temperature evolution. Thus, one thermocouple was recording the temperature of the flow followed by the flame, while the other was recording the temperature of the water inside the pan. When the program displays water temperature extremely close to 100°C, and the water achieves an uniform boiling state, the flow meters are closed so that the flame extinguishes. Then swiftly, the pan is put back on the electric balance and the new weight value is registered. The difference between the values registered before and after the heating process, represents the mass of water evaporated. Figure 2.2 shows a scheme of the procedure. The left pan portrays the beginning of the experiments, and the right pan portrays the end of the experiments.

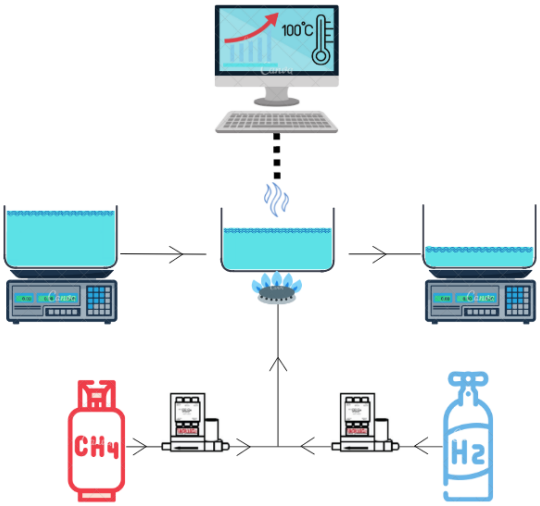

Figure 2.2: Heating Experiment Scheme

The data, such as the water temperature evolution, experiment time, mass of water evaporated and burner power, was acquired. It's essential data to obtain the cooking efficiency, as it's explained in chapter 3.

2.1.2 Flashback Experiments

The experiments to estimate the flashback risk, were carried out both with the pan on top of the burner and without, to each burner the same way. First, the methane flow meter was opened providing the designed power for each burner. For burner $B10$ it was $3000W$, for $B07$ it was $1500W$ and for $B05$ the power was $750W$. Then, gradually, the hydrogen in the mixture was increased by a 5% step, while maintaining the same power. In the process, differences in the flame's color, size and behaviour were captured by the camera. At last, the hydrogen percentage from which flashback is extremely likely to occur was noted, and sometimes flashback was even captured.

2.1.3 Sound Intensity Experiments

The sound intensity measuring was performed by placing the microphone at a $12cm$ radial distance from the burner center. The experiments were conducted under the designed power provided for each burner, amid a 5% step increase of hydrogen percentage in the mixture. The flashback conditions, mentioned before, were considered for this experiments, using the pan on top of the burner.

2.1.4 PIV Experiments

The PIV technology requires several components to study the flow behaviour: a computer, a synchronizer, a power unit and a camera. Still, the experiments required the components that provide the combustion. Besides the cooktop burner and the pan, the experiments used a system of plastic tubes to drive methane and hydrogen flow from the compressed cylinders into the burner. The system of plastic tubes, passed through the flow meters so that the flow rate could be controlled and adjusted. In addition, after passing

the flow meters, the flow passes by a container filled with aluminium oxide particles, and only then it reaches the burners. In fact, the aluminium oxide is introduced in the flow so that the PIV technology can capture the flow behaviour. Apart from the aluminium oxide, all of the PIV components were controlled by the laboratory computer. Indeed, figure 2.3 shows a scheme of the connection between the components towards its target, the flow around the pan. While the combustion components are on the left side, the most of the acquisition components are on the right side. Yet, the aluminium oxide is placed on the left side. In particular, after the flow meters and before the burners, so that no material would be endangered.

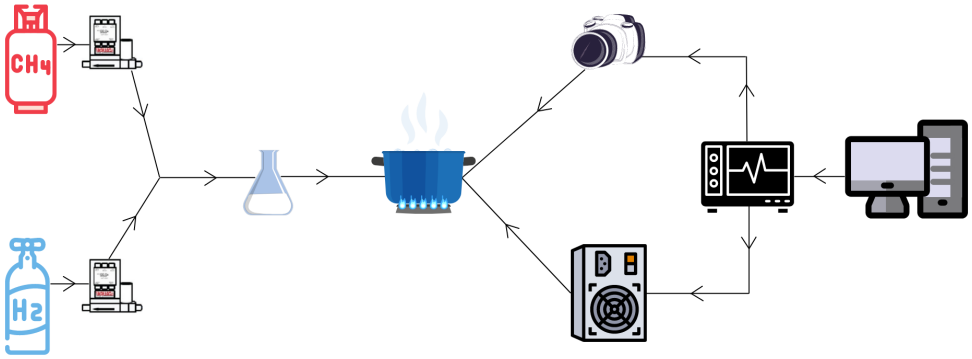

Figure 2.3: PIV Experiments Scheme

The PIV experiments consisted in obtaining the flow velocity field and its magnitudes around the pan. To that end, the PIV system requires a 90 degree angle between the camera and the laser, according to the position of the aimed flow field. For that reason, and due to laboratory technical restrictions, there were only one possible position between the Acquisition system and the Combustion components. As consequence, not all burners could be selected to the PIV experiments. Indeed, only burner A was available to conduct the experiments as it is in figure 2.4.

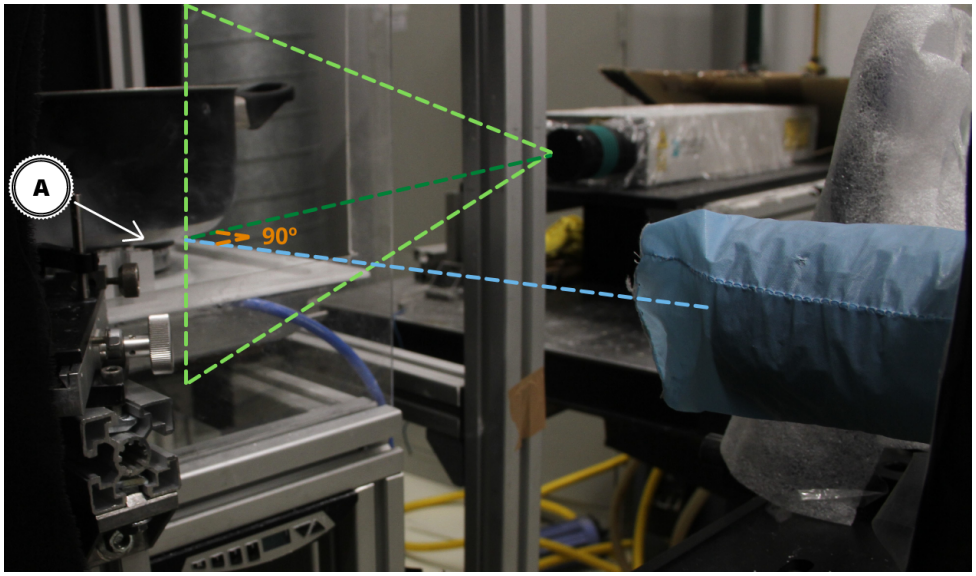

Figure 2.4: PIV Main Components Positions

The pan was supported by three aluminium blocks instead of the usual grid, so that it was possible

obtain velocity results for the flow near the bottom of the pan. However, the supporters resulted in extra positioning restrictions, since both the camera and the laser beam require an unblocked/unspoiled shoot window. Still, that must be achieved without compromising the pan stability. Consequently, it was found non possible positioning that provides the flow velocity field for the all region at once. Instead, it were used two different sets of positioning that allowed to study all the region, by separating it into two different regions, each appointed for each positioning set. For once, a positioning set allowed a clear image of the flow between the burner head and the bottom of the pan, figure 2.5(a). Whereas, the other positioning set provided a clear image of the flow alongside the pan surface, from the burner holes to the pan handle, figure 2.5(b).

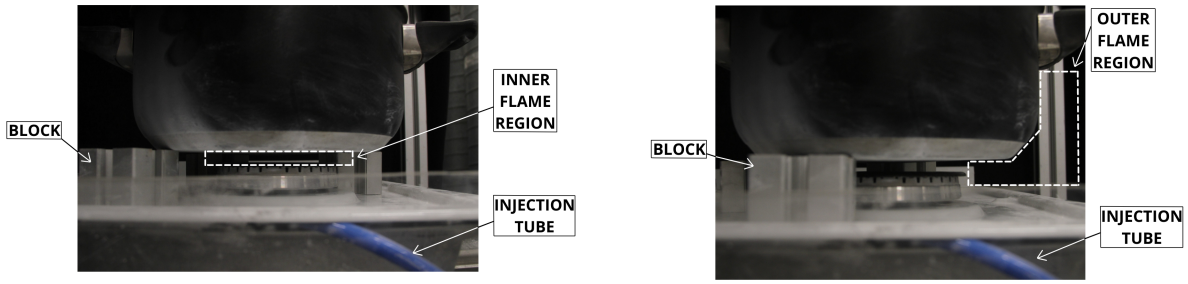

(a) Positioning Set 1

(b) Positioning Set 2

Figure 2.5: PIV Regions

Nevertheless, it turned out to be quite a minor drawback. The PIV acquisition settings provide the user with a wide range of values for two parameters, the trigger rate and the time between pulses. The trigger rate is the frequency at which the pair of laser pulses is shot, while the time between pulses is the time between the laser 1 and the laser 2. It is crucial to determine and respect the minimum acceptable value for the last parameter otherwise the obtained results would be adulterated. Indeed, the time between pulses depends on the flow velocity, the interrogation area, the overlap of the interrogation area, and on the resolution of the acquired images. Therefore, if one expects velocities with considerably different magnitudes according to a region/zone, then logically a time lapse fitted for each region should be consider. As a matter of fact, in the region between the burner top and the pan bottom or inner flame region, the expected magnitude velocity is significantly lower than the expected magnitude velocity for the outer flame region. After all, the separation of the flow region in two different regions, due to forced positioning restrictions, ended up being favorable for the expected accuracy of the results. Moreover, besides the two different regions considered, the experiment also contemplated different operating conditions dependent on the power of the burner and the proportion of blended methane-hydrogen mixture, which is duly detailed in table 2.2.

Although the experimental conditions are defined, one has to be aware of the steps to follow in order to control the acquisition system. It is important to turn on the equipment by a specific order: 1) the laser power unit; 2) the camera; 3) the synchronizer; 4) then Dynamic Studious program can be started on the laboratory computer, otherwise the program will not successfully recognize all the components. Afterwards, one can use the remote control to turn on both the pump and the laser. The system should

Table 2.2: PIV Experimental Conditions

Region	Power(W)	Hydrogen(%)	Trigger Rate(Hz)	Time between Pulses(us)
Inner Flame	1500; 3000	0; 40	15	10000; 5000
Outer Flame	1500; 3000	0; 40	15	500; 300

be fully operational and ready, though it still remains to set a scale for the acquired data. Indeed, it can be achieved be acquiring a photography of the survey area with a millimetre scale paper positioned near the scope region, placed sideways to the laser beam and facing the camera. This step, is also extremely useful to focus the camera's image as much as possible, by adjusting the lens opening as well as the zoom.

Finally, reflections may seriously damage the results. Therefore, the experiments were conducted with the minimum luminosity at the laboratory, and the experimental platform was covered with layers of black fabric as much as possible. Additionally, it was used a lens ($\lambda = 532nm$) to filter the flame's luminosity.

2.2 Components Detailed Information

The experimental set up is constituted by several components. First of all, it was based on an aluminium platform made from smaller parts connected through joints. The platform provided a great deal of flexibility and possibilities to arrange every component. Apart from the platform, the set up is constituted by several components that can be found in figures 2.6, 2.7 and 2.8.

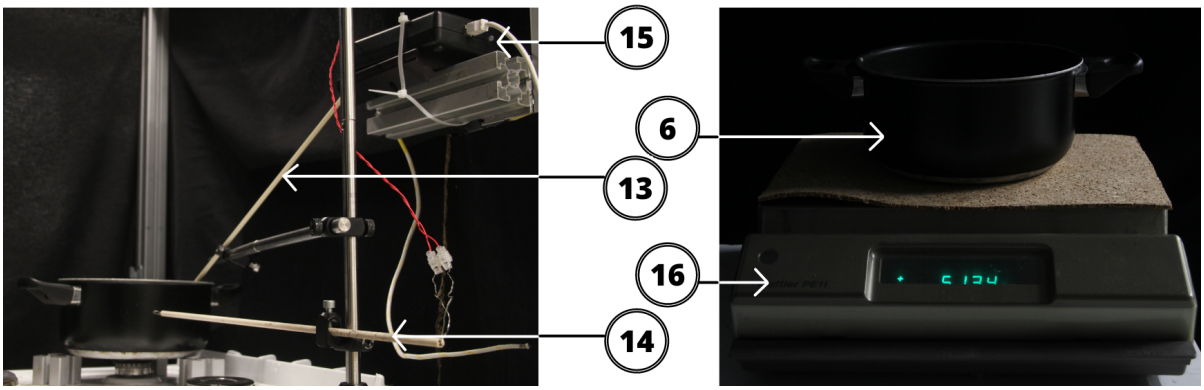

Figure 2.6: Thermocouples, Acquisition Board and Electronic Balance

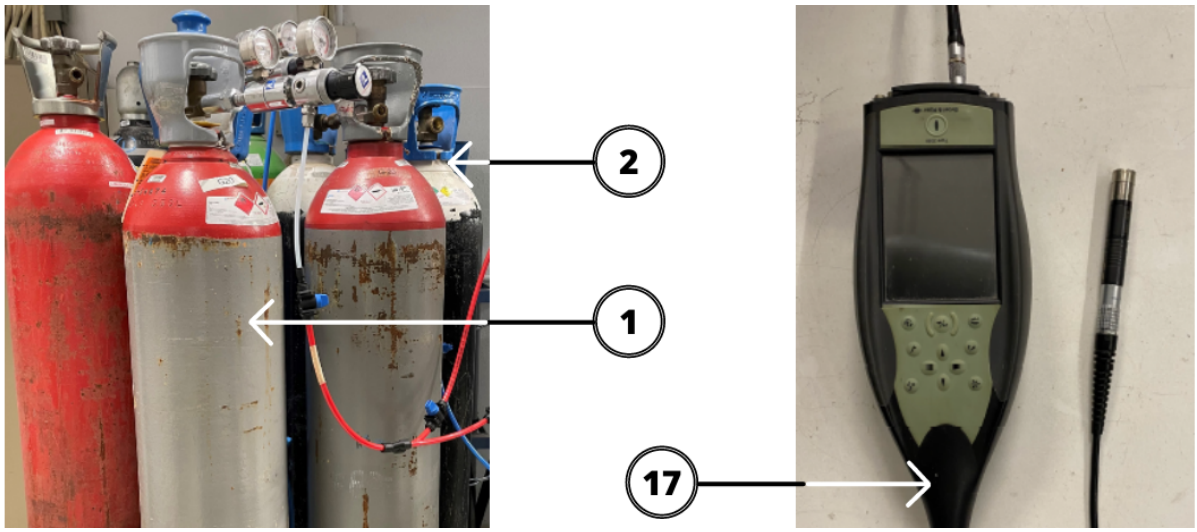

Figure 2.7: Gas Cylinders and Microphone

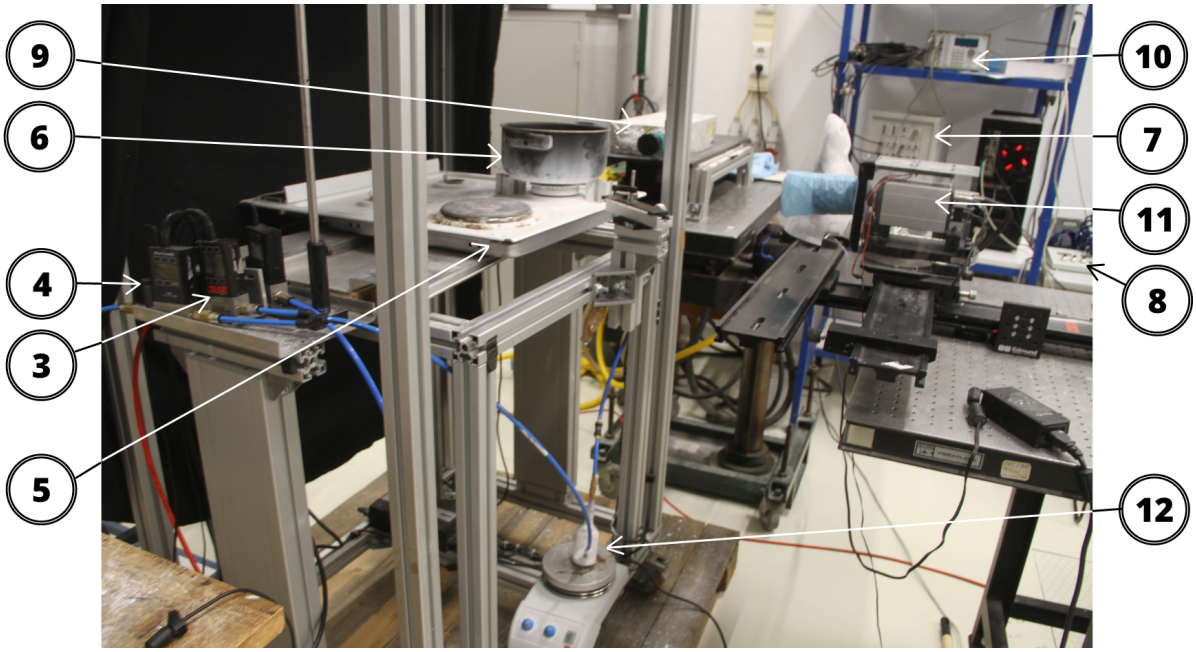

Figure 2.8: Main Experimental Set Up

The numbers inside the circles of figures 2.6, 2.7 and 2.8, correspond to the components listed in table 2.3. The components are divided in 2 different groups, Combustion and Data Acquisition. The Combustion group displays the required components so that the fuel gas is injected to the cooktop, burning when in the burner head. Whereas, the Data Acquisition group displays the components used to record useful data to the current study. In addition, the table lists a brief description of the function/objective of each component. Still, detailed information regarding each component is given in the sub sections 2.2.1 and 2.2.2.

Table 2.3: Experimental Components

Components			
Group	Number	Name	Objective
Combustion	1	Methane Cylinder	Storage compressed methane
	2	Hydrogen Cylinder	Storage compressed hydrogen
	3	Alicat Flow Meter	Control methane flow rate
	4	Alicat Flow Meter	Control hydrogen flow rate
	5	TEKA Cooktop	Provide combustion platform
	6	Pan or Pot	Storage water
Data Acquisition	7	Power and Cooler Unit	Laser control
	8	Remote Controller	Facilitate end user controls
	9	Laser	Highlight flow particles
	10	BNC Synchronizer	Control the timing
	11	ANDOR Camera	Capture particle's positions
	12	Aluminium Oxide Powder	Track the flow
	13	Inside thermocouple	Measure water temperature
	14	Outside thermocouple	Measure outside flow temperature
	15	Acquisition Board	Detect electric voltage
	16	Electronic Balance	Measure water mass inside the pan
	17	Microphone	Measure sound intensity

2.2.1 Combustion Group

As indicated before, the components of the combustion group play a crucial role providing the combustion of different fuel blends.

Cooktop Burner

The Teka model E/60.3 3G 1P AL is a self aerated stove. It is designed so that, a significant part of the air necessary to the combustion is pulled by the gas jet. Thus, an amount of air is mixed with the fuel gas before the burner port. Plus, it is designed to deliver the fuel gases into three different burners. The injectors of the burners have different dimensions, according to the dimension of each burner. However, for the scope of the study, the burners present different head diameters and number of exit holes. Also, the burners are designed to provide different powers. Table 2.4 resumes the burners features and figure

2.9 shows the cooktop.

Table 2.4: Cooktop Burners

Burner	Diameter(cm)	Holes	Power(máxW)
B10	10	28	3000
B07	7	21	1750
B05	5	18	1000

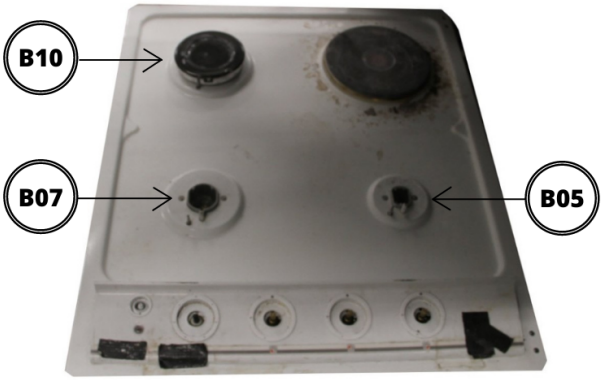

Figure 2.9: TEKA E/60.3 3G 1P AL

Pan

The pan's materials are mostly aluminium, coated with a non-stick black external layer. Yet, it has a ferritic stainless steel disk at the base so that the pan can be used for induction heat transfer as well. Approximately, the pan is $12cm$ high, it has a base diameter of $16cm$ and a top diameter of $18cm$, plus it weighs $513.5grams$. Moreover, based on its materials, the pan's estimated thermal conductivity and specific heat are $220W/mK$ and $900J/KgK$, respectively.

Gas Properties

As mentioned before, the present work is focused on two main gases, Natural Gas and Hydrogen. NG is formed deep beneath the Earth's surface and its main component is methane. It is also constituted by smaller amounts of hydrocarbon gas liquids and non hydrocarbon gases. As an example, GALP PORTUGAL commercialises NG with up to 90% of methane in a molar basis, while the remaining 10% are distributed along several derived hydrocarbons.

As a consequence, it was considered that there are no major implications for the scope of the study if one consider only methane as a representative for NG. Therefore, the experiments were performed using only methane, instead of NG. Both the purchased methane and hydrogen were delivered by AirLiquide. The delivery ensures that methane has a guaranteed purity level of 99.995%, and hydrogen has a guaranteed purity level of 99.999%.

Flow Meters

The Alicat flow meters allowed to impose different quantities and fractions of mixtures into the stove. One flow meter controls the amount of methane, while the other controls the amount of hydrogen. The flow meters operate on the basis of controlling the pressure difference between its inlet and outlet, according to the demand imposed by the user. However, the flow meters have a different range of capacity: 0-0.5 SLPM; 0-1 SLPM; 0-5 SLPM; 0-20 SLPM(Standart Liters per Minute). In addition, it is important to select the controller that operates at the closer range of the demanded gas in order to increase the accuracy of the controller itself. Yet, it is pivotal to respect those range of capacities, in order to avoid overheating and therefore damaging the flow meters. Therefore, to each gas was designated a flow meter according to the volumetric flow required for each mixture, which is detailed in the section 2.4.

2.2.2 Acquisition Group

As mentioned before, the acquisition group is constituted by plenty of components, though not necessarily linked with each other. As a matter of fact, some components don't even belong to the same experiments. While the components $7-12$ belong to the PIV experiments, the components $13-16$ belong to the Water Heating experiments, and finally the component 17 belongs the Sound experiments.

Power Unit, Laser and Remote Control

The PIV system is mainly constituted by a power supply unit, a laser and a remote control, all of them from the DANTEC DYNAMICS. The power unit, model LPU450 with a $450W$ capacitor charger, also contains an inbuilt water to air heat exchanger that works as a cooler. The laser head is the ultimate feature of the laser system, which produces infrared laser light at $1064nm$. The camera cannot detect near infrared light, thus the laser light is converted to visible green light at $532nm$ by a harmonic generator. Finally, the laser functionality can be manually controlled using the remote control. It provides the user with classic options such as start/stop, pump's on/off, shutter open/close, plus laser intensity. Indeed, the laser can increase up to a $15Hz$ repetition rate and $65mJ$ per pulse, which converts it into an intense light for the human eye. Thus, being advisable to operate the equipment using the eye protection goggles.

Camera and Synchronizer

The ANDOR camera, model Zyla 5.5 sCMOS, captures 5.5 million pixels per image with a pixel size of $6.5\mu m$, due to its $22mm$ diagonal sensor. The particles are captured in a black and white image, yet it is extremely important to keep the camera way from direct laser light exposure or even intense reflections. Moreover, the camera shooting rate is controlled by the synchronizer BNC Model 575. It has an accuracy of $1ns$ and a delay resolution of $250ps$, which makes it a great precision timing device.

Thermocouples and Acquisition Board

The thermocouples were type R, embedded in a ceramic tube in order to not only prevent the wires from touching each other but also to prevent them from losing their shape. The DT9828 acquisition board

was from Data Translation, and provided readings with an overall accuracy better than $0.1K$.

Electronic Balance and Microphone

It was used an electronic balance to measure the water mass inside the pan, the Mettler PE11 which supports up to $11kg$. It has a readability of $0.1g$ and stabilization time of approximately $2.5sec$. Plus, a $0.1g$ maximum deviation is guaranteed under standard operating conditions. The microphone was the 4185 type, from Bruel Kjaer. It can measure sound intensity from $10db$ up to $150db$, plus it ensures a maximum sound distortion of 0.01%. At last, the microphone was placed at a radial distance of $12cm$ from the burner center.

2.3 Data Treatment

Regarding the temperature evolution inside or outside the pan, the system relied on two thermocouples connected to the acquisition board. The temperature evolution was obtained with delay when compared to real time process, which leads to further data corrections. Moreover, the PIV experiments rely on a few data processing steps, so that the images captured can be translated into useful information.

2.3.1 Temperature Correction

While the fluid is in direct contact with the tip of the thermocouples, the temperature at the tip increases as the water temperature increases. Still, the acquisition board only detects the increase in the differential voltage. The QuickDAQ program reads the differential voltage and translates it into temperature. Thus, the program is actually giving the thermocouple tip temperature and not the water temperature. Yet, if the heat transfer process from the water to the thermocouple tip were instantaneous, the temperature read between both would be the same and the program would be giving the water temperature. Therefore, in order to obtain the real temperature evolution of the fluid, one must know how much time is needed to the thermocouple meet the temperature of the fluid. That delay or time constant, can be obtained trough an energy balance at the tip of the thermocouple, which is given by the expression 2.2.

$$\frac{dU}{dt} = \dot{Q}_{conv} + \dot{Q}_{cond} + \dot{Q}_{rad} \tag{2.2}$$

Yet, assuming that the heat transfer through conduction and radiation is an extremely small percentage of the heat transfer due to convection, than these can be neglected. Therefore, expression 2.2 can be elaborated further into expression 2.3, by only considering heat transfer through convection.

$$\rho c V \frac{dT_b}{dt} = A\,h\,(T_f - T_b) \tag{2.3}$$

It is known that $\frac{\rho c V}{A\,h} = \tau$, as being the time constant or time delay. Thus, τ can be introduced into the expression above. Therefore, by following the steps in expression 2.4, it becomes possible to obtain according to the temperature difference between the fluid and the tip, divided by the tip temperature evolution over time. Therefore, to obtain tau one needs to have all these three parameters.

$$\frac{dT_b}{dt}\tau = (T_f - T_b) \Leftrightarrow \tau = \frac{(T_f - T_b)}{\frac{dT_b}{dt}} \tag{2.4}$$

Actually, the water boiling temperature at atmospheric pressure is 100°C. Thus, by heating the water inside the pan until it reaches a boiling state, and then quickly diving the thermocouple in the water, the program was supposed to immediately read a 100°C. Instead, the program showed the temperature evolution in time and it took a while to reach the 100°C, which provides the user with the three parameters needed to obtain τ. Yet, that experiment is vulnerable to human errors. Therefore, in order to reduce that margin and obtain the most accurate value for τ, 10 experiments were conducted for each thermocouple, resulting in the values presented in figure 2.10 (a).

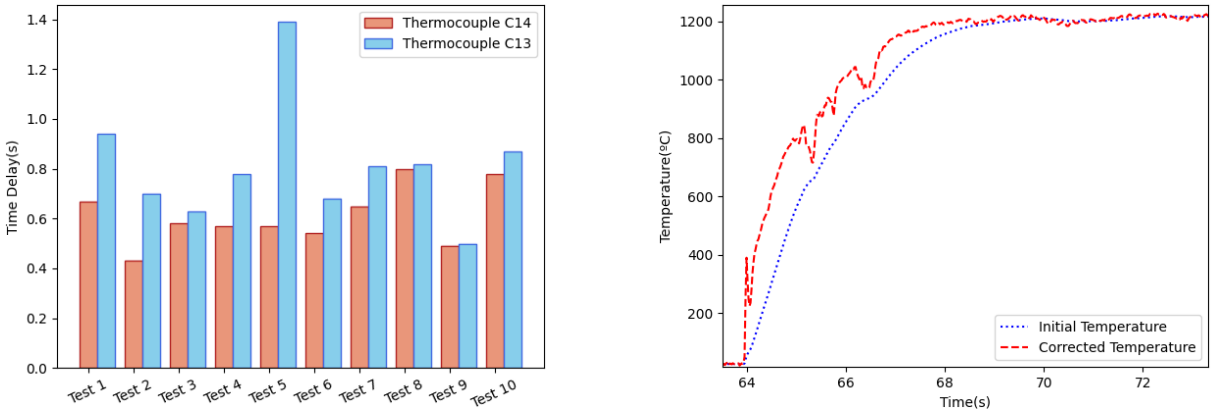

(a) Obtained τ Values

(b) τ Effect on Temperature Evolution

Figure 2.10: Temperature Correction

From the values obtained, an average τ was assumed for each thermocouple. For component 13, the thermocouple inside the water, $\tau = 0.73818$. While for component 14, the thermocouple outside, $\tau = 0.55273$. Figure 2.10 (b) shows the effect of τ on the temperature evolution of the flow next to the flames, over the time interval in which ignition occurs. Indeed, it shows that if one intends to obtain the temperature where the thermocouple is placed, a time correction must be applied. Otherwise one is only obtaining the temperature of the thermocouple tip.

2.3.2 PIV Analysis

The DynamicStudious program provides the user with plenty of possible analyses. Thus, in order to obtain the most accurate results, besides of the experimental set up, it also depends of the user's sensibility while using the program. Firstly, besides the flow region, the camera also captures part of the pan and of the burner. Therefore, in order to decrease the analyses time, one should define a mask to black out regions with no interest such as those in figure 2.11, and then apply the defined mask to all of the images taken.

(a) Inner Region (b) Outer Region

Figure 2.11: PIV Applied Masks

Secondly, there are three possible analysis to obtain the velocity vectors: Average Correlation analyse, Cross Correlation analyse and Mean Pixel Value analyse.

The Average Correlation develop a correlation function for each pair of images taken by the camera, one correlation for each image sequence. Nevertheless, the Average Correlation averages the correlation function of each interrogation areas at each location for all the images, thus resulting in a single average correlation providing a single velocity field. Therefore, sequences of images with no particles in a certain location, will provide a despair correlation that can greatly affect the average velocity driving it to null. Thus, it entails that one should record a sufficient number of images, so that the total sum of particles in each region is reasonable, minimizing the impact of images with no particles.

The Cross Correlation analyse relies on the same principle as before, it also analysis each image sequence providing several correlations yet, it does not averages the correlations. Instead, it does provide several velocity fields and it's up to the user to decide how to achieve the final velocity field. For once, DynamicStudio suggests applying the Vector Statistics command which converges all the velocity fields into a single average velocity field. Thus, providing the mean velocity vectors in an unique graphic. Unfortunately, again it ends up sharing the same drawback of requiring sufficient image sequences, in order to minimize the impact of frames with no particles.

The Mean Pixel Value analyse runs for all sequences of image pairs and condenses all the first images into a first average image, as well as all the second images into a second average image. Thus, it only provides a single velocity field, given by a single correlation between both the averaged images. No further Statistic analysis is required, yet it only works well if there is no background noise. Plus, in a conceptual view, it is not a proper way to obtain results.

All in all, the Average Correlation and the Cross correlation seemed to be the most appropriate approaches, yet according to DynamicStudious Cross Correlation should be the most suitable option. Indeed, it manages to provide the user with the ultimate vector velocity field, while avoiding to average all the correlation functions (which are classified as a crucial parameter).

At last, in order to visualize the vector magnitude field apart from only the vectors length, the Scalar

Map command provides a coloured image according to a magnitude coloured scale. However, all of the graphics referent to the PIV results, which are present in chapter 4, were post treated using Tecplot 360 EX 2018 R2. Indeed, the program provides the user with customized options that allow faster conclusions and turns out to be more appealing.

2.4 Uncertainty Analysis

2.4.1 Flow Controllers Uncertainty

The flow controllers company mentioned in section 2.2, suggests that the total uncertainty of a certain flow, depends on both the flow measured and the flow meter full capacity. It is given by equation 2.5, where U_Q stands for the uncertainty of the flow rate and Q_m stands for the measured flow rate, while $Q^i_{\max}$ stands for the maximum flow rate capacity of the i flow controller.

$$U_Q = \pm \left(0.008 Q_m + 0.002 Q^i_{\max}\right) \tag{2.5}$$

In fact, one aims at reducing the total uncertainty as much as possible. Such can be achieved by selecting the flow meter with the minimum flow rate capacity, as long as it fulfills the intended flow rate. To that end, according to the required flow rate for each experiment, the most suitable flow meter was selected. Therefore, the higher flow rate uncertainties ended up being the ones, for the measured volumetric flow rates close to the flow meter's scale. Table 2.5 lists the situations that led to the maximum uncertainty and relative error.

Table 2.5: Max. Uncertainty and Relative Error for each gas volumetric flow rate

Flow meter	Max. Q_m (SLPM)	$Q^i_{\max}$ (SLPM)	Max. U_Q (SLPM)	e_Q (%)
CH_4	5.0000	5	0.0500	1.0000
CH_4	0.9657	1	0.0097	1.0045
H_2	9.1139	10	0.0929	1.0193
H_2	5.0000	5	0.0500	1.0000
H_2	0.9657	1	0.0097	1.0045

Nevertheless, the flow controllers uncertainty directly affects the hydrogen molar fraction as well as the power provided by the burner. Therefore, both parameter's uncertainty must consider the flow controllers uncertainty.

H_2 Mole Fraction Uncertainty

The hydrogen mole fraction, f_{H_2}, can be traduced by the hydrogen flow rate divided by the sum of itself with the methane flow rate. Still, to estimate the uncertainty of hydrogen fraction, the error propagation

from the flow meters uncertainty must be considered. Expression 2.6 provides the hydrogen fraction uncertainty, $U_{x_{H_2}}$, based on the basics of error propagation [72, 73].

$$U_{x_{\mathrm{H_2}}} = \pm \frac{Q_{\mathrm{H_2}}}{Q_{\mathrm{CH_4}} + Q_{\mathrm{H_2}}} \sqrt{\left(\frac{U_{Q_{\mathrm{H_2}}}}{Q_{\mathrm{H_2}}}\right)^2 + \left(\frac{\sqrt{U_{Q_{\mathrm{H_2}}}^2 + U_{Q_{\mathrm{CH_4}}}^2}}{Q_{\mathrm{CH_4}} + Q_{\mathrm{H_2}}}\right)^2} \tag{2.6}$$

As a consequence, the maximum uncertainty should happen for experiments conducted under two situations. The first term of expression 2.6 suggests that the higher the x_{H_2}, higher the $U_{x_{H_2}}$. In addition, both $U_{Q_{H_2}}$ and $U_{Q_{CH_4}}$ are known to be higher when the flow meter is forced to operate close to its full capacity. Table 2.6 shows that, the maximum relative error stands for the experiments conducted under the maximum x_{H_2} admitted (80%). Ultimately, the table bellow show that the relative error for the x_{H_2} is never above $\sim 2\%$.

Table 2.6: Max. Uncertainty and Relative Error for x_{H_2}

Power (W)	f_{H_2} (%)	$U_{Q_{CH_4}}$ (SLPM)	$U_{Q_{H_2}}$ (SLPM)	$U_{f_{H_2}}$ (%)	$e_{f_{H_2}}$ (%)
3000	60	0.0377	0.0500	0.7353	1.2255
3000	80	0.0282	0.0929	1.0630	1.3288
1500	30	0.0278	0.0096	0.4100	1.3667
1500	80	0.0191	0.0465	1.0793	1.3492
750	50	0.0097	0.0097	0.6151	1.2302
750	80	0.0066	0.0278	1.2842	1.6052

Burner's Power Uncertainty

The U_P, is again deduced according to the formulas of error propagation [73]. This time, in addition to the CH_4 and H_2 volumetric flow rates, the LHV for each gas must also be included. In fact, expression 2.7 gives the U_P for every experiment, though obviously the second term is null for experiments with only CH_4.

$$U_P = \pm \sqrt{\left(U_{Q_{\mathrm{CH_4}}} LHV_{\mathrm{CH_4}}\right)^2 + \left(U_{Q_{\mathrm{H_2}}} LHV_{\mathrm{H_2}}\right)^2} \tag{2.7}$$

The greater the flow rate uncertainty, the greater the power uncertainty. As so, according to the previous table 2.5, the highest power uncertainty should occur for experiments under volumetric flows close to the flow meter's maximum capacity. Indeed, table 2.7 lists the higher values for the power uncertainty and its relative uncertainty. The maximum U_P happens for the experiment conducted under $3000W$, without H_2 admixture. It's noteworthy that, due to the nature of the LHV units, the units of the volumetric flow uncertainty must be adjusted to m^3/s.

Table 2.7: Max. Uncertainty and Relative Error for U_P

Power (W)	$U_{Q_{CH_4}}$ (10^{-7} m^3/s)	$U_{Q_{H_2}}$ (10^{-7} m^3/s)	U_P (W)	e_P (%)
3000	8.3799	———	30.0000	1.0000
3000	5.7692	8.6538	22.6699	0.7557
1500	3.7102	1.5901	13.3931	0.8929
750	1.6090	1.6090	7.4979	0.9997

2.4.2 Electronic Balance Uncertainty

The electronic balance, used to weight the water mass inside the pan before and after it reached the boiling point, has a maximum deviation of $0.1g$ thus the maximum relative error of its measures is 0.021%.

2.4.3 Acquisition Board Uncertainty

Based on data-sheet information, the acquisition board is subjected to a reading precision which for a 95% confidence level, it corresponds to ± 0.18°C. Consequently, the maximum relative uncertainty corresponds to the lowest temperature registered, thus it is 1.2%.

2.4.4 PIV Uncertainty

The PIV's uncertainty is a subject that has been discussed in the late years. Indeed, the pursuit for enhanced methods suitable for different experimental conditions and results is at full steam. *DynamicStudious* provides the user with two different methods, the Sciacchitano, Wieneke and Scarano method [74], called Particle Disparity, and the Charonkos and Vlachos method [75], called Peak Height Ratio, which is the one most popular today.

The Particle Disparity method, focus on the displacement vectors resulted between the individual particles from the first image, and its pair on the second image. If particle pairs in the vicinity of a vector all show similar displacements, the uncertainty is considered small. If on the contrary, there is a fluctuation in the vector displacement value for its vicinity, then the uncertainty is higher. Unfortunately, in spite of the fact that, mathematically, one only requires two pairs of particles to perform the analysis, the authors suggest up to 7 matches of particles for achieving reliable statistics.

Peak Height Ratio method, relies on the empirical relationship between the radial error, and the ratio between the highest and the second highest correlation peak, thus returning the radial uncertainty. As so, the bigger ratio between the correlation peaks the smaller uncertainty. In other words, since similar images imply higher peak-to-peak ratio, the more similar the images, the lower the associated uncertainty.

Therefore, reflections or seeding, which refers to an uniform density of particles in the frames, are major aspects to consider. The PIV's data treatment process as well as its uncertainty deeply relies on the similarity between images, particularly from the same sequence. Actually, it's easy to realize that if by any reason the particles feeding is interrupted, even briefly, it will lead to frames with no particles,

endangering the final results as previously explained. Similarly, if a reflection happens it may obscure particles nearby and prevent them from being captured by the camera, thus resulting in the same issue. These are major aspects to be aware of when conducted the experiments, as they can greatly jeopardise the result's quality and accuracy.

All in all, the Peak Height Ratio presented itself as a better option as it has no requirements for achieving reliable statistics. Nevertheless, its outcome for every experiment, table 2.8, turned out slightly higher than what one would intend.

Table 2.8: PIV Experiment's Relative Uncertainty

Region	Power(W)	Hydrogen(%)	Max. Unc. (%)	Modal Unc. (%)	Min. Unc. (%)
Inner	1500	0	15.02	12.5-13.5	8.17
Inner	1500	40	15.19	11.0-11.5	10.45
Inner	3000	0	16.33	13.0-13.5	10.21
Inner	3000	40	15.52	14.0-14.5	8.21
Outer	1500	0	16.28	12.0-12.5	7.35
Outer	1500	40	15.08	12.0-12.5	7.60
Outer	3000	0	19.06	14.5-15.0	8.17
Outer	3000	40	15.93	12.0-12.5	7.35

The relative uncertainty values obtained, could have been lower if a better seeding had been achieved. However, the relative uncertainty corresponds to the flow's velocity and, in chapter 4 it will be showed that the magnitude of the Inner region velocities are lower than the magnitude of the Outer region velocities. Actually, lower velocities foster higher relative uncertainties. Thus, perhaps why the modal and the minimum uncertainty of the Inner region was slightly higher then the one from the Outer region. Still, the experiments were quite susceptible to reflections known to increase the absolute uncertainty. Therefore, not surprising, the maximum uncertainty was detected close to the burner's and pan's surfaces. Furthermore, the relative uncertainty for the Outer region gradually increases along the flow. Actually, it happens as the velocity along the flow decreases but also due to the fact that it is considered a free flow. Therefore, logically, the further away the flow is from the origin, the more susceptible it is to variations. In particular, if it must go around the pan. However, it is also true that it was difficult to achieve a constant Alumina feeding. Indeed, an uniform feeding is pivotal for achieving a proper and constant seeding known to greatly benefit the results and minimize the uncertainty. Yet, connecting the fuel and Alumina pipe to the burner without compromising the seeding, turned out to be a challenge. The results stand for the best available connection without drilling through the cooker plate sheets, until the burner inlet.

Chapter 3

Cooking Efficiency Models

Along the document, cooking efficiency has been stated as one of the main parameters of this study. Yet, the cooking efficiency itself, has been defined by many ways so far. In 2011, Oberascher et al. [76] chose to boil eggs, for instance. The efficiency was rated according to a scale created by his own, in which the properties and consistency of the egg yolk were the key parameters. Later in 2018, Zhao et al. [70] chose to boil water and suggested the cooking efficiency as the heat absorbed by the water over the heat released by the fuel. Ultimately, one had to conduct an energy balance over the system to obtain the efficiency of the process. It seemed the most reliable and easily implemented method, thus it was adopted in the current study. However, the cooking efficiency can be affected by multiple factors, under different operating conditions. While Zhao et al. study only addressed a certain operating condition, the current study addressed several operating conditions, as it's detailed in the heating experiments (section 2.1 in table 2.1). Therefore, it explored the impact of the following factors: burner diameter; burner power; hydrogen fraction in the $NG - H_2$ mixtures; water mass.

In addition, the current work sought to develop a second method to determine the cooking efficiency, yet to be explored in the literature. For once, it is based on the heat transfer equations, thus it was required to understand the flue behaviour. To that end, the PIV experiments were fundamental to pursue this second method.

The present study develops two different models to determine the cooking efficiency, each related to a certain theoretical background and to a certain experiment. Still, it was developed a final mathematical function, which uses the cooking efficiency results, to create a dependency between all the operating conditions. So that, the results can be extrapolated and, under similar operating conditions, the cooking efficiency can be predicted.

3.1 Model 1

This method is according to the Zhao et al. suggestion, which stands that through the combustion of a gas, energy is released and can be provided to a system. While a certain quantity of the combustion energy is lost to the surroundings, some of the energy is transferred to the pan and, in this case to

the water inside. However, the efficiency of the cooking process relies only on the useful energy from the combustion reaction, as that being only the energy that goes into the water. Therefore, the energy required to increase the temperature of the pan, is considered as dissipated energy. Initially, efficiency is given by the ratio between the energy rate into the water and all the energy provided by the combustion, $\eta = \frac{\dot{Q}_{in}}{\dot{Q}_{comb}}$.

The first step is to conduct an energy balance to the control system, identified as the mass of water in the pan. The figure 3.1 suggests the internal energy balance as expression 3.1, further developed into expression 3.3. In which, the variation of the internal energy relies on both the energy that enters the system and on the variation of the water mass, as the water evaporated in the heating process. Ultimately, the energy given to the water or the useful energy from the combustion, can be achieved by expression 3.4.

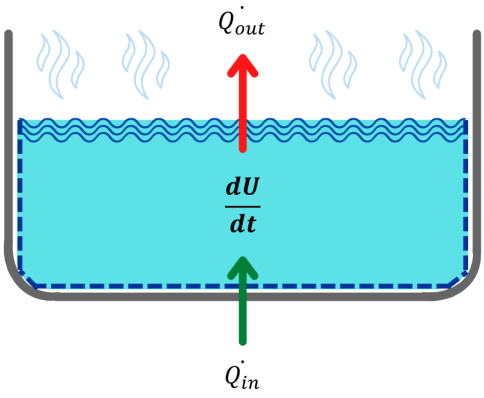

Figure 3.1: Heat Balance to the Water

$$\frac{dU}{dt} = \dot{Q}_{in} - \dot{Q}_{out} \tag{3.1}$$

$$\Leftrightarrow \quad \int \frac{dU}{dt}\, dt = \int \dot{Q}_{in}\, dt - \int \dot{m}_{evap} h_{fg}\, dt \tag{3.2}$$

$$\Leftrightarrow \quad \Delta U = Q_{in} + h_{fg}\, \Delta m_w \tag{3.3}$$

$$\Leftrightarrow \quad Q_{in} = \Delta U - h_{fg}\, \Delta m_w \tag{3.4}$$

Although, the internal energy was given by expression 3.1, it can also be given by expression 3.5. which can be integrated in the experiment time period, resulting in expression 3.7.

$$\frac{dU}{dt} = Cp_w \frac{dT_w}{dt} m_w + Cp_w \frac{dm_w}{dt} T_w \tag{3.5}$$

$$\Leftrightarrow \quad \int \frac{dU}{dt}\, dt = \int Cp_w \frac{dT_w}{dt} m_w\, dt + \int Cp_w \frac{dm_w}{dt} T_w\, dt \tag{3.6}$$

$$\Leftrightarrow \quad \Delta U = Cp_w\, (m_{wf} T_{wf} - m_{wi} T_{wi}) \tag{3.7}$$

Thus, it becomes possible to obtain the useful energy provided to the water by combining both expressions 3.3 and 3.7. In addition, if the total energy provided from the combustion reaction is replaced

by, the mass of fuel multiplied by its low heating value, it leads to the final expression 3.8 to determine the cooking efficiency.

$$\Rightarrow \quad \eta = \frac{Cp_w \left(m_{wf} T_{wf} - m_{wi} T_{wi}\right) - h_{fg}\, \Delta m_w}{m_{fuel}\, LHV} \tag{3.8}$$

All in all, the efficiency expression depends only on variables obtained through the experimental method of heating the water. The evaporated water is obtained through the difference of the mass measured with the balance, before and after the experiments. The temperature is given by the thermocouples, and the fuel mixture is imposed by the flow meters.

3.2 Model 2

This model approaches the heat transfer process in a more detailed context. Although, radiation is neglected (as in the previous method), it is relevant to consider if the heat transfer is either by conduction or convection. The cooking efficiency given by this model relies on the fraction between the heat provided by each heat transfer process, and all the energy released by the combustion of a certain gas mixture, $\eta = \frac{\dot{Q}_{cond} + \dot{Q}_{conv}}{\dot{m}_{fuel}\, LHV}$.

It is heat transfer by conduction where the flames interact with the pan bottom. Though, it is heat transfer by convection along the flow of the combustion products. The conduction happens due to the temperature difference between the flames and the pan bottom. Whereas, the convection heat transfer happens due to the temperature difference between the flue and the pan's surface. Thus, it was considered heat transfer to the water from the moment when the pan walls reach a stationary temperature. However, it is not known the precise moment when the pan reaches a stationary temperature. Therefore, it had to be considered that as soon as the experiment begins, the pan has already reached its stationary temperature. In contrast, in order to avoid over calculating the useful energy given to the system, the energy required to heat the pan until its stationary temperature must be subtracted. To that end, the cooking efficiency expression becomes, $\eta = \frac{\dot{Q}_{cond} + \dot{Q}_{conv} - \dot{Q}_{pan}}{\dot{m}_{fuel}\, LHV}$.

Actually, the PIV experiments proved to be crucial to cope with the heat transfer convection equations, as it allowed to identify relevant convection regions, and it made possible to distinguish between natural convection and forced convection. According to the fundamentals of heat transfer [77], either if it is forced or natural convection, depends on either if $\frac{Gr}{Re^2} << 1$ or $\frac{Gr}{Re^2} >> 1$. Hence, knowing the flow velocity magnitude, in order to determine Reynolds number, was a pivotal outcome from the PIV experiments. In addition, it revealed that for most of the convection regions, the heat transfer nature is natural convection. Indeed, the overall heat transfer was divided in several regions along the pan walls, according to the nature of the heat transfer process, figure 3.2.

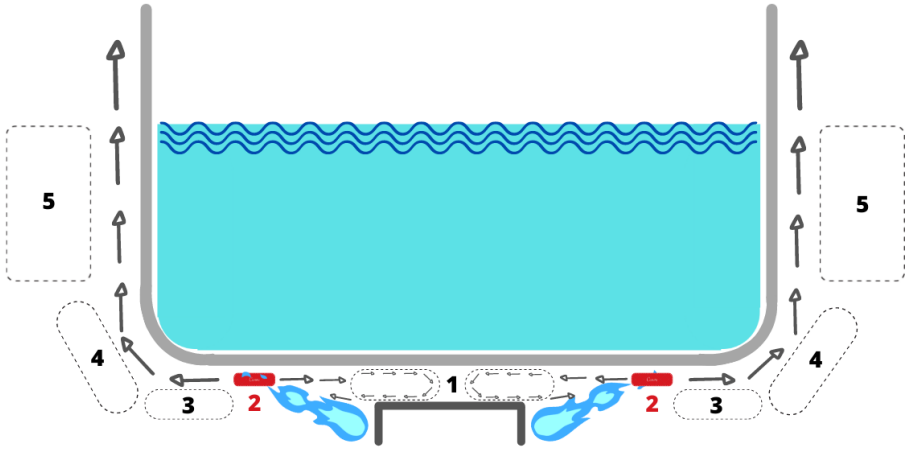

Figure 3.2: Regions of Heat Transfer

As the figure 3.2 suggests, there are up to 5 different regions of heat transfer. The first is placed above the burner surface and below the pan outside bottom. In fact, section 4.3 shows that the PIV experiments led to the identification of a recirculation bubble in region 1, with flow velocity magnitudes corresponding to natural convection. The fundamentals of heat transfer state that, for the lower surface of a horizontal cold plate geometry, the average Nusselt number for natural convection is given by expression 3.9. Which, multiplied by the combustion products thermal conductivity, and divided by the fraction between the burners surface area and its perimeter, leads to the convection coefficient, expression 3.10. Parameters such as thermal conductivity and kinematic viscosity for instance, used to calculate the Rayleigh number, will be properly addressed later on this chapter. Curiously, right above the edge of the burner head, the PIV detected a vortex caused by the flow leaving the burner holes. Although, the vortex partially blocks the return flow from the recirculation bubble, its effect on the heat transfer was not considered.

$$Nu = 0.54\, Ra^{\frac{1}{4}} \tag{3.9}$$

$$h = \frac{Nu\, \kappa_{mix}}{\frac{A_s}{p}} \tag{3.10}$$

On the contrary, for region 3 next to the flames tip until the pans bottom edge, the $\frac{Gr}{Re^2}$ decreases substantially to bellow 1. Therefore, for region 3 it is heat transfer through forced convection. Therefore, for a laminar flow over a flat plat under an uniform heat flux, the Nusselt number and the convection coefficient are given by the foregoing expressions 3.11 and 3.12.

$$Nu = 0.453 Re^{\frac{1}{2}}\, Pr^{\frac{1}{3}}, \quad Pr \geq 0.6 \tag{3.11}$$

$$h = \frac{Nu\, \kappa_{mix}}{x} \tag{3.12}$$

As the combustion products flow over the bottom of the pan until reaching the edge, then the flow tries to keep up with the curvature of the pan and flows over the side wall. Region 4 was designated for the pan curvature. Whereas, from the location where the curvature ends until it reaches the waterline height, it's region 5. In regions 4 and 5 there is natural convection, and the Nusselt number is obtained through

expression 3.13, which serves as input for the previous expression 3.12 in order to obtain the convection coefficient. However, region 4 relies on figure 3.3, as a simplification for the bottom edge curvature, so that the same expression could be applied. Although, for region 4, the typical $Ra = \frac{g\beta(T_s - T_f)x^3}{v^2}$ must be adjusted. The gravitational force as input must be multiplied by $\cos\theta$, in which θ is the angle of the curvature simplification.

$$Nu \;=\; 0.68 \;+\; \frac{0.67\, Ra^{\frac{1}{4}}}{(1 \;+\; (\frac{0.492}{Pr_{mix}})^{\frac{9}{16}})^{\frac{4}{9}}} \tag{3.13}$$

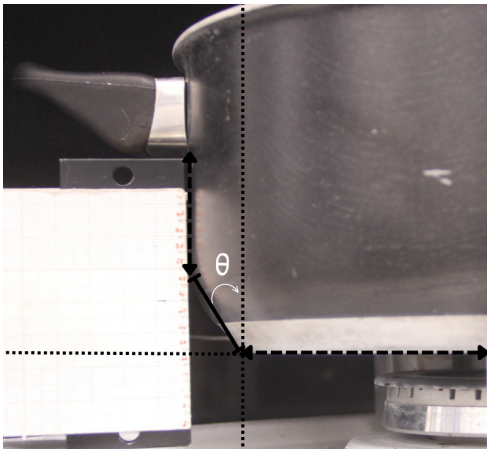

Figure 3.3: Curvature Simplification of the Bottom Edge

All in all, the heat rate transfer by convection is given by expression 3.14, applied for regions $1, 3, 4$ and 5, in which the parameters are adjusted for each region. For regions 1 and 3, the pan bottom temperature was assumed as uniform. While for regions 4 and 5, the pan wall temperature were distinct. The area of region 1 is a circle, the area of region 5 is crown shaped though. The contact area for region 5 is pretty straightforward but, the area of region 4 was calculated accordingly with the curvature simplification. In addition, as mentioned in the previous chapter, the temperature of the flow was measured experimentally. As suggested in [78], it was assumed an average flow temperature for each region, in order to obtain the convection heat transfer.

$$\dot{Q}_{conv} \;=\; A\, h\, (T_{flow} - T_{pan}) \tag{3.14}$$

At last, the rate of heat transfer by conduction happens in region 2, in which the flames extend along the pan bottom. It's possible to apply directly the expression 3.15, from fundamentals of heat transfer, in which the pan temperature is equal to the one in region 1 and 3.

$$\dot{Q}_{cond} \;=\; \frac{\kappa_{mix}\, A}{\Delta x}\, (T_{flame} - T_{pan}) \tag{3.15}$$

Therefore, the cooking efficiency associated to this method can be written in function of all regions, according to its heat transfer nature, expression 3.16. However, for a few experiments conducted under

high operating burner power, the propagation of the flames along the pan bottom increased to such an extent so that, it covered all region 3. Instead, region 3 ceased to exist and became part of region 2. Therefore, for those experiments, the cooking efficiency expression does not include the third heat transfer term.

$$\eta = \frac{\dot{Q}_{conv_1} + \dot{Q}_{cond_2} + \dot{Q}_{conv_3} + \dot{Q}_{conv_4} + \dot{Q}_{conv_5} - \dot{Q}_{pan}}{\dot{m}_{CH_4} LHV_{CH_4} + \dot{m}_{H_2} LHV_{H_2}} \tag{3.16}$$

As briefly mentioned, the Prandtl number, the Rayleigh number, the Nusselt number and the Reynolds number of the flow gas mixture, are pivotal to calculate the heat transfer. To that end, it is required to previously determine gas properties such as the kinematic viscosity, dynamic viscosity, thermal conductivity, thermal diffusivity, specific heat and density. Usually, these components would be easily obtained for each gas, using normalized tables of gas properties. However, for a mixture of gases, in Perry's Handbock [79] it is suggested expressions 3.17, 3.18 and 3.19, in which the properties of the mixture are depended on the molar fraction of each gas component.

$$C_{p,mix} = \sum_{i=1}^{C} y_i C_{p,i} \tag{3.17}$$

$$\kappa_{mix} = \frac{\sum y_i \kappa_i M_i^{\frac{1}{3}}}{\sum y_i M_i^{\frac{1}{3}}} \tag{3.18}$$

$$\mu_{mix} = \frac{\sum y_i \mu_i M_i^{\frac{1}{2}}}{\sum y_i M_i^{\frac{1}{2}}} \tag{3.19}$$

Plus, the ideal gas law allows to write the density of a mixture as expression 3.20, in which the temperature value is adjusted for each region. The gas constant of the mixtures can be obtained through expression 3.21, that relies on both the mass fraction and molar mass of each component.

$$\rho_{mix} = \frac{P}{R_{mix} T} \tag{3.20}$$

$$R_{mix} = \sum \frac{m_i}{m_t} \frac{R}{M_i}, \quad R = 8.314 KJ/kmolK \tag{3.21}$$

The components of the flow mixture gas are no less than the products of the combustion reaction, of burning the fuel mixture with atmospheric air, as mentioned before. However, the type of gases which result from the combustion, depends on either if it is a rich or lean reaction. In order to classify the reaction, a ϕ ratio measurement through a spectrometer experiment was performed. It was obtained $\phi = 1.23$, for $0\% H_2$ admixture, which classifies the reaction under rich conditions.

Thus, considering f as the molar fraction of hydrogen admitted in the fuel mixture, the combustion reaction itself is given by expression 3.22, where the combustion products are CO_2, CO, H_2O and N_2.

$$\begin{aligned} \mathrm{fH_2} + (1-\mathrm{f})\mathrm{CH_4} + \frac{(2-1.5\mathrm{f})}{\phi}\,(\mathrm{O_2} + 3.76\ \mathrm{N_2}) \rightarrow (\frac{4-3\mathrm{f}}{\phi} + 2\mathrm{f} - 3)\mathrm{CO_2} + (\frac{3\mathrm{f}-4}{\phi} - 3\mathrm{f} + 4)\mathrm{CO} \\ + (2-\mathrm{f})\mathrm{H_2O} + 3.76\frac{(2-1.5\mathrm{f})}{\phi}\mathrm{N_2} \end{aligned} \tag{3.22}$$

However, amid hydrogen admixture it is expected a change in the ϕ value. Unfortunately, the spectrometer calibration curves were not fitted for $CH_4 - H_2$ combustion, so it was not possible to measure ϕ for other than non hydrogen admixture. In that context, the worked developed by de Vries, Mokhov and Levinsky [17] addressed in the State of the Art, proved to be extremely useful to assume the ϕ values for the remaining experiments with hydrogen admixture. Therefore, this method considers the combustion reaction product's properties, which consequently affect the heat transfer coefficients.

3.3 Prediction Function

The economist Paul Douglas and its mathematician colleague Charles Cobb, in 1928 published both together an econometric model which, at that time was intended as a production function [80]. It provided a relationship between independent production inputs, that result in a dependent production output. Nowadays, it is widely known and it has become more and more useful for other purposes, as long as it is applied in a statistical basis. The original model stands that, the output Q can be estimated by the multiplication of the inputs L, K, E raised to a given exponent l, k, e. Expression 3.23 stands as the original model. It's a non linear function, though if Q, L, K, E are positive values, the logarithm function can be linear in l, k, e. For once, α is used to impose small corrections.

$$Q \;=\; \alpha\, L^{l}\, K^{k}\, E^{e} \tag{3.23}$$

The work developed at the present study, puts together all the results from the cooking efficiency experiments and attempts to culminate in a final expression, that predicts the cooking efficiency. The following parameters as the independent variable: Burner Power; Burner Radius; Number of Burner Exit Holes; Pan Radius; Water Mass; Hydrogen Fraction. The exponents are considered the output elasticities, and its values were obtained by the Mathematica software. The program seeks for the best exponent values, so that the operating conditions for each experiment, result in the cooking efficiency closest to that previously obtained by models 1 and 2.

Hence, for this particularly case, the expression above turned into expression 3.24, as the variables were duly substituted. As a first approach, it was implemented two input ratios in order to simplify the expression, and reduce the number of exponents. One between the Burner Power and the Number of Exit Holes, while the other between the Burner Radius and the Pan Radius. Nevertheless, despite confirming and validating certain trends, it ended up revealing inaccurate results. Thus, it were raised other hypotheses based on expression 3.25, aiming at more accurate results. As these attempts increasingly revealed the dynamics of the interaction between the parameters, the sensitivity towards the study itself also increased, which led to a small mathematical adjustment in the H_2 fraction term. Expression 3.26

stands as the mathematical function, that provides the closest results to the reality portrayed in models 1 and 2.

$$\eta \;=\; \alpha \left(\frac{P}{nh}\right)^{A} \left(\frac{R_b}{R_p}\right)^{B} m_w^F \, f_{H_2}^G \tag{3.24}$$

$$\eta \;=\; \alpha \, P^A \, R_b^B \, nh^F \, R_p^G \, m_w^J \, f_{H_2}^H \tag{3.25}$$

$$\eta \;=\; \alpha \, P^A \, R_b^B \, nh^F \, R_p^G \, m_w^J \, (f_{H_2} + 1)^H \tag{3.26}$$

Cobb and Douglas claim that, the output elasticity measures the impact that each input has on the output. For instance, if $A = 0.3$ means that a 1% increase in the Burner Power, results in a 0.3% increase in the cooking efficiency. Moreover, if the the output elasticity is equal to 1, which is the same as $A + B + F + G + H + J = 1$, it holds that the function display constant returns to scale (CRS). Therefore if one doubles the input values, the output value will be twice as large. However, in the case that the output elasticity is less than 1 or more then 1, then the function display decreasing returns to scale (DRS) or increasing returns to scale (IRS). On one hand, if $A + B + F + G + H + J = 0.7$, then doubling the input values means a 70% increase to the output. Whereas, on the other hand, if $A + B + F + G + H + J = 1.3$, doubling the input values means a 130% increase to the output. Nevertheless, in the event of $A + B + F + G + H + J < 0$, -0.3 for instance, then doubling the input values results in a 30% decrease on the dependent variable.

All in all, the exponents values translate the most interesting conclusions about the role of each macro parameter on the cooking efficiency. Plus, the following chapter shows the accuracy of expression 3.26, and enhances it as a function for predicting the cooking efficiency.

Chapter 4

Results and Discussion

This chapter is divided in 5 sections. Section 1, 2 and 3 , approach the results from both the flashback risk, sound intensity and PIV experiments. Then, in section 4, the cooking efficiency obtained for both models is compared, and insights about the impact of the operating conditions are discussed. In addition, it is conducted an analysis of slow cooking vs fast cooking, focused on sustainability and end user financial costs. In section 5, the results from the prediction function are compared to the ones from models 1 and 2, and the impact of the operating conditions are further discussed. At last, it's explored the advantages and limits of implementing a few adjustments, to the prediction function.

4.1 Flashback Risk

The flashback risk was previously defined as a crucial target to the study. It was stated as a phenomenon which may occur amid hydrogen admixture, leading to overheating the burner head. So that, it endangers the cooking process and the appliance's lifetime.

As mentioned before, the experiments contemplated two different scenarios, flashback risk experiments with the pan and without the pan. Experiments simulating real life cooking, thus using the pan, led to the identification of flashback from $50\% - 55\%$ H_2 admixture. Figure 4.1 shows the flame's appearance evolution amid hydrogen admixture. Apart from a slight decrease on the flames size, the flames remain unchanged until up to 10% H_2. The 25% H_2 stage, marks the beginning of the appearance of random orange tips in the flames, and two flame zones become discretely outlined. As hydrogen percentage increases, the orange tips become more and more usual, and the different flame zones become more and more distinct. At 50% H_2, the two flame zones are clearly visible. One in the inner zone in intense light blue tones, while the other is in the outer zone in violet blue tones. At this stage, the flames become really short and flashback may occur at any time.

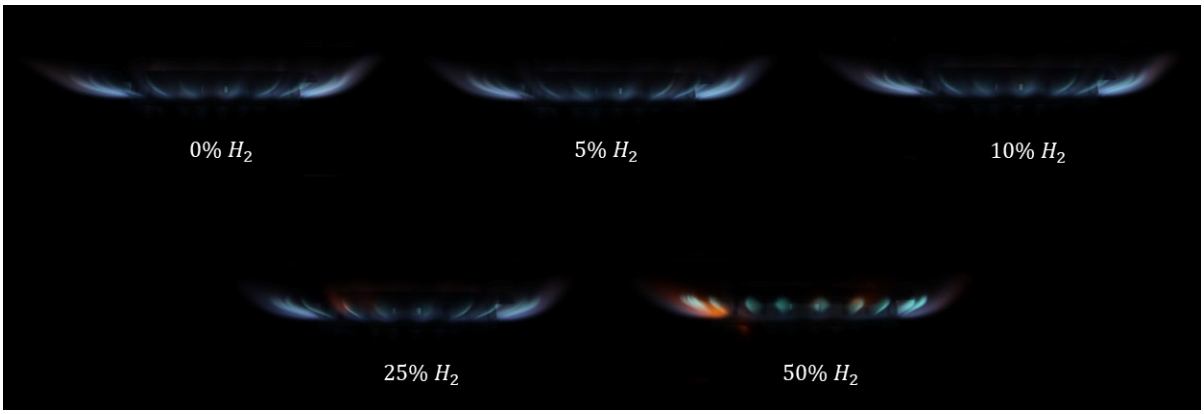

Figure 4.1: Flames Appearance with Pan - B10 1500W

On the other hand, for experiments conducted with no pan, the flames flashed back to the burner from close to 80% H_2 admixture, which is a major difference compared to that obtained with the pan. Figure 4.2 shows the flames appearance for H_2 fractions close to that range. For 70% H_2, the flame's tips are continuously orange, the flame's zones are completely defined and, the intensity of its tones is even higher than on the brink of flashback with the pan. For 80% H_2, there is no distinction between flame zones, as almost all of the flame's body becomes sunny yellow, flashback may happen at any moment. Actually, for 85% H_2, flashback happens as soon as the flame is ignited. The image on the right shows a flashback situation in which, although there is flame propagation through the burner holes, the flames are not only in violet tones with orange tips, but also remarkably less intense than before.

Figure 4.2: Flames Appearance without Pan - B10 1500W

Moreover, figure 4.3 shows an unique experiment in which after occurring flashback ($a.f.$), the flow meters were allowed to remain opened for a few seconds. Initially, 120 seconds after occurring flashback, the flame's tips turned to sunny colors and a red dark spot began to appear very faintly, in the centre of the black burner head. Then, along time the flame's yellow tips start propagating through all the flame's body. Plus, as the flame underneath went on increasing the burner temperature, the red dark spot turned to reddish tones, spreading over more and more area and increasing in intensity. At 200 s $a.f.$, it was about time to turn off the hydrogen flow meter, so that the inner flame extinguishes and stops causing the overheating of the burner. Consequently, as the fuel flow significantly decreased, the exit flames diminished in size, as it can be noted in the 210 s $a.f.$ picture. Afterwards, as expected the reddish tones start losing its intensity and become more and more faint. In the meanwhile, although

quite unpredictable, the flames tend to increase in size and gradually recover their blue hue.

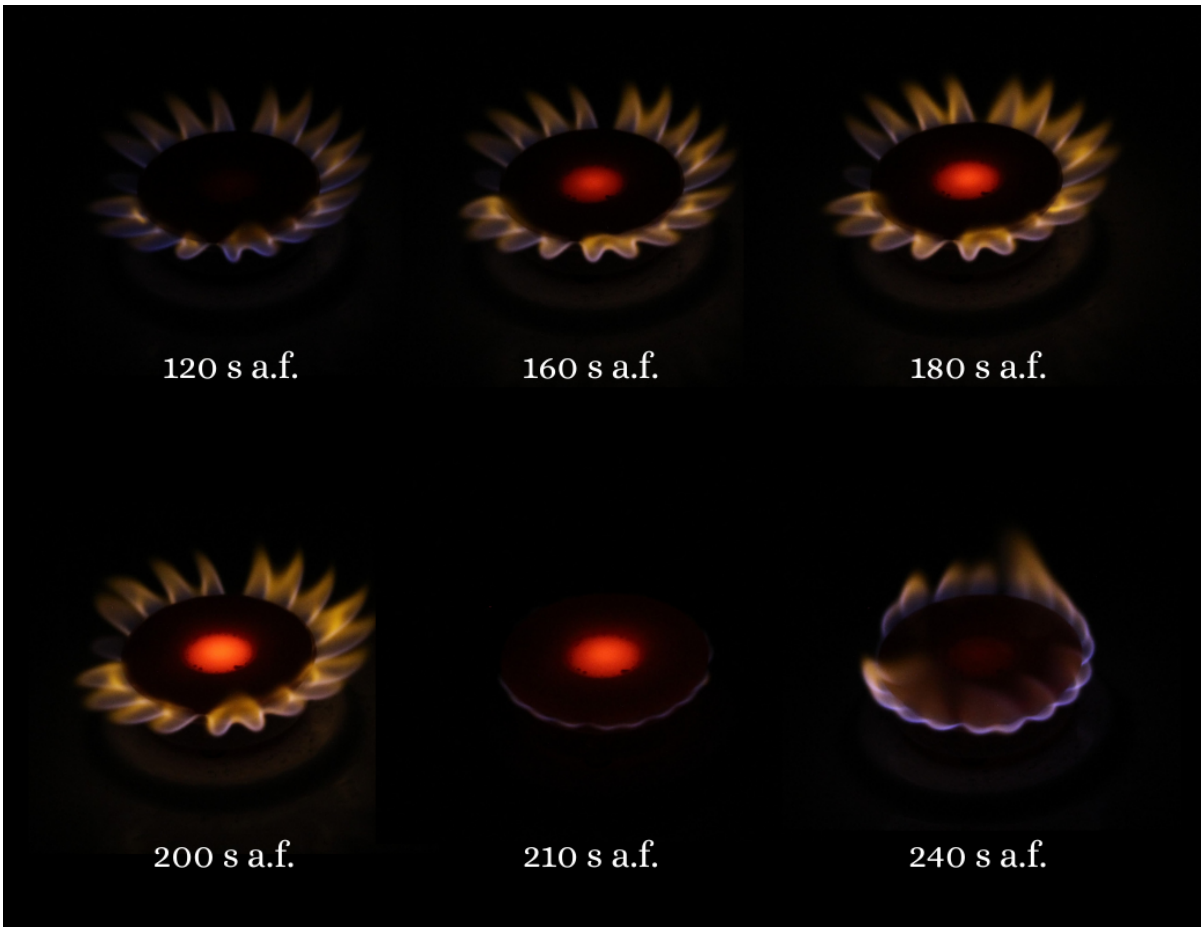

Figure 4.3: Burner Color during Flashback - B10 1500W

Finally, it is worthy to point out that the flashback limits for each situation were equal for all the three burners. In addition, for experiments with the pan placed above the burner, the flame tips interacting with the pan bottom make it more difficult to the flames to stabilize, thus increasing the flashback risk.

4.2 Sound Intensity

Usually, the human ear is able to pick up the sound from the resulting natural gas flames of cooking with a gas stove. The Decibel Scale, figure 4.4 (a), shows that humans are relatively sensitive to decibel variations. The background laboratory sound pressure level was close to 44 dB, thus considered a moderate noise environment.

Actually, considering $0\%H_2$ admixture, in figure 4.4 (b) three the ranges of noise for each burner are clear: for the bigger diameter burner, the associated noise level is $77dB$ close to the very loud maximum limit; for the medium diameter burner, the noise level is still very loud, around $72dB$; for the smaller diameter burner, the noise level is moderate, close to $57dB$. Still, for all burners, the noise level suffered a constant increase, as hydrogen was gradually added.

Figure 4.4 (b) shows that the maximum sound intensity recorded for each burner, was for the higher

hydrogen fraction imposed (50%). Such led to a maximum increase of $\approx 8\%$ for the larger burner, $\approx 6\%$ for the medium burner and $\approx 11\%$ to the smaller burner. Therefore, the smaller burner was the most affected by the hydrogen admixing. Even though, hydrogen appears to have a low impact on the noise intensity, when considering the Decibel scale one can realize quite the opposite. For instance, for the smaller burner, as soon as hydrogen percentage comes close to $\approx 25\%$, it becomes a very loud source of noise. In fact, as hydrogen percentage was gradually increasing, it was possible to hear a distinct "zzzz" noise increasing as well. Dangerously, from $20\%H_2$ mixtures onwards, the larger burner became an extremely loud sour of noise.

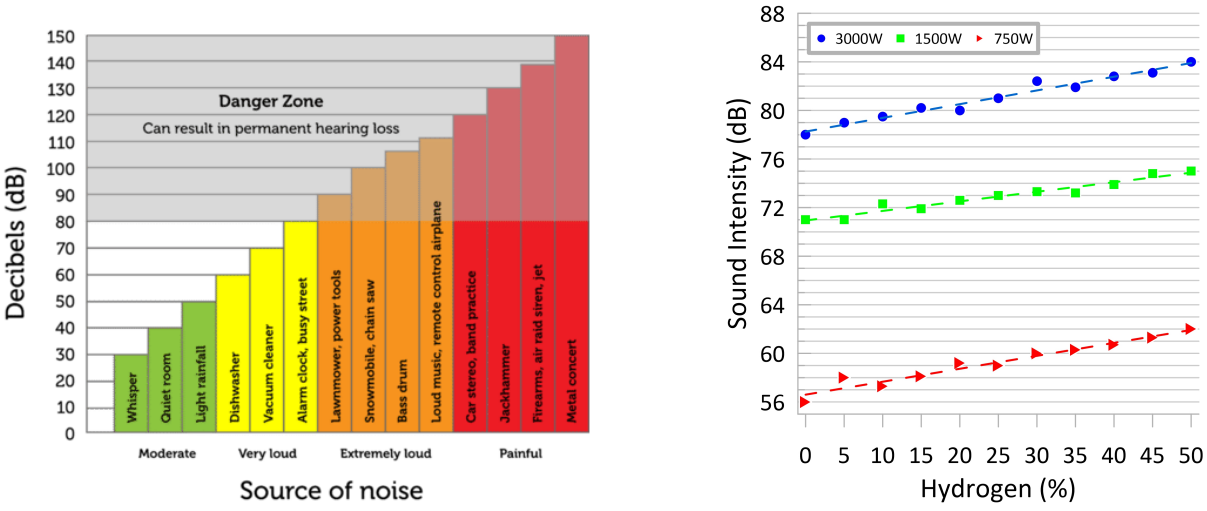

(a) Decibel Scale

(b) Burner's Sound Intensity with Pan

Figure 4.4: Sound Intensity

It's note worthy that throughout the experiments, the flames sound played a helpful role upon identifying flashback moments. One of flashback features is a suddenly different sucking sound, followed by an extremely loud and constant storm sound.

4.3 PIV

As mentioned in chapter 2, the PIV procedures and post data treatment provide visual information about the velocity vectors of a certain flow. Indeed, the velocity vectors were defined as critical for the cooking efficiency model 2, detailed in chapter 3. The experiments conducted focused on: the two different regions (Outer and Inner), already mentioned in chapter 2; two different powers ($1500W$ and $3000W$); two different hydrogen admixtures ($0\%H_2$ and $40\%H_2$), table 2.2. All in all, the experiments resulted in 8 images, each for a certain condition.

Outer Region Results

The PIV results lead to similar images for all the outer region cases. Figure 4.5 shows the $1500W - 0\%H_2$ case; figure 4.6 corresponds to the $3000W - 0\%H_2$ case; figure 4.7 shows the $1500W - 40\%H_2$; figure 4.8 is relatively to the $3000W - 40\%H_2$ case. It was drawn both the pan with the water inside and part of

the burner, so that it could be easily understood. Yet, the draw isn't assigned to neither the color legend nor the X/Y scale. In fact, the scale has its origin placed at the center of burner head surface. The figure shows the flow exiting the burner head and going diagonally to the pan bottom. Then, it proceeds to the bottom edge, where it reaches its maximum velocity. The flow keeps up with the pan edge curvature, and it follows ascending close to the pan side wall. In particular, the figures revealed a vortex above the burner exit and bellow the pan bottom.

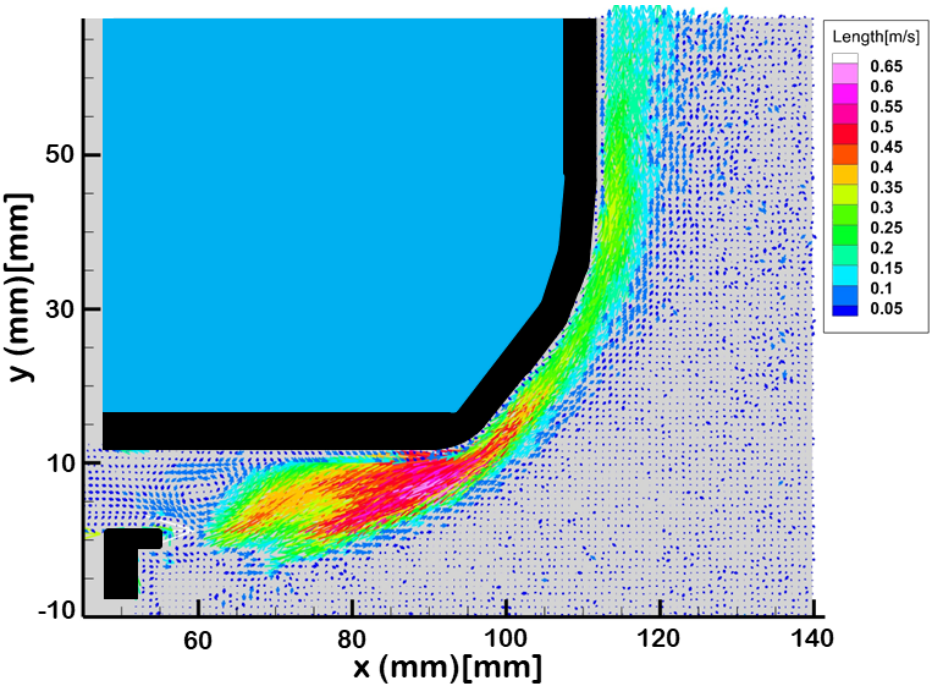

Figure 4.5: Velocity Field for $1500W - 0\%H_2$

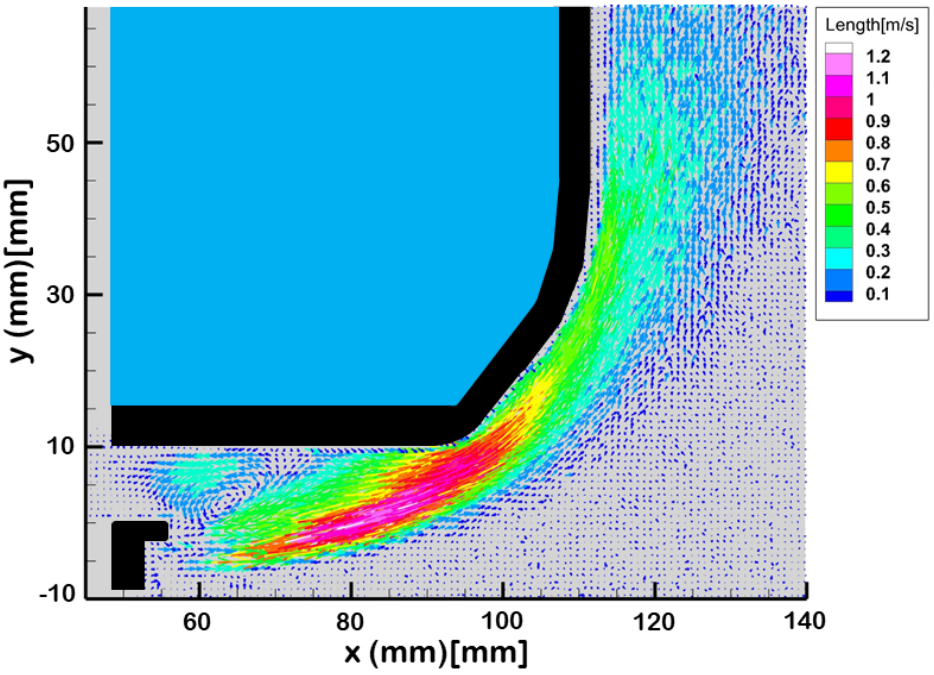

Figure 4.6: Velocity Field for $3000W - 0\%H_2$

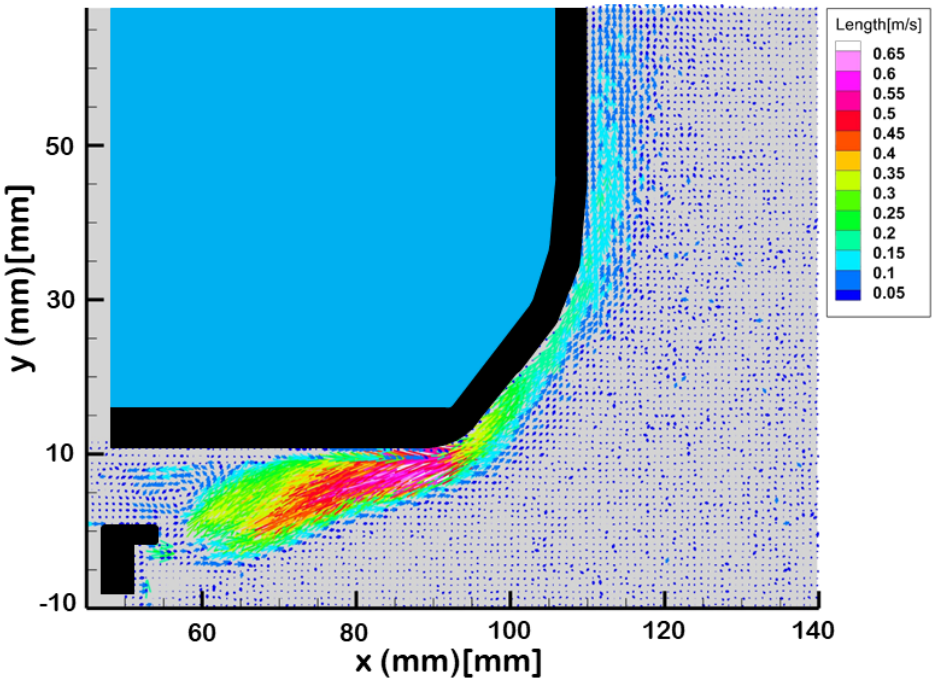

Figure 4.7: Velocity Field for $1500W - 40\%H_2$

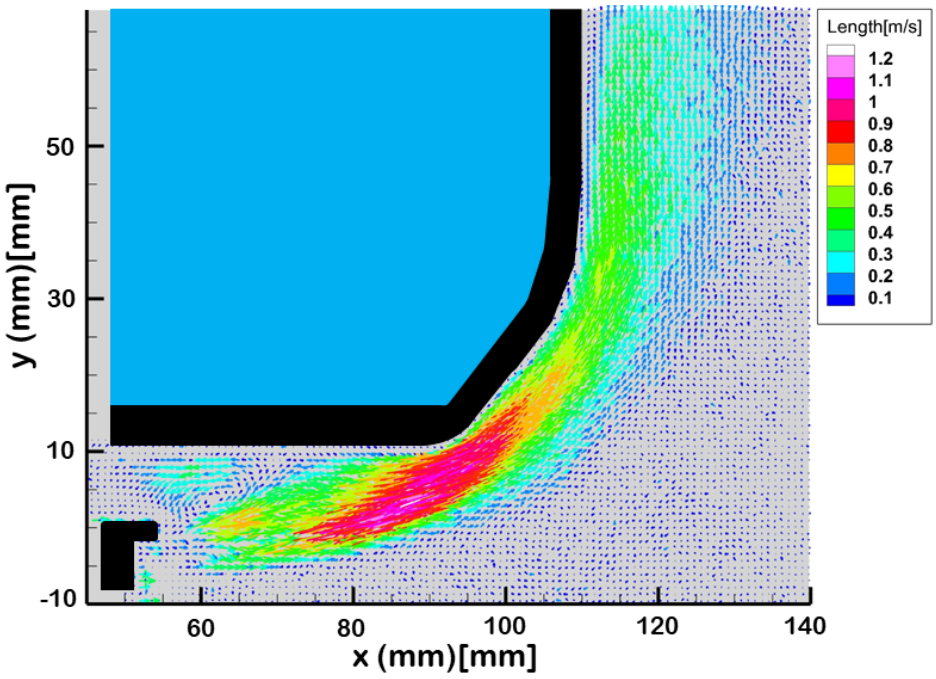

Figure 4.8: Velocity Field for $3000W - 40\%H_2$

As mentioned in chapter 3, the PIV experiments lead to identifying several heat transfer zones. In fact, it allowed to better understand the nature of the heating process and to make the distinction between forced and natural convection, according to the velocity vectors magnitude (length). Actually, figure 4.9, which is a zoomed view of the burner exit region of figure 4.5, might enlighten the flow behaviour. It can be more easily seen that, as the flow leaves the exit hole and comes closer to the pan bottom, it starts

to separate at the region between the $(X, Y) = (65 - 69, 8 - 10)$ coordinates. While the most of the flow moves horizontally in the right direction, a small share moves horizontally to the left. Eventually, some of the left flow is drawn into the vortex. However, the inner region images will show that the flow keeps moving on, towards the center of the pan's bottom surface. In addition, the inner region experiments proved to be pivotal to explain the horizontal vectors in the right direction into the vortex, and placed just on top of the burner head at the $(X, Y) = (50 - 57, 0 - 4)$ coordinates.

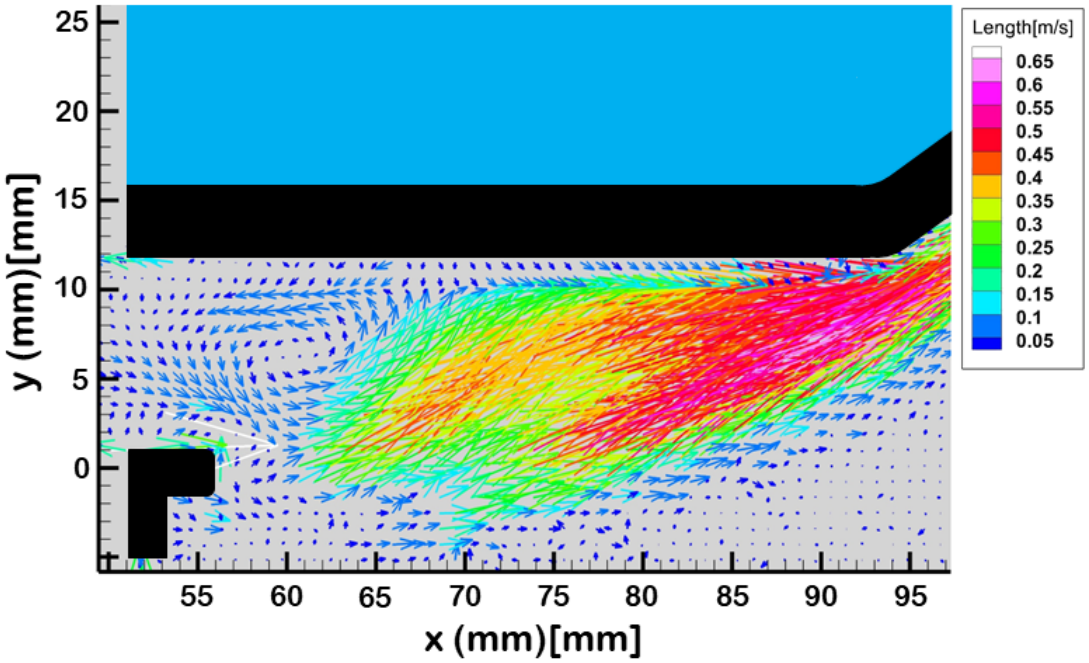

Figure 4.9: Zoomed View of Fig. 4.5

Although all figures display both a similar flow behaviour and a vortex, there are a few differences.

On one hand, if one compares both pairs of figures for the same hydrogen percentage (thus, different power), that is, comparing figure 4.5 with 4.6 and figure 4.7 with 4.8, for the double of the power it was obtained almost the double of the maximum flow velocity. For both figures 4.5 and 4.7 ($1500W$) the flow near the edge of the pan's bottom reached a maximum velocity of $0.60m/s - 0.65m/s$. Whereas, for figures 4.6 and 4.8 ($3000W$), the maximum velocity recorded was $0.90m/s - 1.00m/s$. Such, proves to be a very positive sign to the veracity of the results. Since double the power means double the volumetric flow rate, while the burner exit area remain constant, it should be expected to obtain near twice the maximum velocity.

In addition, the results clearly show an increase on the area affected by the flow. The increase is particularly noticeable in the pan's lateral, where the flow thickness limit has increased from $X = 120$ to $X = 135$, for figures 4.5-4.6, and $X = 115$ to $X = 130$ for figures 4.7-4.8. Therefore, twice the power resulted in a lateral flow area about $15mm$ thicker. Even though, in other zones, the same effect isn't that easily quantified, it must not be overlooked. Especially in figures 4.5-4.6, the increase in the velocity field area after the burner outlets, is quite remarkable.

Besides, the vortex was also affected by doubling the burner power. The magnitude of the vectors

around the vortex increased to values close to double, from $\approx 0.10m/s$ to $\approx 0.20m/s$. Such, immediately resulted in a clear benefit for the visualization of the vortex, as it became more defined and even slightly larger. Plus, as the power increased, the vortex center also moved further to the right. For figure 4.5, the vortex center is at $(X, Y) = (60, 7)$, while for figure 4.6 it is at $(W, Y) = (64, 3)$. For figures 4.7-4.8, the similar happened, thus meaning that doubling the burner power resulted in an adjustment in the vortex center position, $4mm$ in the X direction towards the right and another $4mm$ in the Y direction downwards.

Comparing figure 4.5 with 4.7 and figure 4.6 with 4.8, there is almost non difference for the maximum absolute velocity recorded. However, the results show that the flow area was affected. The images clearly show a decrease in the area of the velocity field of the flow, especially between figures 4.5-4.7. This results are in agreement with the literature review in chapter 1. It states that as the hydrogen mixture increases, the laminar combustion velocity also increases, resulting in a decrease in the flame size. In particular, the flow thickness over the pan's lateral zone suffers a $5mm$ decrease, steeping from a thickness limit $X = 123$ to $X = 118$, for figures 4.5-4.7. Again, the position of the vortex undergoes a further adjustment. Whereas for figure 4.5 the vortex center is at the $(X, Y) = (60, 7)$ coordinates mentioned before, for figure 4.7 it is at $(X, Y) = (57, 4)$. Therefore, from pure methane flames to $40\%H_2$ flames, the vortex moved $3mm$ in the X direction towards left and another $3mm$ in the Y direction downwards.

Finally, the vortex and the flow behaviour can be better understood by complementing the analysis with the results from the region between the center of the burner head, and the center of the pan's bottom.

Inner Region Results

As the flow reaches the pan bottom its majority heads towards the edge, yet some of it flows towards the center of the pan bottom. Figures 4.10, 4.11, 4.12 and 4.13, show that the flow moves towards the center. Where, due to the burner geometry, it meets the flow arriving from all the other radial directions and an interesting phenomenon occur - the flow displays axial symmetry on the $X \approx 0$ axis and it shows a re-circulation bubble on both sides. For figures 4.10, 4.11, 4.12 and 4.13, the blue area is the water inside the pan and the black area just next to it represents the outline of the pan bottom. The other black area bellow the vectors, represents the burner head. Again, these areas are not to scale with the X/Y axes and don't correspond to the color legends above the figures.

Still, from figures 4.10 and 4.12 to figures 4.11 and 4.13, the burner power doubled from $1500W$ to $3000W$. As a consequence, the maximum velocity recorded increased to approximately the double, from $0.03m/s$ to $0.07m/s$. Double the power is achieved by doubling the volumetric flow. In addition, taking on account that the burner exit area remained constant, then the velocity is expected to double. Such meets the results and fosters its consistency, which is a good indicator. In the meanwhile, the flames are known to shorten as the hydrogen percentage in the fuel mixture increase. Therefore, the flames became closer to burner head, yet it wasn't noticed any effect on the magnitude of the velocity field whatsoever. In fact, from figure 4.10 to figure 4.12 or from figure 4.11 to figure 4.13, though the hydrogen percentage increased from 0% to 40%, the maximum velocity recorded remained the same.

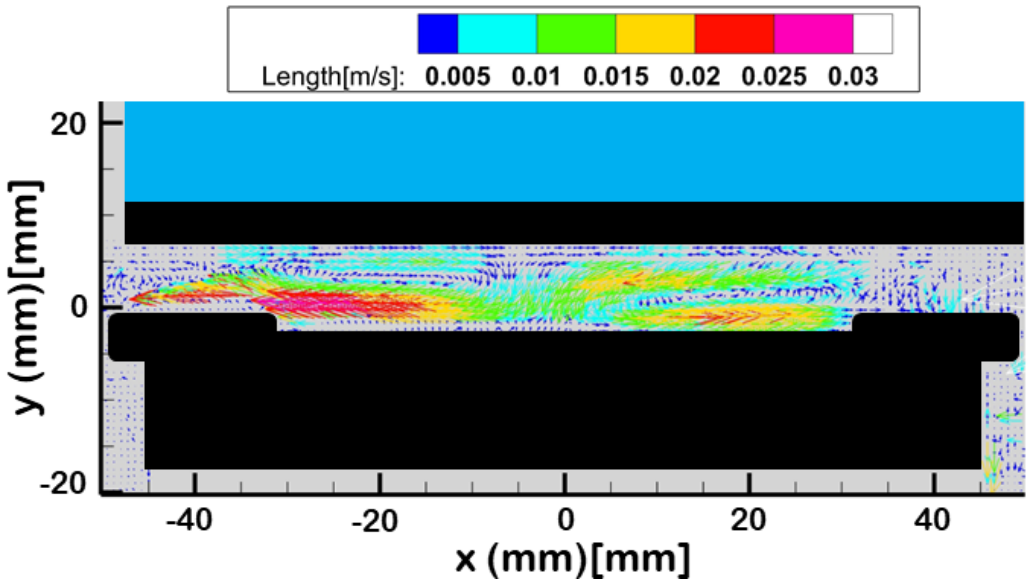

Figure 4.10: Velocity Field for $1500W - 0\%H_2$

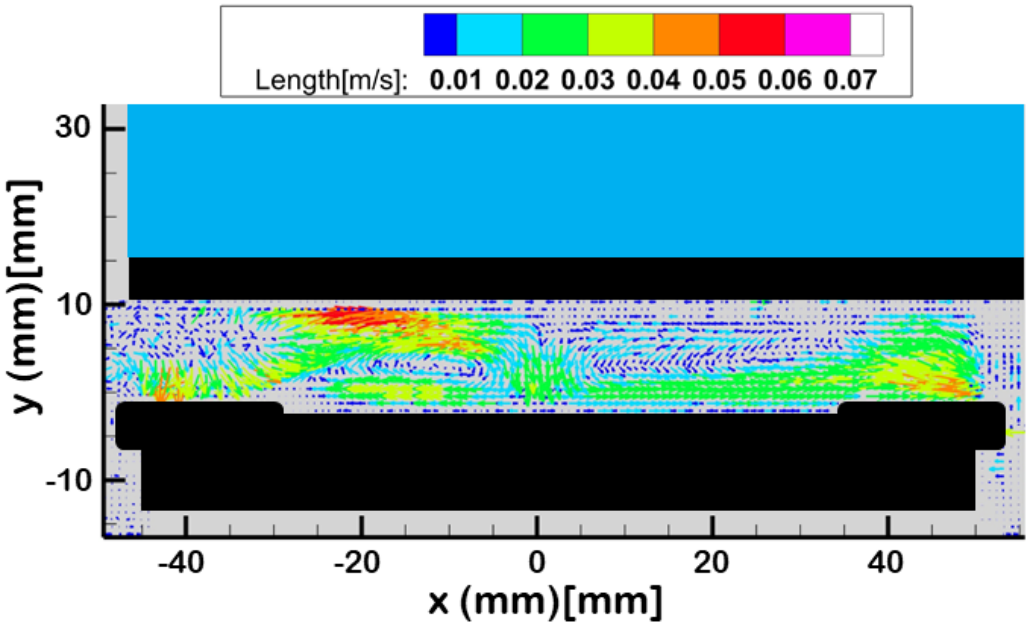

Figure 4.11: Velocity Field for $3000W - 0\%H_2$

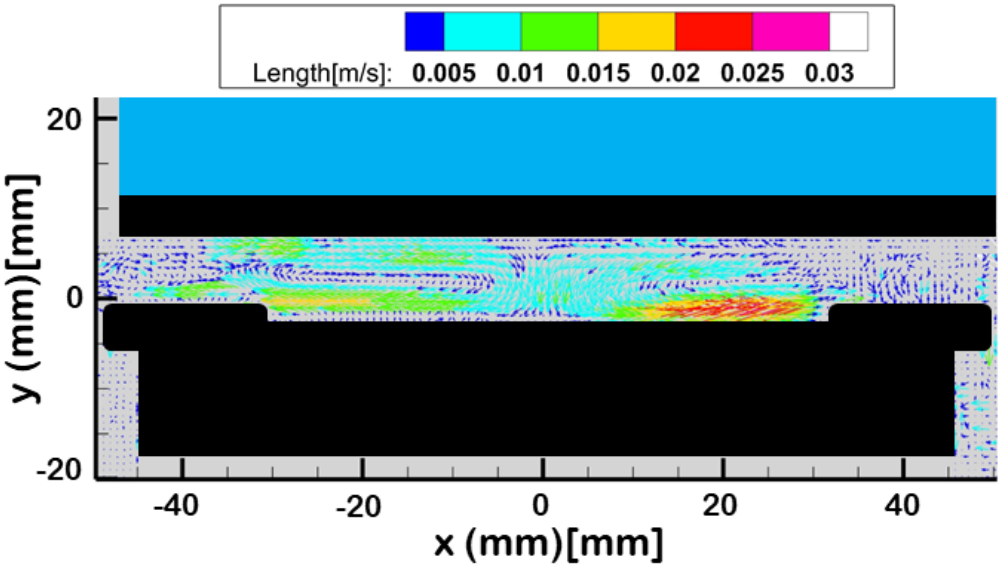

Figure 4.12: Velocity Field for $1500W - 40\%H_2$

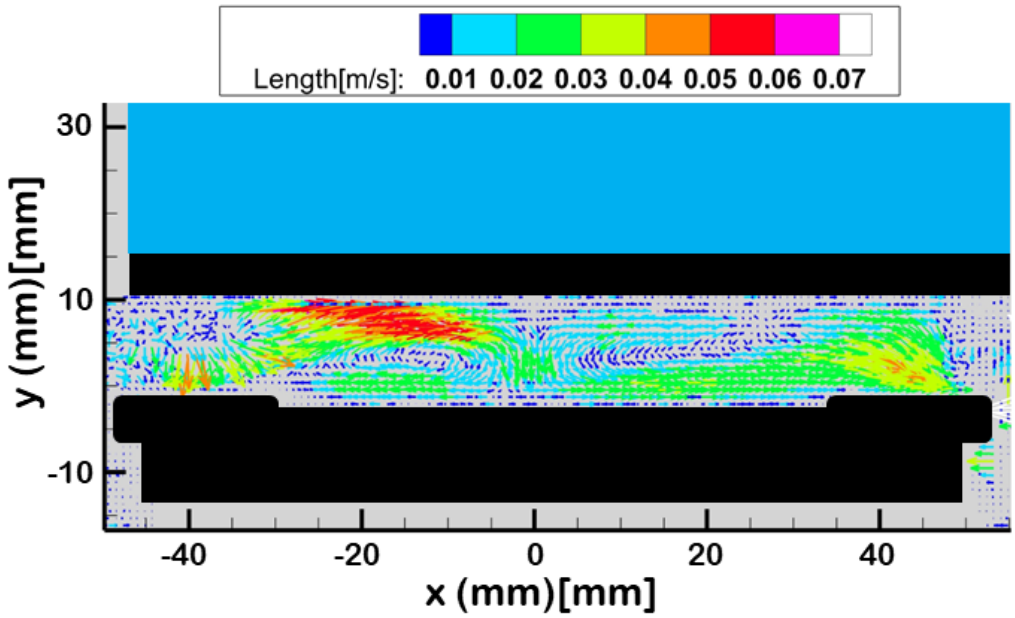

Figure 4.13: Velocity Field for $3000W - 40\%H_2$

In fact, the previously called interesting phenomenon can be explained by the following reasons. At first, the temperature measurement revealed that, as the flow is closer to the centre its temperature decreases. Actually, one of the heat transfer principles behind the process of heating the pan stands that, as the flow advances, it is losing energy to the base of the pan. In addition, the flow closer to the bottom of the pan should be less hot than the flow closer to the burner head. The principles of thermodynamics [81] state that, at a constant pressure, a temperature decrease of a certain gas will be followed by an increase on its density. Therefore, the density of the higher part of the flow becomes higher as it approaches the centre of the pan bottom. This, combined with the fact that the flow from opposite directions meets at the center, causes the flow reaching the center to move downwards to the burner head. Then, as it gets

near the surface of the burner head, the flow turns in the opposite direction to the one it came from at the beginning. It keeps on moving back, towards the edge of the burner head, where it meets the vortex. Afterwards, it ends up joining the new exit flow coming from the burner holes and moving towards the pan edge.

Actually, figure 4.14 is a zoomed view of the center region of figure 4.12 for $1500W - 40\%H_2$, so that the turn in the flow's direction can be easily visualised.

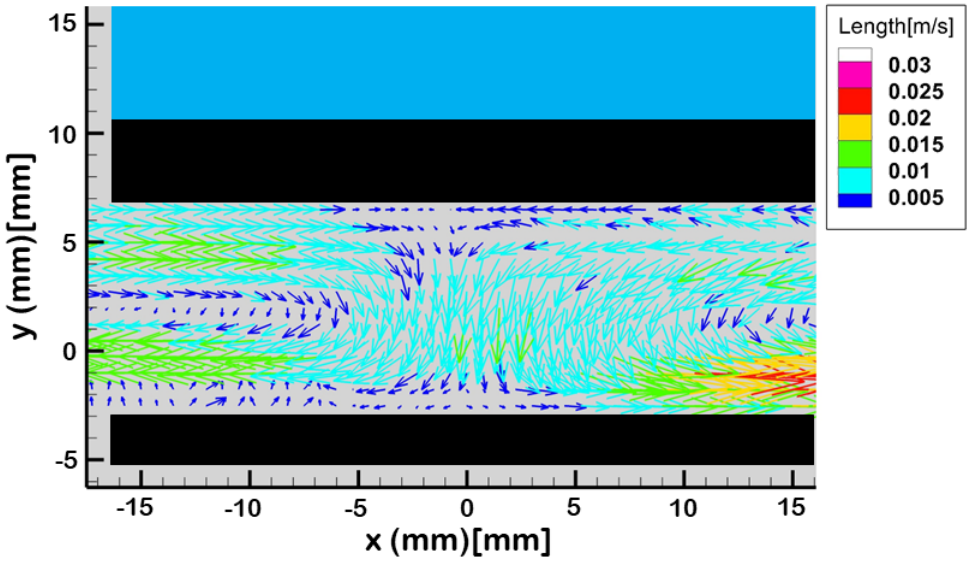

Figure 4.14: Zoomed View for $1500W - 40\%H_2$

These results were affected by the reflections, due to the experimental display of the aluminium blocks supporting the pan. Which, made it difficult to achieve a total uniformity of results. Sometimes a certain zone displayed the larger vectors, sometimes the same zone displayed a loophole on the velocity field. In particular, the region of the edge of the burner head was seriously jeopardised, making it impossible to record the vortex or even sometimes the incoming flow. In addition, the time between pulses was decreased, in order to ensure a clear visualization of the smaller vectors (lower velocities), which implies not properly recording larger vectors (higher velocities).

Still, an unique attempt of recording the vortex under special conditions was rewarded with figure 4.15, as a zoomed view, entirely focused on the left side vortex. In fact, the time between pulses was adjusted to as short as possible, which fosters the recording of fast flow regions, while sacrificing the visualization of slow flow regions. Hence, the figure stops displaying vectors the further way from the vortex and the closer to the vortex center. Still, for the slow region, it was possible to compare the results with the one obtained for the figure 4.11, under the same hydrogen and power conditions. Although it isn't possible to visualize in the figure bellow, the direction of the vectors remained much the same, traducing the same flow behaviour. Plus, again, the magnitude of the vectors near the symmetrical axis ranged between approximately $0.01 - 0.05m/s$. Whereas, for the region near the inside rim edge of the burner head ($X \approx -25$), the velocity proved to be slightly higher, approximately $0.1m/s$ instead of the $0.07m/s$ identified above.

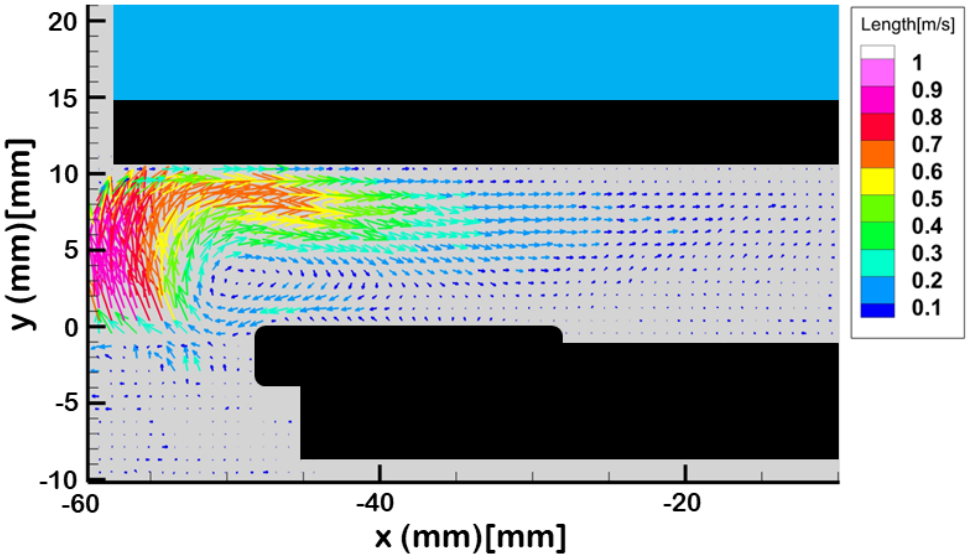

Figure 4.15: Vortex for $3000W - 0\%H_2$

Nevertheless, the vector map of the vortex resulted quite different from that shown in the results for the outer region. It is now possible to visualise in detail, a clear evolution of the velocity magnitude as the flow travels through the vortex. Actually, before, the vortex vectors displayed uniform velocities ranging approximately between $0.01m/s - 0.20m/s$. Now, it turns out that the vortex vectors display several velocities, ranging from approximately $0.01m/s$ up to a momentary $1.00m/s$. However, it's important to recall that this experiment was entirely focused on recording the vortex. Thus, the camera lens could be adjusted to capture a much narrower and therefore more focused window. Nonetheless, the vortex created by the interaction of the flow exiting the burner holes with the burner head, ends up playing a pivotal role accelerating the flow towards the center of the pan.

Finally, the PIV outcome proved to be priceless to the development of the model 2 introduced in chapter 3. It allowed to better understand the heat transfer process, by revealing not only the existence of a vortex but also of a re-circulation bubble. In addition, it provided data to help mainstreaming the heat transfer process for the other burners. The impact of each heat transfer region can now be quantified, while the cooking efficiency results are properly addressed.

4.4 Heating Time and Cooking Efficiency

Heating Time

Model 1 in section 3.1, explained that the time of the Heating experiments was fundamental to assess the cooking performance. Figure 4.16 shows the cooking time for experiments conducted for $0.5L$ of water, and figure 4.17 shows the same for experiments under $1L$ of water. In both of them, the symbols show the recorded time for each experiment, according to the hydrogen admixture and the operating conditions. The doted lines are the resulting trend of the time evolution.

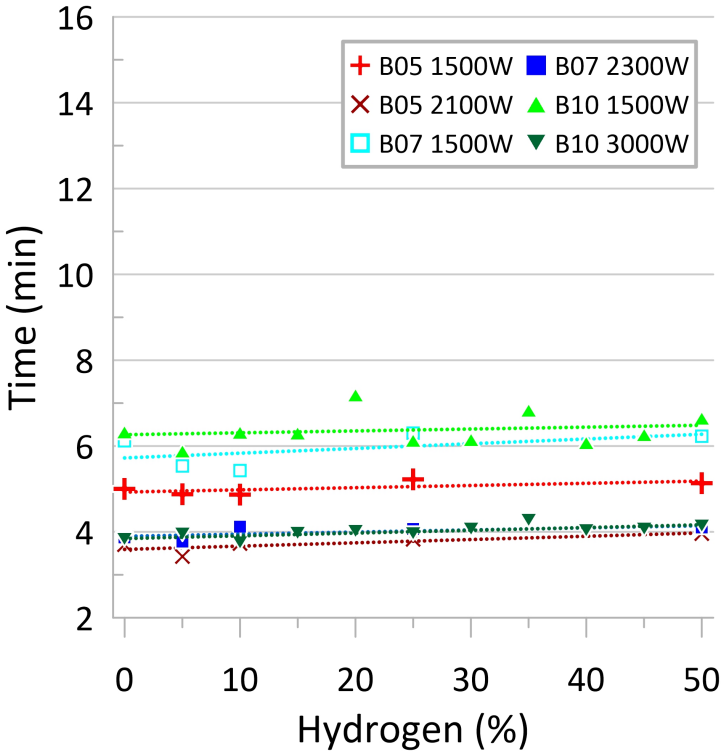

Figure 4.16: Cooking Time for $0.5L$ of Water

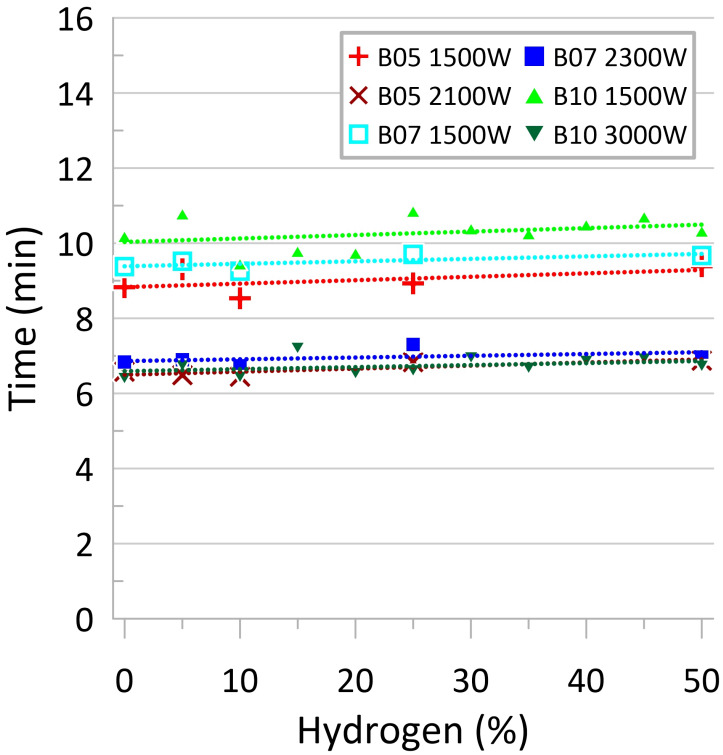

Figure 4.17: Cooking Time for $1L$ of Water

Figures 4.16 and 4.17 show that regardless the water volume and the operating conditions, as the hydrogen percentage increases, there is a slight increase in the time required to heat the water. The

results are consistent with what was observed in the flashback experiments. As the percentage of hydrogen increased, the flames became shorter. Therefore, taking more time to heat the water and leading to the positive slopes of the trend lines. For figure 4.16, most of the experiments lead to approximately a 2% time increase step, for every 10% hydrogen addition. Whereas, for figure 4.17, the time step increase is approximately 1%. Therefore, the smaller the volume of water, the more susceptible it is to time increase in percentage. Still, quantitatively, for figure 4.16 or for figure 4.17, a 2% or a 1% time increase can be translate for both, as an increase between $4s - 7s$, according to the operating conditions. Indeed, the slope of the trends for each figure is very similar. However, figure 4.17 for twice the water volume than figure 4.16, should show close to double of the required time. Yet, for most of cases, the increase was only $\approx 50\%$. Therefore, it proves that the water convection currents play an important role in distributing the heat throughout its entire mass.

Furthermore, from figure 4.16 to 4.17, the order of the time required for each burner operating at a certain condition, remains unchanged. For both figures, the operating conditions of the $B05 - 2100W$, $B07 - 2300W$, $B10 - 3000W$ experiments, lead to a faster water heating. Curiously, for these conditions, all the burners operated at higher powers for which they were designed. Logically, higher powers foster a faster heating process. In fact, the lower power ($1500W$) cases, required more time for the water to reach a boiling state.

At last, in burner $B05$, it was conducted a few experiments simulating slow cooking conditions, by operating the burner at $750W$. Those experiments, required between $24 - 26$ minutes to heat $1L$ of water, until it reached a boiling state. Despite requiring so much time, the slow cooking experiments stand as the most efficient heating process, as will be seen further on.

Cooking Efficiency - Model 1

For the figures 4.18 and 4.19, the symbols show the cooking efficiency for each heating experiment conducted. Whereas, the doted lines show the tendency for a specific operating condition, amid hydrogen admixture.

Actually, both figures show trend lines with negative gradient. Thus, the higher the percentage of hydrogen in the mixture, the less efficient the heating process will be as expected. Such, is coherent with the time results from the figures 4.16 and 4.17. As the more hydrogen, the shorter the flames, and the longer it will take to heat the water. The longer it takes to reach the same boiling state, more energy will be expended. Thus, leading to a less and less efficient heating process.

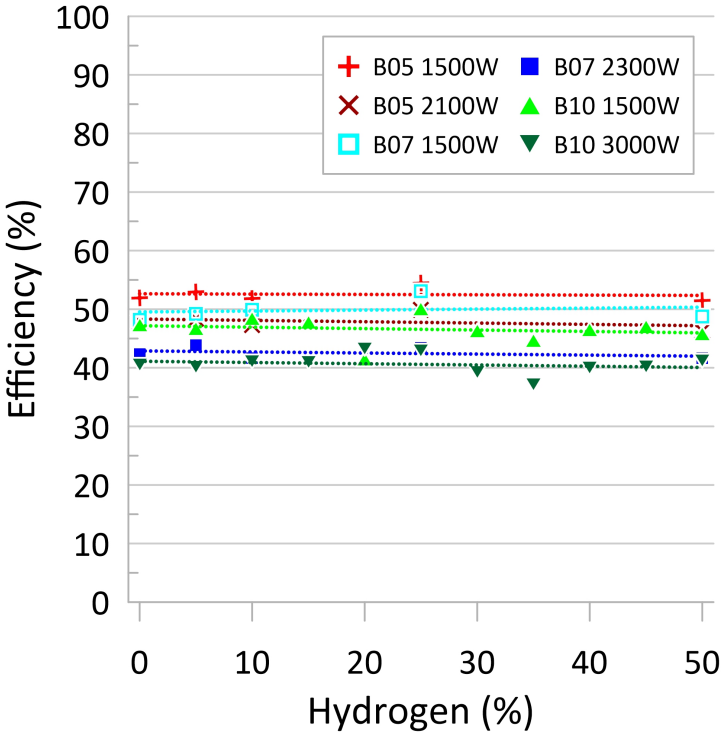

Figure 4.18: Model 1 - Cooking Efficiency for $0.5L$ of Water

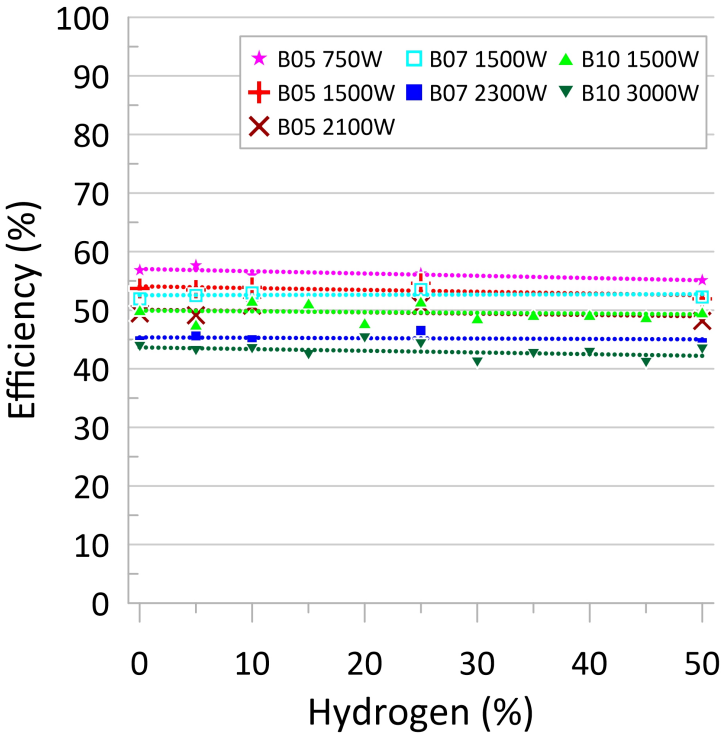

Figure 4.19: Model 1 - Cooking Efficiency for $1L$ of Water

From figure 4.18 to figure 4.19, again the order of the cooking efficiencies for a certain operating condition, remains unchanged. Though, for the same operating condition, the cooking efficiency increases. For instance, the experiment $B10-3000W-1L$ is $\approx 2\%$ more efficient than the experiment $B10-3000W-$

$0.5L$. In fact, in the experiments for $1L$ of water, the cooking efficiency is between $2\% - 3\%$ higher than, the exact same experiment for $0.5L$ of water. Therefore, the effect of the water convection currents, is now proved to be beneficial to the cooking efficiency.

In addition, for both figures, the higher power experiments turned out to be the least efficient, ranging from 40% to 45%. Even though, experiments under higher power are time-saving, as it require less time to heat the water, they are not the most energy efficient. In the meanwhile, experiments conducted at $1500W$ presented efficiencies between $50\% - 55\%$. In figure 4.19, the efficiency of the $B05 - 750W$ experiments, oscillates between $55\% - 58\%$. Thus, proving to be the experiments with the highest cooking efficiency experiments. It clearly shows that, despite requiring a considerable amount of time, slow cooking is more interesting from an energy-driven point of view than fast cooking.

Cooking Efficiency - Model 2

Model 2 led to cooking efficiency results very close to those obtained for model 1. Both figures 4.20 and 4.21, turned out to be very alike to figures 4.18 and 4.19. Clearly, it was possible to obtain similar trend lines, both in terms of the gradient and the range of results. Again, the results respected the previous relation between cooking efficiencies. As low power entails higher efficiency, and high power entails lower efficiency. Plus, just like before, from $0.5L$ to $1L$ of water, the efficiencies range step up between $2\% - 3\%$.

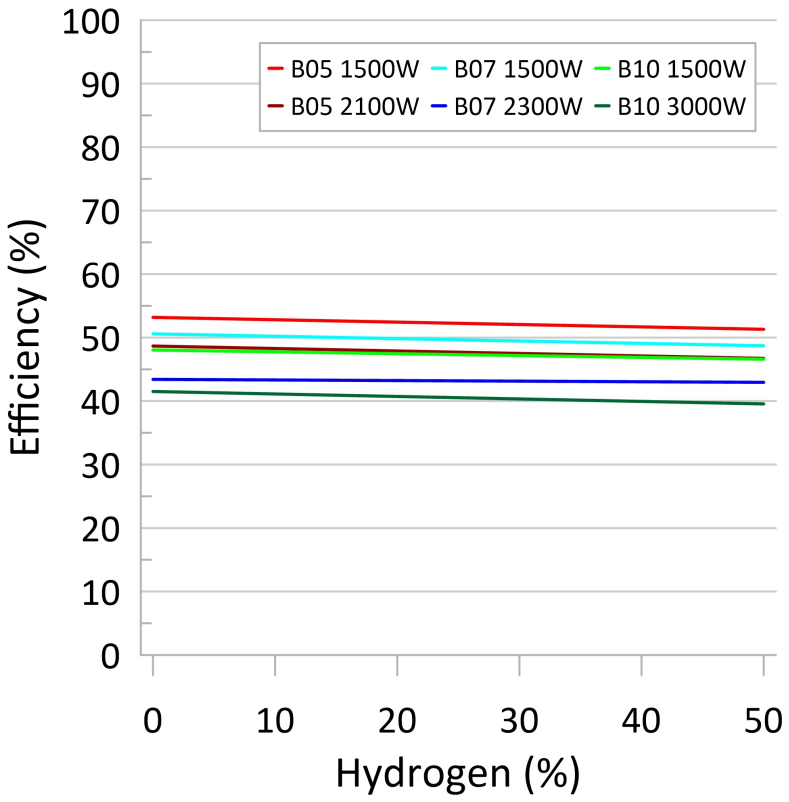

Figure 4.20: Model 2 - Cooking Efficiency for $0.5L$ of Water

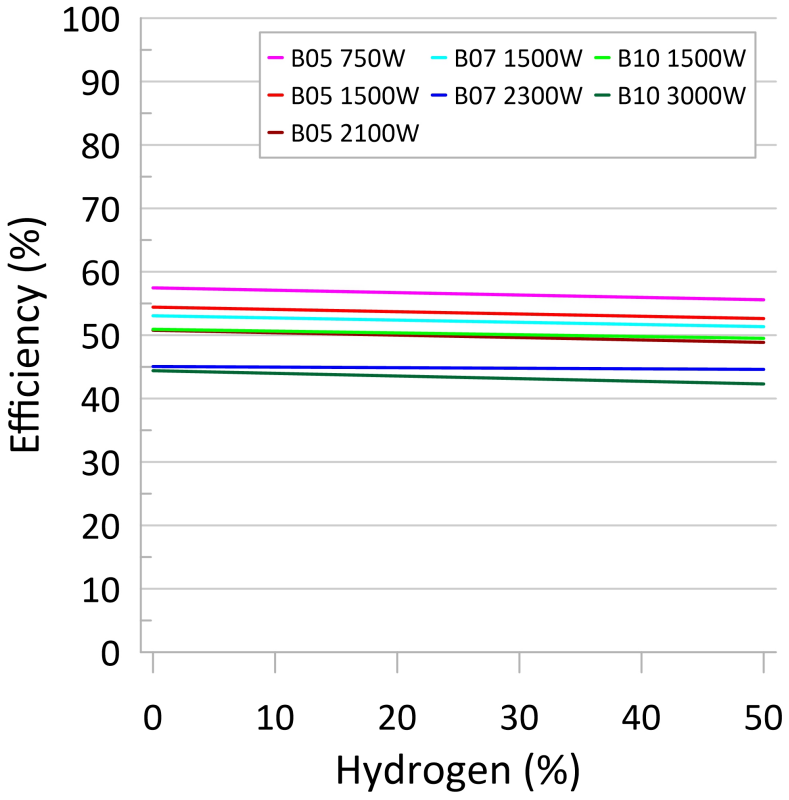

Figure 4.21: Model 2 - Cooking Efficiency for $1L$ of Water

As explained in section 3.2, model 2 allows to quantify the heat transfer rate for each region, according to its nature. In fact, the heat transfer by conduction proved to play a pivotal role on the heat transfer process. Along the experiments, its contribution to the cooking efficiency ranged from 55% up to a remarkable 75%. Therefore, always exceeding the contribution of the heat transfer by convection. The 75% mark was achieved under the $0.5L$ experiments. Since, logically, a less amount of water implies a lower water level. Thus, a lower convection heat rate at the vertical wall of the pan. Figure 4.22, for instance, shows in red the heat rate from conduction and in blue the heat rate from convection. Clearly, despite decreasing as hydrogen percentage increases, the red line is always above the blue line. In fact, as the hydrogen percentage increases, the flames shorten. Therefore, the area of conduction decreases, leading to a lower heat rate by conduction. Curiously, the opposite effect happens to the heat rate from convection. The other lines display the convection heat rate by region and, it can be noted a significant increase in the heat rate of the post flame region (pink line). As the radius of the conduction area gets shorter, the horizontal distance between the flame tips and the edge of the pan bottom gets larger. Therefore, the area of the post flame region increases, which results in a higher rate of heat transfer by convection. In the meanwhile, as the conduction radius decreases, so does the pre flame or inner region radius as well. Therefore, leading to an extremely slight decrease, to the rate of the heat transfer in the pre flame region. Duly displayed by the purple line in figure 4.22.

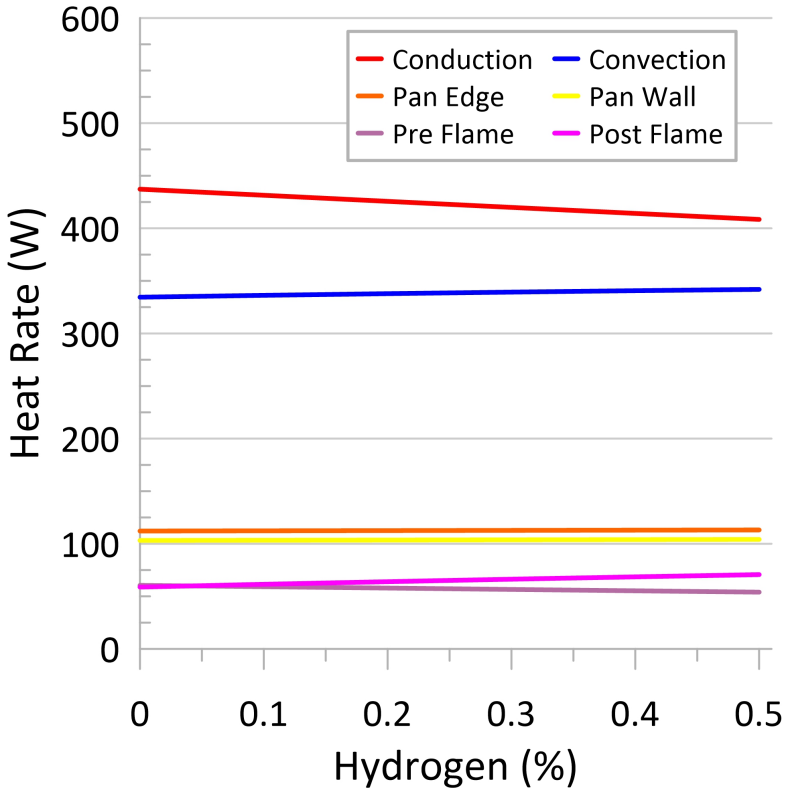

Figure 4.22: Heat Transfer Sources for $B10 - 1500W\ 1L$

It's worth nothing, as hydrogen increases it's expected that the convection heat transfer in both the pan edge and pan wall regions slightly decreases. Even though, in the figure 4.22, the orange and yellow lines convey the that its slope is zero, it's slightly negative. For the time being, the impact on the end user financial costs, due to small variations in the cooking efficiency, is an open question.

Cooking Efficiency Impact on the End User Cost

Bearing in mind the user's point of view, there are 3 main factors that are considered as crucial: the financial cost; the operating time; the type of cooking. The operating time, relies on if the cooking type is either slow cooking or fast cooking. Such, depends on each user, according to its daily routine and cooking intentions. Nonetheless, by knowing the cooking efficiency of both options, it becomes possible to estimate the associated financial cost.

Assuming the average price of $0.09 euros/kWh$ stated in chapter 1, and considering the end user aware for the fact that, putting the lid on the pan shortens the cooking time. Then, under non hydrogen admixture, choosing slow cooking rather than fast cooking or, choosing to heat the water under the $B05 - 750W - 1L - 0\%H_2$ with a 57% efficiency rather then the $B10 - 3000W - 1L - 0\%H_2$ with a 44% efficiency, means that the end user spends 0.0169€ instead of spending 0.0216€. Thus, saving 0.0047€ or $\approx 22\%$ of its costs, each time the end user heats $1L$ of water until it reaches a boiling state.

In the meanwhile, as hydrogen percentage increases the financial gap between both options risks widening. Considering two case scenarios, one assumes that the H_2 price would be $0.12 euros/kWh$, as the best prediction approached in chapter 1. The other scenario assumes the H_2 price equal to

$0.24 euros/kWh$, as the worst prediction. Considering the cooking time and efficiency of two different $NG-H_2$ blends. It becomes possible to determine the financial cost of heating $1L$ of water until $\approx 100°C$, for both case scenarios, and for an end user that prefers slow cooking rather than fast cooking. Table 4.1 uses C^+ to show the best prediction cost and C^- for the worst prediction cost. Note that, the last column on the right shows the cost reduction for each scenario, if the end user chooses slow cooking instead of fast cooking.

Table 4.1: Cooking Prices to the End User

H_2 (%)	Slow cooking (€)	Fast Cooking (€)	Cost Reduction (%)
0	0.0169	0.0216	21.76
20	$C^+ = 0.0174$	$C^+ = 0.0229$	24.02
20	$C^- = 0.0190$	$C^- = 0.0250$	24.00
50	$C^+ = 0.0189$	$C^+ = 0.0253$	25.30
50	$C^- = 0.0243$	$C^- = 0.0326$	25.46

For the best case scenarios, blending hydrogen in the fuel has a low impact on the absolute value for the end user costs. In fact, for $20\%H_2$ mixtures it barely increases. Even for $50\%H_2$ mixtures, it only increases 0.0020€ for slow cooking and 0.0037€ for fast cooking. However, for the worst case scenarios, the increase on the costs absolute value already makes its mark on the overall picture. For blends with $20\%H_2$, the increase could rise until $\approx 12\%$ or to $\approx 16\%$, if it's slow cooking or fast cooking. But for blends with $50\%H_2$, the increase could escalate to $\approx 44\%$ for slow cooking or $\approx 51\%$ for fast cooking.

All in all, the cost forecast is still subject to a very wide range of values. Thus, the best way for the user to minimise its impact, is to adopt more sustainable practices, such as slow cooking. Still, either if slow cooking is the best option or not, depends on each end user financial fund, time availability, or even cooking knowledge. Nonetheless, sustainability is in the spotlight and undeniably, slow cooking is the proper way to address the upcoming future. As so, the development of some method or expression that predicts the cooking efficiency under different operating conditions, could prove to be a very useful tool in the energy saving reality.

4.5 Cooking Efficiency Prediction Function

As mentioned in chapter 3, this study used the Cobb and Douglas production function to match the cooking efficiency obtained by both model 1 and 2. If it proves to be accurate, it may stand as a reliable function, to predict the cooking efficiency amid variations in the input parameters, without requiring an experimental validation.

Eventually, it's important to recall the expression 3.26, $\eta = \alpha P^A R_b^B nh^F R_p^G m_w^J (f_{H_2}+1)^H$, as the mathematical function that led to the most promising results.

Although the independent parameters are the same for both model 1 and 2, the function is able to match more accurately the cooking efficiency of model 2, than the cooking efficiency resulted from model 1. For both figures 4.23 and 4.24, the green line shows the cooking efficiency of model 1 and 2, while the circles show the cooking efficiency given by the mathematical functions (MF). Therefore, the closer the circles are to the green line, the better it is for the accuracy of the results. In addition, the more circles are overlaid on the line, the wider the range of applicability of the modelling function, for predicting the cooking efficiency under conditions more distant from those under which the study was carried out.

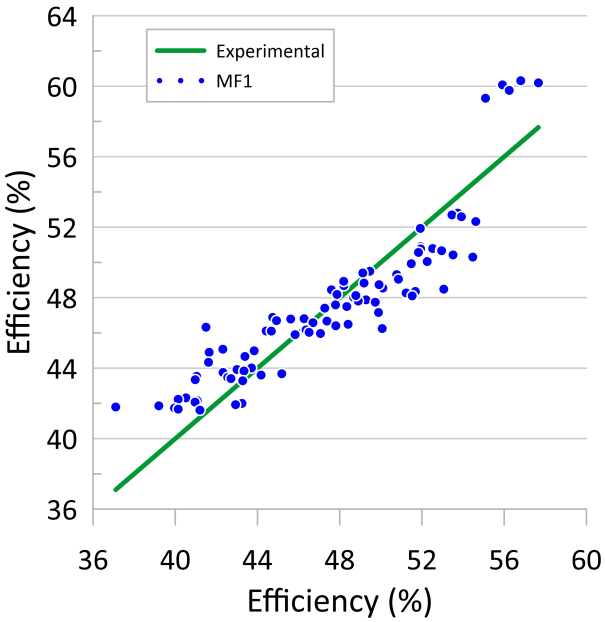

Figure 4.23: Cooking Efficiency of Model 1 VS Modelling Function 1

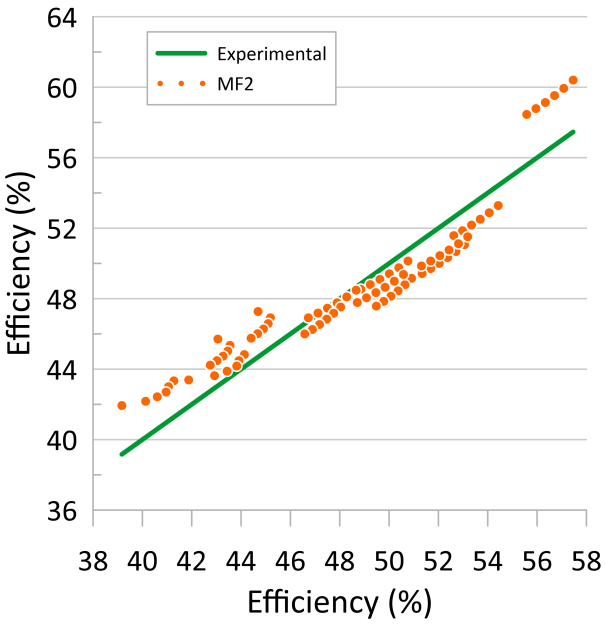

Figure 4.24: Cooking Efficiency of Model 2 VS Modelling Function 2

It is easy to distinguish a clear difference between both figures. In figure 4.23 the circles are way more scattered. Whereas in figure 4.24, the function managed to cope with the trends displayed in figures 4.20 and 4.21, delivering a more organised layout. Even though the cooking efficiency of model 1 displayed a trend, the efficiency data itself did not followed a constant behaviour. In fact, the MF1 function proved to be sensitive to the small random variations in the cooking efficiency of model 1. Such, resulted in a deviation range up to 5, either by default or by overshoot. The function that tries to match model 1 presents a standard relative error of 4%. Yet, the maximum relative error computed was close to 10%. It was for the experiment at the lowest cooking efficiency, $B10 - 3000W - 0.5L$.

The MF2 manage to provide a considerable shorter deviation range, between -2 by default and 3 by overshoot. Nonetheless, the standard relative error remained about 4%. However, the maximum relative error decreased to 6.5%, still for the $B10 - 3000W - 0.5L$ experiment.

It is worth noting that, the function finds it easier to generate accurate results if the cooking efficiency input values follow a more defined pattern, as is the case with model 2. Although R^2 isn't valid to assess the absolute fitness of a non linear regression, it can can be an interesting parameter to compare the fitness between both regressions. For the MF1 (that tries to match the results of model 1), $R^2 = 0.998214$. Whereas, for the MF2, $R^2 = 0.998944$, thus being slightly larger. Again, proving that MF2 is better than MF1. Indeed, there are a few differences between the exponents values of expressions 4.1 and 4.2, as the modelling functions for model 1 and 2.

$$\eta = \frac{100\, m_w^{0.0567076}}{(1+f_{H_2})^{0.0410296}\, P^{0.191894}\, R_b^{0.0796761}\, nh^{0.0653071}\, R_p^{0.273914}} \tag{4.1}$$

$$\eta = \frac{100\, m_w^{0.0487829}\, nh^{0.0562911}\, R_p^{0.0132213}}{(1+f_{H_2})^{0.0806579}\, P^{0.180782}\, R_b^{0.152138}} \tag{4.2}$$

At first, for MF1, J is the only positive exponent, while the remaining exponents are all negative. Therefore, it means that the more water is in the pan, the higher the cooking efficiency, which is in line with the cooking efficiency results obtained for the experiments. However, on the contrary, the higher the remaining parameters, the lower the cooking efficiency. Such, does not complies with some of the conclusions drawn from the previous experiments. Still, the cooking efficiency trend lines were negative as the hydrogen percentage increased. Thus, it supports the fact that hydrogen fraction is rightfully placed in the function denominator. In addition, for the same burner type, higher power resulted in a lower efficiency. Therefore, the power should be and it's in the denominator. The burner radius is also rightfully placed in the denominator, since for the same power, larger sized burners resulted in a lower cooking efficiency. Unfortunately, both the pan radius and the burner exit holes, appear misplaced in the denominator.

From all the results stated so far, it was possible to conclude that the closer the flames are to the edge of the pan, the lower the cooking efficiency. Logically, under the same operating conditions, the larger the pan radius, the further way the flames from the edge of the pan bottom. Thus, the higher the expected cooking efficiency. Along the same line, for the same burner power, as the number of exit holes increases, the lower the flow exit velocity. Thus, the less the flames stretch, being further away from the edge of the

pan bottom. Therefore, the more exit holes there are, the higher the cooking efficiency. Ultimately, the cooking efficiency is directly proportional to both the pan radius and the number of burner exit holes. Therefore, they should be part of the modelling function numerator.

On the other hand, for MF2, J, F and G are all positive exponents, whereas A, B and H are negative exponents. Thus, for this function, the cooking efficiency is higher the more water there is in the pan, the more burner exit holes there are and the larger the radius of the pan. For once, the cooking efficiency is also higher as the less hydrogen is admitted, the lower the burner power and the smaller the burner radius. Now, the function for model 2 not only provides more accurate results but also, it is coherent with the facts described above. Remarkably, the burner power and radius are the independent variables that have the most effect upon the cooking efficiency, since they present by far the higher exponents. On the contrary, both the water mass and the pan radius display a very small effect on the cooking efficiency, since they are parameters not that much explored in the experimental process. In particular, it was only used a single pan, as it is stated in chapter 2. Still, the overall exponent value is equal to -0.2952826. While, for MF1 it is equal to -0.5951132. Thus, doubling the independent variables for MF1, results in a significant higher decrease on the cooking efficiency.

Although for both modelling functions, the relative error was not that significant, efforts were made to improve the functions. So that, the absolute deviation decreased. In fact, it was found out that, the it may not be interesting to incorporate the cooking efficiency data of the experiment that most reflects slow cooking, the $B05 - 750W$. Though, for the refined modelling function 1 (RMF1), figure 4.25 shows an arrangement as much or even more scattered than the one previously in figure 4.23. However, for the RMF2, figure 4.26 already displays a distinct advantage, by not incorporating the symbols of the $B05 - 750W$ experiment. Indeed, from figure 4.24 to figure 4.26, the orange circles came really close to the green line. Even sometimes ended up overlapping completely one another, which is known to be an excellent prelude to very promising results.

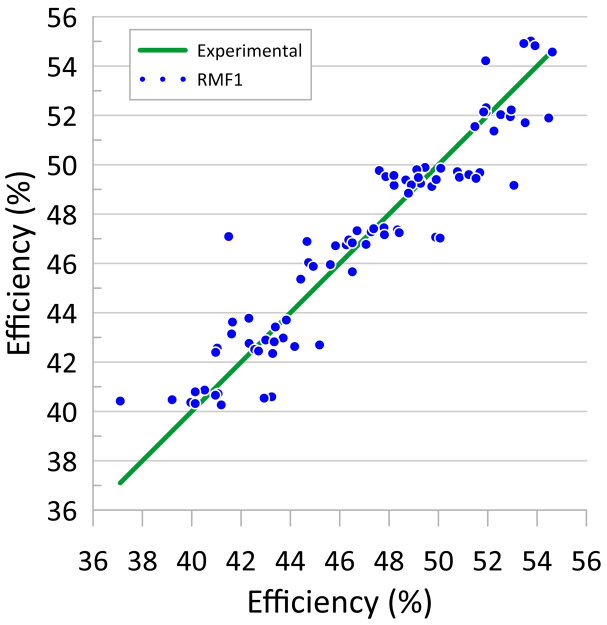

Figure 4.25: Cooking Efficiency of Model 1 VS Refined Modelling Function 1

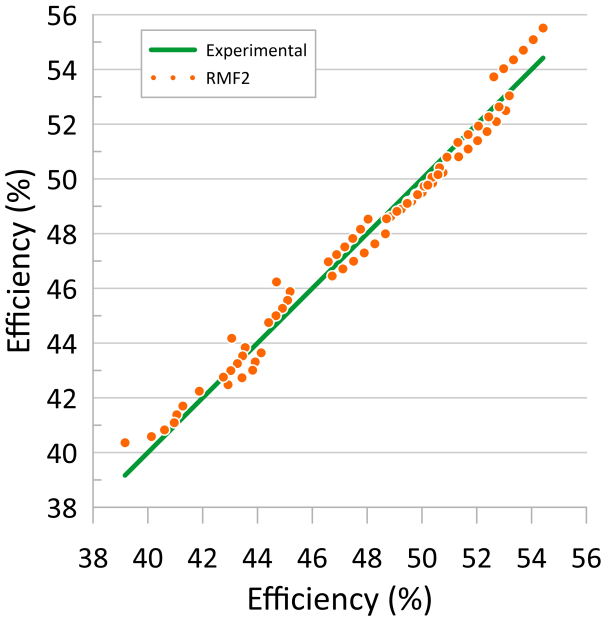

Figure 4.26: Cooking Efficiency of Model 2 VS Refined Modelling Function 2

For the RMF1, the standard deviation slightly decreased, though the maximum deviation clearly increased. Nonetheless, the decrease in the standard deviation, was rewarded with a $R^2 = 0.999053$. Thus, slight higher than the previously $R^2 = 0.998214$, for the MF1.

In the meanwhile, for the RMF2 the deviation range remarkably decreased by half. It is now between -0.9 by default and 1.5 by overshoot. Therefore, both the maximum and the standard errors substantially decreased. The first from 6.5% to 2%, and the second from 4% to 1.1%. Logically, the R^2 value proved to be favourable to the modelling function without the $B05 - 750W$ data. Now $R^2 = 0.999862$, while before $R^2 = 0.998944$. As so, the best fitted modelling function is the RMF2 > RMF1 > MF2 > MF1.

The different reality on the deviation for the RMFs, was followed by a few adjustments on the exponents values. The most relevant was for the RMF1. Since, unlike before, it now has the number of exit holes in the numerator, as it is given by expression 4.3. It is a step forward, to more correctly represent the relationship of the independent variables with the cooking efficiency. Even though, despite decreasing its effect, as its exponent is lower, the pan radius remained in the denominator. Thus, the RMF1 still doesn't fulfill all the physics behind the heat transfer process. Noteworthy, both the burner power and particularly the burner radius, have now a major impact on the cooking efficiency. The sum of the exponents for the RMF1 is -0.5557426. Although slightly lower then for the original MF1, it still traduces the same trend.

$$\eta = \frac{100\, m_w^{0.0725677}\, nh^{0.101351}}{(1+f_{H_2})^{0.0362993}\, P^{0.290599}\, R_b^{0.20681}\, R_p^{0.195953}} \tag{4.3}$$

Expression 4.4 for the RMF2, respected the appropriate relationship between the variables, as all remained in the same positions as before. Moreover, the number of exit holes, which once was not that relevant, now plays a significant part. Its exponent almost quadrupled, following what has been argued as its rightful importance. The burner power and the burner radius also assumed even more importance,

since its exponents value almost doubled. In the meanwhile, the pan radius exponent is now almost zero, which in a certain way is fair given that all data have the same value for that variable. Even though the exponent of the water mass increased, considering the overall increase in all the exponents, it ended up losing 22% of its relevance in the cooking efficiency. Apart from all that, the hydrogen fraction slightly decreased its weight. Though soon in section 4.4, it was clear that the hydrogen admixture as a low impact in the cooking efficiency. The sum of the exponents for the RMF2 is -0.362977. This time slightly higher then for the original MF2, still also traducing the same trend.

$$\eta = \frac{100\, m_w^{0.0657813}\, nh^{0.211938}\, R_p^{0.0000517512}}{(1+f_{H_2})^{0.0805429}\, P^{0.296993}\, R_b^{0.263212}} \tag{4.4}$$

After all, both modelling functions benefit from not including the $B05-750W$ experiment. In fact, RMF2, manages to provide extremely reliable results. For the RMF1, the improvement had a minor advantage on the standard error but, from the physics point of view of the heat transfer process, it greatly enhanced the credibility of the expression.

Finally, the best function to predict the cooking efficiency of a cooktop burner, operating under certain conditions, is the MF2. It led to more accurate and consistent results than the MF1. Besides, its expression proves to properly interpret the effect of each independent variable on the cooking efficiency. However, if one wants to obtain results for a shorter applicability range, and at the same gives more importance to small variations in the cooking efficiency, then the RMF2 is the most suitable tool. Since, it accurately predicts the cooking efficiency, thus achieving the best fit between closer operating options.

Chapter 5

Conclusions

The main goal of the current work was to assess the impact of hydrogen and natural gas blends on the performance of domestic cooktop burners. The interchangeability of domestic cooktop burners was defined by its capacity to safely perform usual functions, while delivering the expected outcome, without requiring any further adjustments. Thus, there are interchangeability parameters regarding the safety of the appliance and its fitness for purpose. The safety parameters are concerned about issues that might shorten the life time of the appliance or even jeopardise the end user healthy. In this framework, flame stability plays an important role to avoid flashback issues, and to minimize noises dangerous for the end user hearing. The main fitness for purpose parameters concerning the end user are both the cooking efficiency, under which the appliance performs, and the associated financial cost.

To this end, several experiments fuelled by mixtures from 0% to 80% H_2 were conducted: flashback risk experiments in order to realize which mixtures made the flames become unstable; burner noise experiments to quantify the sound pollution and how harmful the noise caused by the flames can be; water heating experiments to determine the cooking efficiency; PIV experiments to understand the flow behaviour and provide a different approach (stated in section 3.2) able to determine the cooking efficiency. Given that today, there is a wide range of operating conditions under which a domestic cooktop burner can operate, it was given a special attention to the effect of the burner power and size on the interchangeability parameters. Such operating conditions, were explored by conducting the experiments above through out 3 different sized burners working under several powers.

The cooking efficiency impact on the financial cost, was finally addressed by using the obtained fuel consumption for slow cooking versus fast cooking experiments, considering NG and H_2 prices both now and in the future. At last, the efficiency results were combined into an overall expression (introduced in section 3.3 and further analysed in section 4.5) that uses as input operating conditions, and provides the expected cooking efficiency as the output. In fact, 2 promising models were developed, so that the cooking efficiency of a domestic cooktop burner, working under different operating conditions, can be predicted without requiring an experimental procedure.

5.1 Achievements

The experiments conducted and the post analyses led to plenty of valuable results, which allowed to achieve interesting conclusions. Most of them were discussed along the chapter 4 yet, some of them together with important insights are listed in the following points:

1. It was detected flashback for $\approx 50\%NG - 50\%H_2$ mixtures, for all 3 burners. Still, there were no significant changes in the flames stability until $\approx 25\%H_2$ admixture. Therefore, the study suggests that the cooktop burner can safely operate under up to $\approx 20\%H_2$ admixture.

2. The burning noise steadily increases as the hydrogen percentage in the fuel mixture increases (figure 4.4 (b)). In addition, when larger domestic burners (designed to operate up to a maximum of $3000W$) are powered from $25\%H_2$ mixtures onwards, it start to emit noise within the range of the extremely loud. Such, is not advisable and is labelled within the danger zone.

3. The cooking efficiency slightly decreases, as the hydrogen percentage in the fuel mixture increases. Still, it doesn't puts at risk the thermal output. Therefore, the cooking efficiency parameter is proved to be ensured amid hydrogen.

4. Slow cooking revealed a cooking efficiency $\approx 15\%$ higher than fast cooking, which puts it on the path to sustainability. In addition, slow cooking saves up to 25% of the costs associated with fast cooking.

5. Considering the best and worst predictions of the hydrogen cost to the end user, it was possible to determine the financial cost of using the cooktop burner fuelled by up to $50\%H_2$ mixtures. In fact, it's expected to rise between 3% and 51% (table 4.1), according to both the percentage of hydrogen and if the end user is aware of efficient cooking practises. Still, it's strongly believed that in a matter of time hydrogen will be competitive. For now, financially, the appliance's fitness for purpose is only ensured for mixtures with small percentages of hydrogen.

6. It was determined that small variations in the cooking efficiency (between $0\% - 3\%$), have almost non significant impact on the financial cost of cooking. Therefore, probably using the modelling function 2 is the best option to predict the cooking efficiency accurately, for a wider range of cases.

5.2 Future Work

The current work led to a study focused on the interchangeability limits of hydrogen admission for a domestic cooktop burner. Though, it turned out exploring the impact of several operating conditions on the cooking efficiency. Nonetheless, it remains a topic with much to explore, which will hopefully result in a few improvements in the work undertaken. The 3 following points are the most pertinent to be addressed.

1. The movement of water inside the pan (convection currents), proved to be a mechanism that fosters a higher cooking efficiency. In addition, slow cooking revealed to be the path to sustainability. Therefore, a study focused on the convection currents, may be an interesting way to discover solutions in order to improve the cooking efficiency.

2. The functions developed to predict the cooking efficiency (section 4.5) could be improved, by a study focused on operating conditions further way from the explored. In particular, the height of the pan, the distance between the burner head and the pan bottom, and larger pans dimensions should be deeper explored.

3. Hydrogen has emerged as a solution to the environmental problems of GHGs emissions. However, it's still important to study the risk of producing NO_x emissions.

Bibliography

[1] C. for Climate and E. Solutions. Global emissions, 2013. https://www.c2es.org/content/international-emissions/.

[2] H. Ritchie and M. Roser. co_2 and greenhouse gas emissions. *Our World in Data*, 2020. https://ourworldindata.org/co2-and-other-greenhouse-gas-emissions.

[3] G. Dubois, B. Sovacool, C. Aall, M. Nilsson, C. Barbier, A. Herrmann, S. Bruyère, C. Andersson, B. Skold, F. Nadaud, et al. It starts at home? climate policies targeting household consumption and behavioral decisions are key to low-carbon futures. *Energy Research & Social Science*, 52:144–158, 2019.

[4] E. Commission. Europe energy statistics explained, 2020. https://ec.europa.eu/eurostat/statistics-explained/index.php?title=Energy.

[5] Statista. Energy idustry in europe, 2020. $https://www.statista.com/map/europe/branch/energy-environment$.

[6] IRENA. Majority of new renewables undercut cheapest fossil fuel on cost, 2020. $https://www.irena.org/newsroom/pressreleases/2021/Jun/Majority-of-New-Renewables-Undercut-Cheapest-Fossil-Fuel-on-Cost$.

[7] M. Roser. Why did renewables become so cheap so fast? *Our World in Data*, 2020. https://ourworldindata.org/cheap-renewables-growth.

[8] R. Falkner. The paris agreement and the new logic of international climate politics. *International Affairs*, 92(5):1107–1125, 2016.

[9] H. Chen, J. Song, and J. Zhao. Synergies between power and hydrogen carriers using fuel-cell hybrid electrical vehicle and power-to-gas storage as new coupling points. *Energy Conversion and Management*, 246:114670, 2021.

[10] A. Rabiee, A. Keane, and A. Soroudi. Green hydrogen: A new flexibility source for security constrained scheduling of power systems with renewable energies. *international journal of hydrogen energy*, 46(37):19270–19284, 2021.

[11] F. T. Röben, N. Schöne, U. Bau, M. A. Reuter, M. Dahmen, and A. Bardow. Decarbonizing copper production by power-to-hydrogen: A techno-economic analysis. *Journal of Cleaner Production*, 306: 127191, 2021.

[12] Y. Xie, Y. Cui, D. Wu, Y. Zeng, and L. Sun. Economic analysis of hydrogen-powered data center. *International Journal of Hydrogen Energy*, 46(55):27841–27850, 2021.

[13] U. E. I. Administration. How natural gas is used in the united states, 2020. *https* : $//www.eia.gov/energyexplained/natural-gas/use-of-natural-gas.php$.

[14] H. Council. Path-to-hydrogen-competitiveness, 2020. *https* : $//hydrogencouncil.com/wp-content/uploads/2020/01/Path-to-Hydrogen-Competitiveness_Full-Study-1.pdf$.

[15] G. H. C. Reduction. Scaling up electrolysers to meet the 1.5 c climate goal. *Abu Dhabi (UAE): International Renewable Energy Agency (IRENA)*, 2020.

[16] I. A. Gondal. Hydrogen integration in power-to-gas networks. *International journal of hydrogen energy*, 44(3):1803–1815, 2019.

[17] H. de Vries, A. V. Mokhov, and H. B. Levinsky. The impact of natural gas/hydrogen mixtures on the performance of end-use equipment: Interchangeability analysis for domestic appliances. *Applied energy*, 208:1007–1019, 2017.

[18] B. British Petroleum Company. Statistical review of world energy, 2021. https://www.bp.com/en/global/corporate/energy-economics/statistical-review-of-world-energy.html.

[19] M. R. Hannah Ritchie and P. Rosado. Energy. *Our World in Data*, 2020. https://ourworldindata.org/energy.

[20] IRENA. Solar costs evolution, 2019. *https* : $//www.irena.org/Statistics/View-Data-by-Topic/Costs/Solar-Costs$.

[21] N. R. E. Laboratory. Photovoltaic research efficiency, 2020. *https* : $//www.nrel.gov/pv/cell-efficiency.html$.

[22] P. A. A. Jorge. Solar pv evolution in portugal: Facts, 2021. *https* : $//www.apren.pt/contents/communicationpressrelease/artigo-de-opiniao--evolucao-energia-solar-em-portugal-4283.pdf$.

[23] S. P. Europe. Eu market outlook for solar power 2021-2025, 2021.

[24] E. Commission. Renewable energy statistics, 2020. *https* : $//ec.europa.eu/eurostat/statistics-explained/index.php?title=Renewable_energy_statistics$.

[25] P. E. Ministry. Programa de apoio edifícios+sustentáveis, 2021. *https* : $//www.fundoambiental.pt/apoios-prr/paes-2021.aspx$.

[26] E. Commission, J. R. Centre, J. Olivier, D. Guizzardi, E. Schaaf, E. Solazzo, M. Crippa, E. Vignati, M. Banja, M. Muntean, G. Grassi, F. Monforti-Ferrario, and S. Rossi. *GHG emissions of all world : 2021 report*. Publications Office, 2021.

[27] E. G. Hertwich and G. P. Peters. Carbon footprint of nations: a global, trade-linked analysis. *Environmental science & technology*, 43(16):6414–6420, 2009.

[28] D. Ivanova, K. Stadler, K. Steen-Olsen, R. Wood, G. Vita, A. Tukker, and E. G. Hertwich. Environmental impact assessment of household consumption. *Journal of Industrial Ecology*, 20(3):526–536, 2016.

[29] I. E. Agency. Iea energy and carbon tracker 2020, 2020. https://www.iea.org/countries/portugal.

[30] E. U. A. for the Cooperation of Energy Regulators. Gas factsheet, July 2021. $https : //www.acer.europa.eu/gas - factsheet$.

[31] DGEG. Natural gas balance, December 2020.

[32] IEA. Co2 emissions by source, 2020. $https : //iea.blob.core.windows.net/assets/c3086240 - 732b - 4f6a - 89d7 - db01be018f5e/GlobalEnergyReviewCO2Emissionsin2021.pdf$.

[33] M. Kayfeci, A. Keçebaş, and M. Bayat. Hydrogen production. In *Solar hydrogen production*, pages 45–83. Elsevier, 2019.

[34] A. V. Da Rosa and J. C. Ordóñez. *Fundamentals of renewable energy processes*. Academic Press, 2021.

[35] V. Singh and D. Das. Potential of hydrogen production from biomass. *Science and engineering of hydrogen-based energy technologies*, pages 123–164, 2019.

[36] M. H. McCay and S. Shafiee. Hydrogen: An energy carrier. In *Future Energy*, pages 475–493. Elsevier, 2020.

[37] P. Breeze. *Power system energy storage technologies*. Academic Press, 2018.

[38] M. David, C. Ocampo-Martínez, and R. Sánchez-Peña. Advances in alkaline water electrolyzers: A review. *Journal of Energy Storage*, 23:392–403, 2019.

[39] A. B. T. Nelabhotla, D. Pant, and C. Dinamarca. Power-to-gas for methanation. In *Emerging Technologies and Biological Systems for Biogas Upgrading*, pages 187–221. Elsevier, 2021.

[40] IEA. Hydrogen in north-western europe, April 2021. https://www.iea.org/reports/hydrogen-in-north-western-europe.

[41] B. Widera. Renewable hydrogen implementations for combined energy storage, transportation and stationary applications. *Thermal Science and Engineering Progress*, 16:100460, 2020.

[42] IRENA. Hydrogen:a renewable energy perspective, September 2019. $https : //www.irena.org/ - /media/Files/IRENA/Agency/Publication/2019/Sep/IRENA_Hydrogen_2019.pdf$.

[43] E. Commission, D.-G. for Energy, J. Cihlar, A. Villar Lejarreta, A. Wang, F. Melgar, J. Jens, P. Rio, and K. Leun. *Hydrogen generation in Europe : overview of costs and key benefits*. Publications Office, 2020. doi: doi/10.2833/122757.

[44] C. Fetting. The european green deal. *ESDN Office: Vienna, Austria*, 2020.

[45] G. Kakoulaki, I. Kougias, N. Taylor, F. Dolci, J. Moya, and A. Jäger-Waldau. Green hydrogen in europe–a regional assessment: Substituting existing production with electrolysis powered by renewables. *Energy Conversion and Management*, 228:113649, 2021.

[46] P. Government and DGEG. Roteiro e plano de ação para o hidrogénio em portugal, December 2019. $https://www.ap2h2.pt/download.php?id = 178$.

[47] O. Schmidt, A. Gambhir, I. Staffell, A. Hawkes, J. Nelson, and S. Few. Future cost and performance of water electrolysis: An expert elicitation study. *International journal of hydrogen energy*, 42(52): 30470–30492, 2017.

[48] K. Schoots, F. Ferioli, G. Kramer, and B. Van der Zwaan. Learning curves for hydrogen production technology: an assessment of observed cost reductions. *International Journal of Hydrogen Energy*, 33(11):2630–2645, 2008.

[49] IRENA. Green hydrogen cost reduction, 2020. https://www.irena.org/publications/2020/Dec/Green-hydrogen-cost-reduction.

[50] E. R. dos Serviços Energéticos. Natural gas price - report, 2021.

[51] T. Economics. Europe natural gas price, 2022. https://tradingeconomics.com/commodity/eu-natural-gas.

[52] H. Europe. The colors of hydrogen, 2022. https://hydrogen.revolve.media/colors/.

[53] A. E. Research. Shades of green (hydrogen) - part 2, February 2022. $https://auroraer.com/wp-content/uploads/2022/02/Aurora_Jan22_EU_hydrogen_Shades Of Green-part2_public Report.pdf?fbclid = IwAR3sUbajNjdBLmyAUNWQQhodgIdsIUYoTmZQxd6II56OU-R_hWSSCxfDezs$.

[54] H. R. N. Jones. *The application of combustion principles to domestic gas burner design*. Taylor & Francis, 1989.

[55] CEN. En iso 6976:2005(e). natural gas – calculation of calorific values, density, relative density and wobbe index from composition, 2005.

[56] CEN. En iso 6976:2016(e). natural gas — calculation of calorific values, density, relative density and wobbe indices from composition, 2016.

[57] G. Yu, C. Law, and C. Wu. Laminar flame speeds of hydrocarbon+ air mixtures with hydrogen addition. *Combustion and flame*, 63(3):339–347, 1986.

[58] S. Zheng, X. Zhang, J. Xu, and B. Jin. Effects of initial pressure and hydrogen concentration on laminar combustion characteristics of diluted natural gas–hydrogen–air mixture. *International journal of hydrogen energy*, 37(17):12852–12859, 2012.

[59] H. De Vries, O. Florisson, and G. Tiekstra. Safe operation of natural gas appliances fuelled with hydrogen & natural gas mixtures (progress obtained in the naturalhy-project). 2007.

[60] H. Levinsky. Limitations on h2 addition to natural gas. In *Proceedings Natural Gas Technologies II Conference, GTI-04/0012*, volume 4268, 2004.

[61] Y. Zhao, V. McDonell, and S. Samuelsen. Experimental assessment of the combustion performance of an oven burner operated on pipeline natural gas mixed with hydrogen. *International Journal of Hydrogen Energy*, 44(47):26049–26062, 2019.

[62] J. Hinrichs, M. Hellmuth, F. Meyer, S. Kruse, M. Plümke, and H. Pitsch. Investigation of nitric oxide formation in methane, methane/propane, and methane/hydrogen flames under condensing gas boiler conditions. *Applications in Energy and Combustion Science*, 5:100014, 2021.

[63] F. Schiro, A. Stoppato, and A. Benato. Modelling and analyzing the impact of hydrogen enriched natural gas on domestic gas boilers in a decarbonization perspective. *Carbon Resources Conversion*, 3:122–129, 2020.

[64] S. Choudhury, V. G. McDonell, and S. Samuelsen. Combustion performance of low-nox and conventional storage water heaters operated on hydrogen enriched natural gas. *International Journal of Hydrogen Energy*, 45(3):2405–2417, 2020.

[65] G. L. Basso, B. Nastasi, D. A. Garcia, and F. Cumo. How to handle the hydrogen enriched natural gas blends in combustion efficiency measurement procedure of conventional and condensing boilers. *Energy*, 123:615–636, 2017.

[66] Y. Zhao, V. McDonell, and S. Samuelsen. Influence of hydrogen addition to pipeline natural gas on the combustion performance of a cooktop burner. *International Journal of Hydrogen Energy*, 44 (23):12239–12253, 2019.

[67] C. Karunanithy and K. Shafer. Heat transfer characteristics and cooking efficiency of different sauce pans on various cooktops. *Applied Thermal Engineering*, 93:1202–1215, 2016.

[68] M. Wichangarm, A. Matthujak, T. Sriveerakul, S. Sucharitpwatskul, and S. Phongthanapanich. Investigation on thermal efficiency of lpg cooking burner using computational fluid dynamics. *Energy*, 203:117849, 2020.

[69] E. Gimeno-Escobedo, A. Cubero, J. S. Ochoa, and N. Fueyo. A reduced mechanism for the prediction of methane-hydrogen flames in cooktop burners. *International Journal of Hydrogen Energy*, 44(49): 27123–27140, 2019.

[70] Y. Zhao, S. Choudhury, and V. McDonell. Influence of renewable gas addition to natural gas on the combustion performance of cooktop burners. In *ASME International Mechanical Engineering Congress and Exposition*, volume 52118, page V08AT10A012. American Society of Mechanical Engineers, 2018.

[71] F.-N. Consultancy. Hydrogen appliances, 2018. https://www.fnc.co.uk/resources/a-study-exploring-the-challenges-of-using-hydrogen-for-domestic-appliances/.

[72] F. Quintino. Chemiluminescent analysis of biogas combustion, 2017.

[73] J. Taylor. *Introduction to error analysis, the study of uncertainties in physical measurements*. 1997.

[74] A. Sciacchitano, B. Wieneke, and F. Scarano. Piv uncertainty quantification by image matching. *Measurement Science and Technology*, 24(4):045302, 2013.

[75] J. J. Charonko and P. P. Vlachos. Estimation of uncertainty bounds for individual particle image velocimetry measurements from cross-correlation peak ratio. *Measurement Science and Technology*, 24(6):065301, 2013.

[76] C. Oberascher, R. Stamminger, and C. Pakula. Energy efficiency in daily food preparation. *International Journal of Consumer Studies*, 35(2):201–211, 2011.

[77] F. P. Incropera, D. P. DeWitt, T. L. Bergman, A. S. Lavine, et al. *Fundamentals of heat and mass transfer*, volume 6. Wiley New York, 1996.

[78] Y. A. Cengel and A. J. Ghajar. Heat and mass transfer: fundamentals and applications. 2014.

[79] M. Doble. *Perry's chemical engineers' handbook*. McGraw-Hill, New York, USA, 2007.

[80] C. W. Cobb and P. H. Douglas. A theory of production. *The American economic review*, 18(1): 139–165, 1928.

[81] M. J. Moran, H. N. Shapiro, D. D. Boettner, and M. B. Bailey. *Fundamentals of engineering thermodynamics*. John Wiley & Sons, 2010.